CHALMERS
UNIVERSITY OF TECHNOLOGY

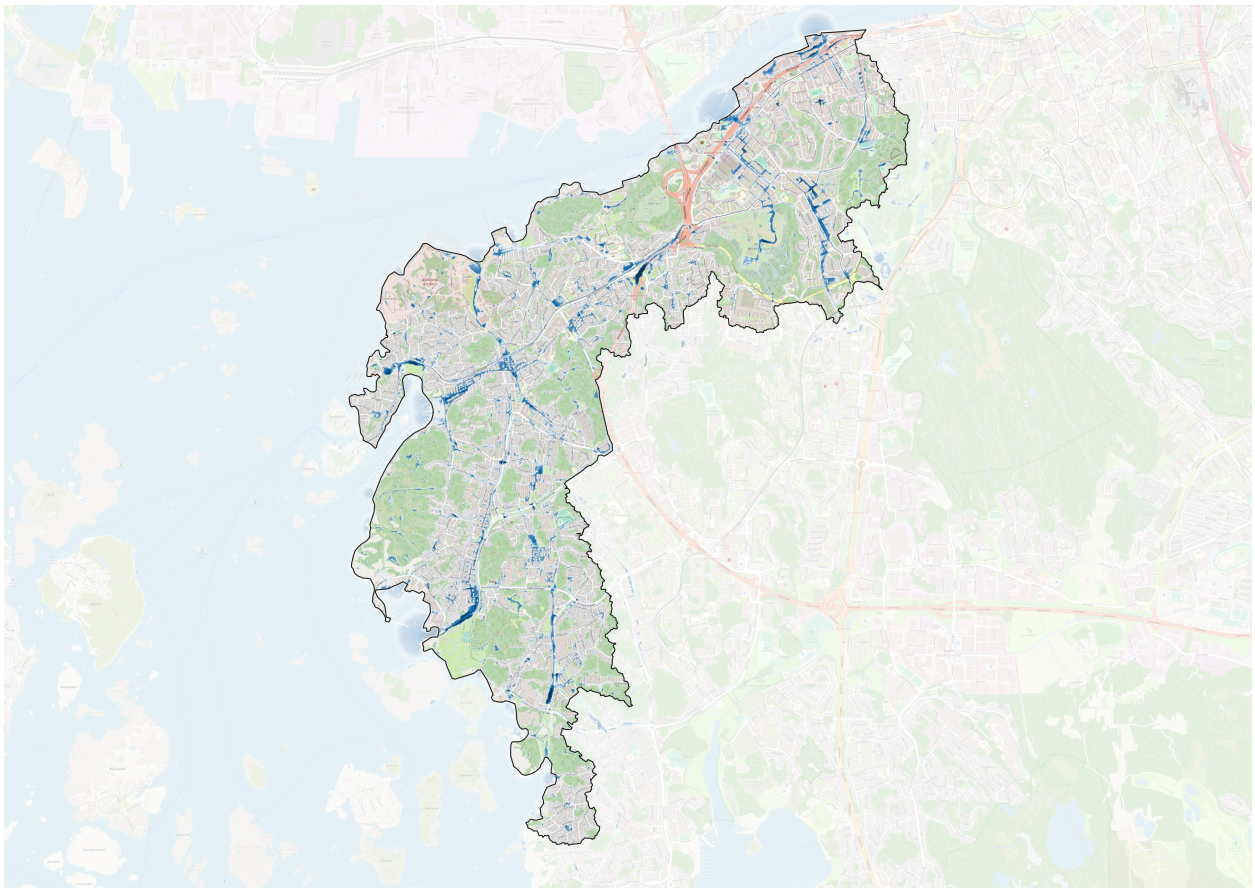

How Pluvial Floods in Urban Areas Vary with Rain Return Period

A Pilot Study to Develop a Tool for Simplifying the Cloudburst Management in Gothenburg

Master's thesis in Master Programme Infrastructure and Environmental Engineering

ALICIA COOPS AND FANNY KARLSSON

DEPARTMENT OF ARCHITECTURE AND CIVIL ENGINEERING
CHALMERS UNIVERSITY OF TECHNOLOGY
Gothenburg, Sweden 2023
www.chalmers.se

Master's thesis 2023

How Pluvial Floods in Urban Areas Vary with Rain Return Period

A Pilot Study to Develop a Tool for Simplifying the Cloudburst Management in Gothenburg

ALICIA COOPS FANNY KARLSSON

CHALMERS
UNIVERSITY OF TECHNOLOGY

Department of Architecture and Civil Engineering
Division of Water Environment Technology
Chalmers University of Technology
Gothenburg, Sweden 2023

How Pluvial Floods in Urban Areas Vary with Rain Return Period
A Pilot Study to Develop a Tool for Simplifying The Cloudburst Management in Gothenburg
ALICIA COOPS
FANNY KARLSSON

Master's Thesis 2023
Department of Architecture and Civil Engineering
Chalmers University of Technology
SE-412 96 Gothenburg
Telephone +46 31 772 1000

Cover: Floods with depths above or equal to 0.2 m due to a 100-year rain within structure plan West in Gothenburg.

Typeset in LaTeX
Printed by Chalmers Reproservice
Gothenburg, Sweden 2023

How Pluvial Floods in Urban Areas Vary with Rain Return Period

Master's thesis in Master Programme Infrastructure and Environmental Engineering

ALICIA COOPS
FANNY KARLSSON

Department of Architecture and Civil Engineering
Division of Water Environment Technology
Chalmers University of Technology

Abstract

Urban floods are the most frequently occurring natural disasters, posing significant threats to cities worldwide. The risk for pluvial floods (i.e. floods due to intense rainfall) is increasing, and thereby, several initiatives have been established worldwide. The aim of this study is to develop a tool to simplify the process of implementing a cloudburst area in different types of residential areas by estimating a manageable rain return period. The study evaluated floods generated by rain from return periods in the range of 10-100 years, in four different residential areas with nearby cloudburst areas, all located in the City of Gothenburg. Further, the study included an evaluation of the site characteristics of each residential area.

Ten rain events (each representing a different return period) were simulated using the hydrodynamic modeling software MIKE+. Simulations were conducted both without and with cloudburst areas. From the results of the simulations without cloudburst areas, a relation between flood and rain return period was established for each residential area separately. No general relation was identified for all investigated areas. However, a correlation was found for two of the areas consisting of townhouses. Based on the correlation between the two areas, a framework for a tool was developed. The developed tool provides an estimation of the manageable rain return period due to the implementation of a cloudburst area in residential areas with townhouses. From the study, it is concluded that to accomplish full utilization of the cloudburst area it is necessary to evaluate both if other measures are required and the most suitable location of the cloudburst area.

From the evaluation of site characteristics, different physical parameters were identified to influence the resilience against floods in different areas, e.g. sewer network capacity, building structure, and depression storage capacity. Further, this study concluded that topography had a distinct impact on flooding in all areas.

Keywords: flood management, hydrodynamic modeling, MIKE+, pluvial flood, rain return period, urban flood.

Acknowledgements

This thesis is the final part of the Master Programme Infrastructural and Environmental Engineering at Chalmers University of Technology in Gothenburg, Sweden. The thesis has been conducted at the Division of Water Environment Technology at the Department of Architecture and Civil Engineering. We would like to thank our examiner Mia Bondelind and our supervisor Sebastien Rauch for your guidance and support. Also, our opponents Klara Djerf and Josefin Hasselberg for helpful inputs and comments.

This thesis would not have been possible without the guidance from Christofer Karlsson at DHI and Dick Karlsson at Stadsutveckling, Enheten för dagvatten och skyfall at the City of Gothenburg. We would like to thank you for your support and interest in our work and for giving us the possibility to be creative and shape the thesis following our interest. You have both supported us during the process and contributed with good discussions and new perspectives. We would also like to thank DHI for allowing us to use MIKE+ and contributing with student licenses, and for sharing the model of structure plan West with us.

A special thanks to Lena Abrahamsson at IT support at Chalmers University of Technology in Gothenburg. Without your help with the student computers, this thesis would not have been possible.

Alicia Coops & Fanny Karlsson, Gothenburg, June 2023

Acronyms

Below is the list of acronyms that have been used throughout this thesis:

CBA	Cost-Benefit Analysis
CDS	Chicago Design Storm
CRED	Centre for Research on the Epidemiology of Disasters
DHI	Danish Hydraulic Institute
EC	European Commission
EPA	United States Environmental Protection Agency
EPA-SWMM	Environmental Protection Agency Storm Water Management Model
EU	European Union
GIS	Geographical Information System
GUFIM	GIS-based Urban Flood Inundation Model
HFSA	Hierarchical Filling-and-Spilling Algorithm
IDF	Intensity-Duration-Frequency
IPCC	International Panel of Climate Change
LNHE	Laboratoire National d'Hydraulique
MCA	Multi-Criteria Analysis
MSB	Myndigheten för Samhällsskydd och Beredskap (Swedish Authority for Social Security and Preparedness)
SMHI	Sveriges Meteorologiska och Hydrologiska Institut (Swedish Meteorological and Hydrological Institute)
UN	United Nations
UNISDR	United Nations Office for Disaster Risk Reduction
USACE	United States Army Corps of Engineering
WHO	World Health Organisation

Nomenclature

Below is the nomenclature of parameters and variables that have been used throughout this thesis:

Parameters

φ	Runoff coefficient [-]
φ_{short}	Runoff coefficient for short-term precipitation [-]
φ_{10}	Runoff coefficient for a 10-year rain [-]
φ_{100}	Runoff coefficient for a 100-year rain [-]
c_f	Climate factor [-]
F	Return period [year]
T	Return period [year]
T_r	Duration [min]

Variables

d_T	Average of maximum depths for a T-year rain $[m]$
$d_{\geq 0.2m,T}$	Average of maximum depths $\geq$ 0.2 m for a T-year rain $[m]$
$FI_{max,T}$	Maximum flow intensity for a T-year rain $[m^3/s/m]$
i_F	Rain intensity $[l/(s \cdot ha)]$
$R_{1,T}$	Ratio of the runoff volume with depths $\geq$ 0.2 m for a T-year rain and the runoff volume with depths $\geq$ 0.2 m for a 100-year rain [-]
$R_{2,T}$	Ratio of the runoff volume with depths $\geq$ 0.2 m for a T-year rain and the total runoff volume for a T-year rain [-]
$V_{tot,T}$	Total runoff volume for a T-year rain $[m^3]$
$V_{d\geq 0.2m,T}$	Runoff volume with depths $\geq$ 0.2 m for a T-year rain $[m^3]$

Contents

List of Figures

List of Tables

1

Introduction

Floods are the natural disasters with the most severe consequences considering human health and economic loss, according to the World Health Organization (WHO) (2013). The organization defines floods as "when an overflow of water submerges land that is usually dry" (WHO, 2013). Another definition, used by United Nations (UN) (2023), is "a general and temporary condition of partial or complete inundation of normally dry land areas from overflow of inland or tidal waters from the unusual and rapid accumulation or runoff of surface waters from any source". The initial cause for flooding to occur varies, however, the most common are intense rainfall, water-level rise, river flooding, or groundwater rise (Houston et al., 2011).

Centre for Research on the Epidemiology of Disasters (CRED) has compiled the number of flood events classified as disasters (either at least 10 death or 100 people affected, or requiring international help (CRED, n.d.-a)), see Figure 1.1. In the figure, it can be seen that the frequency increases with time. According to the International Panel of Climate Change (IPCC) (2021), intensive rain will become more intensive and occur more often due to climate change. Consequently, the risk of floods has increased and is expected to increase even more in the future.

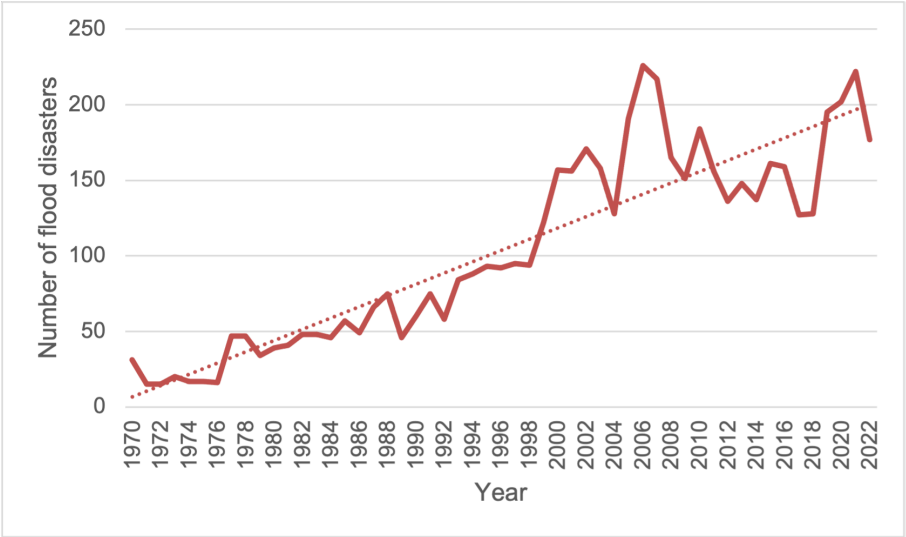

Figure 1.1: Number of flood disasters worldwide per year, 1970-2022 (based on data from CRED (n.d.-b)).

Urban floods are the most frequently occurring natural disaster and pose a significant threat to cities all over the world (Eldho et al., 2018), resulting in disturbances to infrastructure services and socioeconomic activities (Zhou et al., 2019). Both more heavy precipitation but also urbanization will increase the risk of urban floods. Urbanization not only increases the area exposed to floods but also the amount of intensive rains falling on cities (IPCC, 2021). Due to the increased risk of floods, extensive initiatives have been implemented worldwide to increase resilience in cities and these highlight the vitality of addressing how floods will affect an urban area (European Commission, 2023; Jha et al., 2012; Koutsoyiannis & Papalexiou, 2017; UNISDR, 2002). For instance, to understand the correlation between cloudburst events and flood characteristics (Koutsoyiannis & Papalexiou, 2017).

Gothenburg is one example of an urban area with an increased risk of flooding in the future due to increased precipitation, more cloudburst events, sea-level rise, and densification (Stadsbyggnadskontoret, 2019). To enable a dense city with increased resilience against flooding, the municipality has determined several objectives to strive for (Stadsbyggnadskontoret, 2019). Following these objectives, 15 structure plans have been established considering different geographical areas and these aim to concretize how extreme rain events will affect the area and how to prevent such scenarios (Kretslopp och vatten, 2021c). The plans are meant to work as guidance for stakeholders considering the implementation of cloudburst facilities to minimize the risk for and the consequences of flooding (Stadsbyggnadskontoret, 2019). As a complement to the structure plans, Rosén & Nimmermark (2018) developed *FloodMan - Sustainable Flood Management Assessment Tool*, a tool that aims to simplify the process of performing cost benefits analysis (CBA) and multi-criteria analysis (MCA) when planning new flood infrastructure. In the design process today, the structure plans are used to evaluate the risk of floods while FloodMan is used to evaluate the advantages and disadvantages of risk-reducing measures. However, there is no standardized method for evaluating the decrease in risk due to the implementation of a risk-reducing measure.

1.1 Aim

The aim of the thesis is to develop a tool to simplify the process of implementing a cloudburst area in different types of residential areas by estimating a manageable rain return period. The objective is to develop the tool by evaluating flooded volumes generated by rain from return periods in the range of 10-100 years, in different residential areas. The following research questions will be answered to achieve the aim of the thesis:

- Is it possible to create a tool to estimate the increase in flood resilience due to the implementation of a cloudburst area?
- Is there a general relationship between flooded volume and rain return period for the selected areas?
- Which site characteristics impact the flooding in the areas?

1.2 Limitations

The following limitations have been made:

- This study is limited to four residential areas from structure plan West in Gothenburg. All four areas include a cloudburst area that is not incorporated in larger cloudburst facility networks.
- The types of residential areas are limited to three different types i.e. townhouse areas and apartment building areas with- and without enclosed yards.
- The study only considers pluvial floods, i.e. floods that occur due to rainfall.
- The study will evaluate the current situation (2023). The simulated rain events will be customized with a climate factor to include future climate changes in the cloudburst events investigated.

2

Background

The following chapter will provide general information about pluvial flooding. Concepts that are used to describe rain and parameters that affect the severity of a flood will be described. Further, international and national flood management will be explained. This chapter also includes a summary of the concept of flood modeling and some of the tools that are available. At the end of the chapter, previous research similar to this thesis is presented.

2.1 Pluvial floods

The term flood includes coastal flood, flash flood, glacial lake outburst flood, pluvial flood, river flood (fluvial), sewer flood, and urban flood (Seneviratne et al., 2012). Pluvial floods occur due to intensive rain events and are described by Prokic et al. (2019) as floods that occur before the runoff can enter either a recipient, the sewer system, or be infiltrated into the ground. In research, pluvial floods are less studied than fluvial and coastal floods since these often are more extensive considering the affected area and duration (Prokić et al., 2019). The risk for pluvial floods has increased and will, according to IPCC (2021) continue to do so. In addition, Prokic et al. (2019) describe that pluvial floods often have larger economic consequences than fluvial and coastal floods.

Extreme rain events can happen everywhere, however, serious consequences will most likely arise in urban areas (Douglas et al., 2010; Houston et al., 2011; Jha et al., 2012; The European Parliament and the Council, 2007). Walczykiewicz & Skonieczna (2020) presents several possible consequences of pluvial floods, for instance:

- Damage to buildings, estates, and roads
- A reduced capacity in transport- and infrastructure systems
- Disturbances in waste- and drinking-water management

Currently, most of the pluvial floods in Sweden occur during summer (SMHI, 2023). The yearly distribution of precipitation in Sweden will, according to the Swedish Authority for Social Security and Preparedness (MSB), change as a consequence of climate changes (MSB, 2013b). In the future, there will be less total precipitation during the summer months and more total precipitation for the winter months (MSB,

2013b). However, extreme rain will occur more frequently all year (even during the summer months), and hence, the risk of pluvial floods will increase (MSB, 2013b; WHO, 2013).

2.2 Rain concepts

This section will include a description of different concepts commonly used to describe rain events. The selection of concepts is based on the methodology for this thesis, hence concepts that are required to understand to be able to follow the thesis. Other concepts might be mentioned but not further described.

2.2.1 Return period

Return period is defined by a period of time (time interval) and used to describe the probability for an event to occur (Svenskt Vatten, 2016). The concept has several applications, for instance, to describe the probability of a specific rain intensity or volume (Svenskt Vatten, 2016), and is a central element in water management and flood assessment (Vogel & Castellarin, 2016).

The Swedish Meteorological & Hydrological Institute (SMHI) (2021) describes return period as the average time between two events, a statistical measurement based on historical data from observations of extreme weather and series of measurements. From the return period, it is possible to calculate the probability of an event to occur, for instance, the probability of 100-year rain is 1 % each year, independently of other events. Simply explained, there is 1 % risk of a 100-year rain each year, regardless if there where a 100-year rain last year. However, this might also result in no extreme rain of this magnitude during a period of 100 years.

2.2.2 Statistical description of rain events

To be able to statistically describe rain events with different return periods it is necessary to process data from historical rainfall observations (Svenskt Vatten, 2011). In Sweden, the process starts with the establishment of so-called block rains where the rain events are sorted into different blocks considering the maximum mean value of a given intensity. These block rains are thereafter used to develop Intensity-Duration-Frequency (IDF) diagrams (Svenskt Vatten, 2011). An IDF diagram describes the mathematical relationship between rain intensity, rain duration, and return period (Sun et al., 2019). Based on the IDF diagrams, different equations to calculate rain intensity have been established (Svenskt Vatten, 2011). In Sweden, Equation 2.1 is recommended to use for a rain duration of up to 24 hours. (Svenskt Vatten, 2011; Svensson et al., 2020).

$$i_F = 190 \cdot \sqrt[3]{(F \cdot 12)} \cdot \frac{ln(T_r)}{T_r^{0.98}} + 2 \tag{2.1}$$

i_F: Rain intensity [l/s/ha]

F: Return period (T in this study) [year]
T_r: Duration [min]

To model rain it is required to describe how the rain intensity varies for a time serie. For this, a hyetograph is used which is a plot of the average intensity of rainfall against the time interval that is constructed based on either historical rains or design rains (Svenskt Vatten, 2011). A commonly used design rain from IDF diagrams is the Chicago Design Storm (CDS-rain), first established by Keifer & Chu (1957). The CDS-rain is designed using Equation 2.1 to establish a graph where the rain peak (intensity maximum) is located in the middle of the curve (Svenskt Vatten, 2011). The graph is constructed based on maximum rain intensities for different duration and relates to the occurrence of a peak during a rain event and the amount of rain before and after this peak (Marsalek & Watt, 1984) An example of a graph to present a CDS-rain can be seen in Figure 2.1.

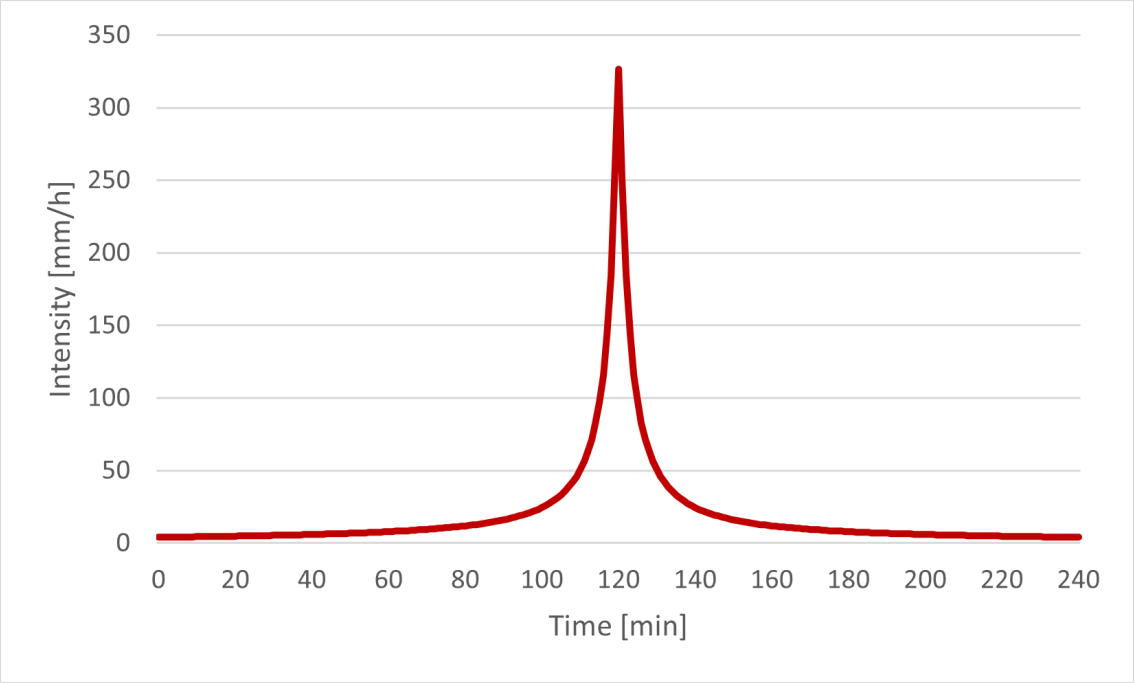

Figure 2.1: Example of a graph that presents the rain intensities (mm/h) for a 100-year CDS-rain with a duration of 240 min (based on Svenskt Vatten (2016)).

2.2.3 Climate factor

Increased precipitation in the future is greatly associated with climate changes and according to SMHI, the rain intensity for a 10-year rain will increase by 15-30 % until the year 2100 (Eklund et al., 2015). To consider the impact of climate change in design rains, that are based on historical data, a climate factor (c_f) is used (Svenskt Vatten, 2016). Climate factors are established by estimations of future climate scenarios and hence, the climate factor might differ depending on the scenario analysed. According to Svenskt Vatten (2016) and Gustafsson & Mårtensson (2017), it is suitable to use a climate factor in the range of 1.2 to 1.5 when evaluating cloudburst in Sweden with a return period of 100 years and above.

2.3 Physical parameters influencing flooding

There are several physical parameters influencing the occurrence and characteristics of flooding (Jha et al., 2012; Prokić et al., 2019; SMHI, 2023). The following sections will present research regarding these parameters and their impact on floods in urban areas.

2.3.1 Topography

Topographic factors include inclination, elevation, and depressions and are important spatial characteristics that affect urban flooding (Zhang, 2020; Huang et al., 2019). Topography affects both infiltration capacity and generation and characteristics of runoff (i.e. velocity, directions, and depths) (Qi et al., 2020). Further, the topography may contribute to increased flood volume by hindering water from reaching the sewer system if inlets are improperly located (Palla et al., 2018). Walczykiewicz & Skonieczna (2020) state topography as one of the two most significant aspects (in addition to surface properties) that influence the risk for urban flooding.

Topography is especially important for low-lying areas and depressions with large contributing areas (Qi et al., 2020). Walczykiewicz & Skonieczna (2020) define depressions as the most vulnerable places in urban areas considering floods. The vulnerability of depressions is defined by the size and slope of the area and surrounding areas that contribute to the flood (Qi et al., 2020).

2.3.2 Infiltration

The influence of infiltration on urban flooding has been analyzed by several researchers (K. Luo & Zhang, 2022; Ren et al., 2020; Qi et al., 2020; Walczykiewicz & Skonieczna, 2020; Wang et al., 2022), and according to Alshammari et al. (2023) insufficient infiltration capacity is one of the dominant factors. Infiltration capacity depends on the characteristics of the soil, e.g. structure, porosity, land cover, and texture (Alshammari et al., 2023). Green areas are associated with a high infiltration capacity, however, during intense rains the infiltration capacity will decrease due to saturation resulting in surface runoff (Svenskt Vatten, 2016).

Impervious areas influence the urban water cycle processes resulting in decreased infiltration capacity and emerged urban floods (Ren et al., 2020). Since urban areas generally are covered by a large fraction of impervious surfaces (e.g. roads, asphalt surfaces, and buildings), a majority of the rain will result in surface runoff (Ren et al., 2020). Walczykiewicz & Skonieczna (2020) state that impervious surfaced areas are one of the main causes of urban flooding. In a study by Wang et al. (2022), imperviousness, and green-space-ratio were identified as the overall dominant factors influencing urban flooding. K. Luo & Zhang (2022) analysed how changes in land cover in China, between 1977 and 2018, have affected the risk of urban floods. According to the study, the amount of impervious surfaces has increased by 140 % for the observed period. The increase in imperviousness resulted in a decreased capacity of cities to reduce surface runoff, by 13 % (K. Luo & Zhang, 2022).

Urban areas in Sweden have, according to MSB (2013b), an infiltration capacity equivalent to a 10-years rain (no climate factor). This indicates an insufficient capacity during heavy precipitation and hence, it is important to ensure that the infiltration capacity enhances or at least remains (MSB, 2013b). The Swedish National Board of Housing, Building, and Planning, Boverket, states that it might be required to restrict the increase of impermeable areas when establishing detailed developments plans and instead implement areas for enhanced infiltration to ensure resilient urban areas (Boverket, 2010).

2.3.3 Sewer network

The sewer network influences urban flooding, mainly due to insufficient capacity in most urban areas (Prokić et al., 2019). Evans et al. (2013) state that urbanization, rapid population growth, and the expansion of impermeable surface areas have led to a significant surge in demand for sewer systems for most urban areas. Commonly there are two methods used for sewer networks, combined and separated. A combined system is when all water (waste, runoff, and drainage) is collected in one system, and a separate system is when wastewater is collected in one system and the remaining water is collected in another (Jha et al., 2012). Combined sewer systems are common in old sewer networks and Prokic et al. (2019) describes that urban areas with combined sewer systems generally are more vulnerable to flooding than urban areas with separated systems.

One of the reasons for the lack of sewer capacity is that the sewer network has not been updated to the same extent as cities have developed (Jha et al., 2012). The Swedish sewer system was developed in the 19th century and since the 1950s, mainly separate systems have been installed to ensure better management of stormwater (Svenskt Vatten, 2016). Although, approximately 13 % of the Swedish sewer network consists of combined systems and these are often located in central parts of urban areas (Räddningsverket, 1997; Svenskt Vatten, 2016). The general sewer network in Sweden is designed to manage normal precipitation and, according to MSB (2013b), a properly designed sewer network is capable to handle the volume of a 10-year rain.

2.3.4 Building structure

Urban floods are highly influenced by spatial characteristics which commonly are associated with infiltration. However, urban forms, building structures, and density also influence urban flooding but have not received as much attention (X. Li et al., 2021). Urban forms (e.g. congestion, location in relation to streets, building height) strongly influence the mean flood depths in urban areas (Bruwier et al., 2020). The most important factor, according to Bruwier et al. (2020), is the building side setback (i.e. the distance between the building and the road) which influences both the water storage and outflow discharge (Bruwier et al., 2020). Further, building height and density are potential driving factors for urban floods since these are associated with impermeable areas and hence the generation of runoff (Qi et al., 2020; Wang et al., 2022).

2.4 Flood management

Inappropriate urban planning and lacking communication between stakeholders result in an increased risk for hazardous floods (Jha et al., 2012). Hence, functioning flood management is important for urban areas that strive for resilience against floods. The following section presents an overview of the flood management agreements in the world, Europe, and Sweden followed by a brief description of the agreements set by the City of Gothenburg.

In 2004, UN released a report on how to reduce losses due to flooding (UNISDR, 2002). The report aims to guide decision-makers to increase resilience against flooding (UNISDR, 2002). In 2012, the World Bank released *Cities and Flooding* with guidance for stakeholders considering urban flood risk management (Jha et al., 2012). Further, in 2015, the *Sendai Framework for Disaster Risk Reduction: 2015-2030*, was established by the United Nations Office for Disaster Risk Reduction (UNISDR) to increase knowledge and reduce the risk of disaster globally (UNISDR, 2015). Considering floods, the framework defines the importance of simplifying flood risk management on a national and local level (UNISDR, 2015).

In the European Union (EU), flood management is governed by the *Floods Directive 2007/60/EC* which was established in 2007 (The European Parliament and the Council, 2007). Following the directive, each member state is obliged to (*i*) map areas vulnerable to floods, (*ii*) analyse the risks (considering human health, environment, cultural heritage, and economic loss) in each area, and (*iii*) establish an action plan to reduce the risks for the areas. Further, the directive gives guidance on which rain events and parameters to analyse, e,g rain events with a return period of 100 years or larger, and flood extension, depth, and flow (The European Parliament and the Council, 2007). The European Commission (EC) (2023) declares that the Floods Directive shall be an iterative process that should be continuously updated in six years cycles (i.e. all three steps should be accomplished every six years).

In Sweden, the obligations stated by the Flood Directive are governed by several regulations. In 2009, the Regulation of flood risks (*SFS 2009:956*) (Försvarsdepartementet, 2009) was adopted which aims to reduce the negative impacts of floods. In SFS 2009:956, MSB is defined as responsible for the preliminary analysis of flood risks and flood mapping and the County Administrative Boards for the development of action plans considering flood risks. To guide the County Administrative Boards, MSB established regulations considering flood risk management (*MSBFS 2013:1*) in 2013 (MSB, 2013a). The municipalities are responsible for flood management when developing comprehensive and detailed development plans, according to *PBL 2010:900* (Landsbygds- och infrastrukturdepartementet, 2010), and as property owners, according to *Jordabalk 1970:994* (Justitiedepartementet, 1970). To guide the municipalities to fulfill their responsibilities, MSB released a report on how to work with cloudburst mapping and flood prevention in urban areas in 2016 (Gustafsson & Mårtensson, 2017). In the guidance the process of cloudburst management is divided into planning, cloudburst mapping, impact analysis, developing structure plans, planning of measures, contingency planning, and follow-up,

and guidance on how to proceed is given for each part (Gustafsson & Mårtensson, 2017).

The City of Gothenburg is, as the municipality, responsible for flood management when developing comprehensive and detailed development plans. Following this, a supplement to the comprehensive plan that considers flood risks was adopted in 2019 (Stadsbyggnadskontoret, 2019). In the supplement, current and future risks are described and strategies to reduce these (e.g. structure plans) are presented. In addition to the comprehensive plan, a cloudburst agreement was initiated between several departments in the city in 2021 (Göteborgs Stad, 2021). The agreement aims to divide the responsibilities considering cloudburst and flood management in the city and clarify the decision-making process (Göteborgs Stad, 2021).

2.5 Flood modeling

To analyse floods, two tools are often mentioned, hydrodynamic models and Geographical Information System (GIS) (Seenath et al., 2016). The difference between the tools is that hydrodynamic models involve water movement and GIS tools do not, instead GIS tools are used to display data by mapping (Seenath et al., 2016). GIS is mostly used for flood mapping, risk mapping, and hazard assessments (Seenath et al., 2016; Di Salvo et al., 2018). Hydrodynamic models are commonly used for flood-related engineering (e.g. flood forecasting) and are more suitable to be used for scenario analysis (Teng et al., 2017). The following sections will include a description of both tools and examples of software.

2.5.1 Hydrodynamic models

Hydrodynamic models are mathematical models that simulate water movement, specific flow rates, and water depth distribution, by solving equations formulated by applying laws of physics (P. Luo et al., 2022; Teng et al., 2017; Randa et al., 2022). Hydrodynamic models could be applied for different dimensions: one dimensional (1D), two dimensional (2D), three dimensional (3D), and coupled 1D-2D (Randa et al., 2022).

For 1D hydrodynamic models, it is assumed that the flow is in one direction, and the flow velocity is homogeneous (Randa et al., 2022). The basis for the model is to represent flow as a series of cross-sections towards the flow direction and the model uses the Shallow Water Equations (Randa et al., 2022; Teng et al., 2017). These models are the simplest representation of flow and can be used in various hydraulic situations where the flow is comparable to one dimension, e.g. open channels and pipes (Teng et al., 2017). One advantage with 1D models is due to the low input requirements resulting in a simple model structure (P. Luo et al., 2022). However, the low input requirements also limit the broad understanding of hydrological processes (Randa et al., 2022).

The 2D hydrodynamic models are the most common setup for flood mapping and flood prediction (Randa et al., 2022). These models represent the floodplain as a

2D field by using the two-dimensional Shallow Water Equations for estimating the horizontal velocity and the depth of the flow (Teng et al., 2017). In comparison to the 1D models, the 2D models provide more information resulting in increased accuracy (P. Luo et al., 2022). Additional advantages are the incorporation of small-scale topography in the model which has been demonstrated to impact the urban flooding (Randa et al., 2022).

Coupled 1D-2D models combine the advantages of the two model types. An application for such models is by using the 2D models to model surface runoff and combining it with a 1D description of the pipe network (P. Luo et al., 2022). These types of models are more suitable for complex sites such as urban areas (P. Luo et al., 2022).

The 3D models can be used to model vertical turbulence, spiral flow, and vortices (Teng et al., 2017). These models are more suitable for catastrophic floods such as tsunamis, flash floods, or dam breaks (P. Luo et al., 2022). The 3D models are complex and often stated to be unnecessary for urban flood modeling since 2D and 1D-2D models provide sufficient information (P. Luo et al., 2022).

2.5.1.1 Hydrodynamic software

There are several hydrodynamic model software developed for pluvial modeling and it is possible to apply most of these for urban flood studies (Teng et al., 2017). However, the strength and limitations of each software need to be considered depending on the aim and application. Three examples of modeling software capable of modeling floods are MIKE+, TELEMAC, and HEC-RAS. Table 2.1 lists the limitations and strengths of the software based on literature obtained by Randa et al. (2022). MIKE+ is a hydraulic modeling software created by Danish Hydraulic Institute (DH) in 2020, with the latest update in 2023, and is a combination of existing DHI software such as MIKE Urban and MIKE 21 (DHI, 2023a). Since MIKE+ is a new software, no studies have been accomplished considering the advantages and disadvantages of the software. Therefore, the strengths and limitations of MIKE Urban and MIKE 21 are presented.

Table 2.1: Summary of strengths and limitations for different hydrodynamic software (based on Randa et al. (2022)). *(Published with CC BY-NC-ND 4.0.)*

Model name	Developer	Strength	Limitations
MIKE 21	DHI	Capable of simulating flow characteristics. Applicable in flood dynamic simulations.	Simulation time steps must be manually calibrated, to ensure model stability, more calibration needed.
MIKE Urban	DHI	Integrated GIS capabilities. Applicable in simulating urban flows.	Inability to capture some hydrodynamics such as shocks and supercritical flows during simulations.
TELEMAC 2D	LNHE	Can simulate permanent and transient hydrodynamic conditions.	Stable under specific conditions.
HEC-RAS 2D	USACE	Wide references, wide range of applicability.	Inability to perform water quality modeling in 2D flow areas.

MIKE+ is based on the Shallow Water Equations and can be used as 1D, 2D, or coupled 1D-2D for modeling distribution-, wastewater- and stormwater networks, collection systems, river networks, and overland flows (DHI, 2023b). Since MIKE+ is a relatively new tool, there is limited literature on the application. However, there is extensive research found about MIKE 21 and MIKE Urban and their application in urban flooding. One example, similar to the objective of this thesis, is a study from Aalborg University where the aim was to analyze rainfall and flooding in relation to return periods in urban areas using both MIKE Urban and MIKE 21 (Tuyls et al., 2018). Apart from research applications, MIKE applications have been used by the City of Gothenburg to model flooding and establish the structure plans (Kretslopp och vatten, 2021c).

TELEMAC-2D is a modeling software developed by Laboratoire National d'Hydraulique (LNHE) (Ata et al., 2014). The software is based on the Shallow Water Equations and the main application is for river and marine hydraulics (Ata et al., 2014). Since TELEMAC-2D commonly is used for coastal areas there is limited literature obtained about its application in urban areas (G. Li et al., 2022). There have been some studies conducted in urban areas though, an example is G. Li et al. (2022) where TELEMAC-2D was used for flood risk assessment. The research scope differs from the aim of this thesis, however, some similarities are found as different rain intensities depending on the return period are simulated. Some limitations are mentioned, such as not being able to model the drainage system. Although, Li et al. (2022) state that TELECMAC-2D is reliable for urban flood simulation.

The third example is HEC-RAS 2D which is a software developed by the US Army Corps of Engineering (USACE). The software can be used in either 1D, 2D, or coupled 1D-2D and solves the Shallow Water Equations and the Diffusion Wave Equation (Brunner, 2023). There are several application possibilities for HEC-RAS-2D such as channel modeling, floodplain modeling, and dam breach modeling (Brunner, 2023). One advantage of HEC-RAS 2D is that it is free to access which could be a reason for its wide references (Randa et al., 2022). An application of HEC-RAS, similar to the topic of the thesis, is Rangari et al. (2019) who used it to analyse the flood risk in urban areas. Their aim was to develop a risk map of Hyderabad, India, by modeling rains with different return periods. Their result showed that, by using HEC-RAS, it is possible to create a general model used to generate risk maps applicable to any region with few input requirements.

2.5.2 GIS-based models

GIS is used to display information, called spatial data, about the earth's physical aspects in a geographical coordinate system (Unwin, 1996). Spatial data could be defined in different ways, such as vectors or rasters, and are used to describe the world with the help of lines and polygons (Unwin, 1996). GIS tools have multiple application possibilities and, in relation to flooding, it is mainly used for spatial analysis (Di Salvo et al., 2018). In contrast to hydrodynamic models, GIS tools are simpler and require less extensive information about the area of interest (Di Salvo et al., 2018). However, this also limits the applicability (Di Salvo et al., 2018).

GIS is extensively adopted for flood modeling, however, not considered the most common method (Xing et al., 2022). Although, for flood mapping and flood risk assessments, GIS based models are commonly mentioned (Chen et al., 2009; Di Salvo et al., 2018; Xing et al., 2022). One example of such model is GIS based Urban Flood Inundation Model (GUFIM) that was developed by Chen et al. (2009). The study aimed to create a model for simplifying the identification of flood risks in urban areas. The model used standard data, IDF diagram, and contour maps, and resulted in a simplified less time-consuming model to be used for urban planning (Chen et al., 2009). Another GIS-based model is the more established Scalgo Live which is a browser-based modeling tool developed by the Danish company Scalgo in 2015 (SCALGO ApS, 2023). Scalgo Live is used by consultant companies and municipalities in Sweden and Denmark for urban planning, risk management, and climate adoption (SCALGO ApS, 2023). Scalgo Live has multiple application possibilities and uses topography and water volumes to determine the flooding in an area (SCALGO ApS, 2023). The Swedish consultant company Sweco used Scalgo Live for cloudburst mapping in Ängelholm municipality, Sweden (Theland, 2019) and described the limited computer times as advantageous. One limitation mentioned was that it does not provide details of water flow and no further analysis of rain duration as the analysis is static (Theland, 2019).

2.6 Previous research

This thesis aims to evaluate the relationship between the rain return period and floods in Gothenburg. During the literature review, few studies similar to this thesis have been found. This section will include an overview of the research available, similar to the aim of this thesis.

Tuyls et al. (2018) analysed the correlation between rain return period and flooded volume and area in Lystrup, Denmark, using 35 historical extreme rain events in a 1D-2D coupled hydrodynamic model. The study defined the relation between rain intensity and flooded volume and area as complex and highly dependent on the characteristics of the studied area. Further, the identification of risk areas was stated as essential to enable efficient flood management (Tuyls et al., 2018). A limitation of the study was that just one area was analysed though, and Tuyls et al. (2018) recommend verifying these results for other areas as further research.

Mediero et al. (2022) examined the correlation between the rain and flood return period in Pamplona, Spain, using a standard, and a stochastic approach. The standard approach refers to the use of design rains in a 2D hydrodynamic flood modeling tool (Mediero et al., 2022). The stochastic approach analyses the probability of a specific water depth for each risk zone and storm event using a Hierarchical Filling-and-Spilling Algorithm (HFSA) called Safer_RAIN, developed by Samela et al. (2020). Figure 2.2 visualizes the results for one of the risk zones analysed as two graphs, one for each approach (Mediero et al., 2022). The graphs represent the correlation between the water depth and rain return period and show similar trends for the standard and stochastic approaches.

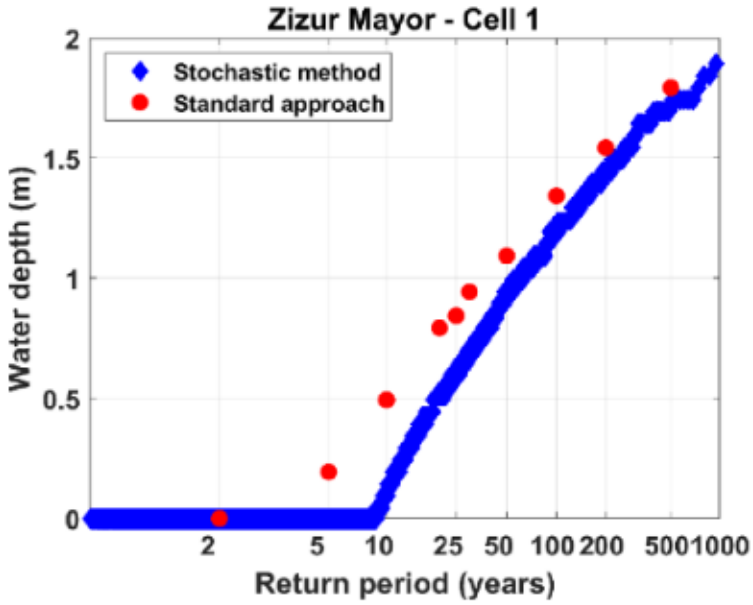

Figure 2.2: The correlation between water depth (m) and rain return period (years) for a risk zone in Pamplona (Mediero et al., 2022). *(Published with CC BY-NC-ND 4.0.)*

Arosio et al. (2020) analysed flood risks in Mexico City using the 1D modeling tool EPA SWMM (a stormwater management model provided by the United States Environmental Protection Agency (EPA)). Figure 2.3 presents the results as a graph where the number of affected (directly or indirectly) elements are visualized in relation to the rain return period. The elements considered were crossroads, fire stations, fuel stations, hospitals, schools, and blocks (Arosio et al., 2020). The graph shows an increasing trend for affected elements with an increasing rain return period.

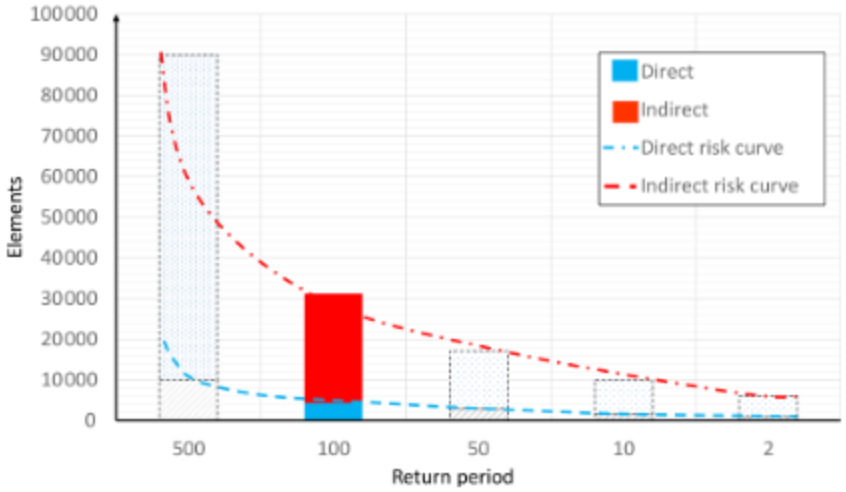

Figure 2.3: The correlation between elements affected (direct or indirect) (-) and rain return period (years), for Mexico City (Arosio et al., 2020). *(Published with CC BY 4.0.)*

Following Arosio et al. (2020), Martina et al. (2020) examined the correlation between flooded areas and water levels for different rain return periods in Mexico City. The study was conducted by modeling CDS-rain for different return periods in EPA SWMM and by analysing water depths in GIS (Martina et al., 2020). Figure 2.4 visualizes the results where the graph shows that the flooded area increases with the rain return period.

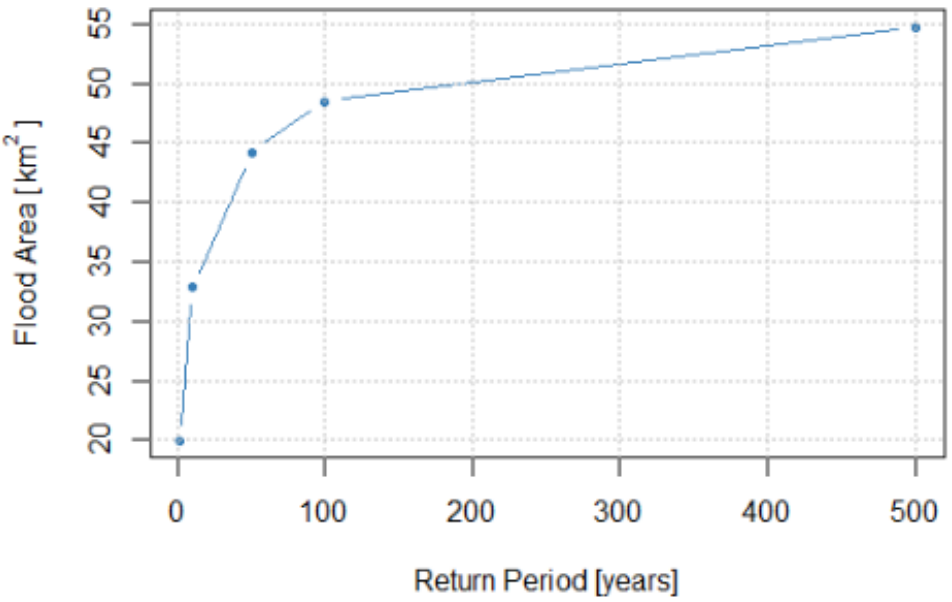

Figure 2.4: The correlation between the flooded area (km^2) and rain return period (years), for Mexico City (Martina et al., 2020). *(Published with CC BY.)*

3

Methodology

This chapter outlines the methodology used in this master thesis. This thesis included a qualitative literature review, a case study, a quantitative data analysis of the results generated from modeling using MIKE+, and tool development.

3.1 Literature study

This master thesis included a qualitative research part consisting of a systematic literature review to establish further knowledge in the research area. A qualitative research approach is beneficial for gaining more extensive knowledge in a research area (Bell et al., 2019). The literature search was accomplished using a set of keywords, e.g. cloudburst events, pluvial flooding, precipitation, return period, urban areas, topography, infiltration, sewer network, and hydrodynamic modeling. These keywords were used in different combinations and enabled both a more extensive knowledge in some specific areas (e.g. hydraulic modeling) and a broader understanding in others (e.g. differences in how flooding affects urban areas). The search method snowballing was used to find additional literature. Snowballing is when new literature is collected from the sources of other relevant literature (Bell et al., 2019). The method was conducted on collected literature to increase the possibility of finding relevant information.

The literature search was accomplished using Scopus and Google and included both articles from scientific journals and grey literature. Scientific articles were used to gather relevant knowledge within the research area. Also, to gain knowledge about studies with similar objectives as the thesis. Grey literature refers to materials from organizations, government departments, companies, consultants, and other non-academic associations (Kanu et al., 2020). Grey literature was required to establish knowledge about the study area considering previous studies, local conditions, and the process of cloudburst infrastructure implementation in the city of Gothenburg. Both primary and secondary sources were required to be able to answer the research questions. Primary sources include previous studies and the model with simulations received from Kretslopp och vatten while secondary sources included reviews.

3.2 Research design

The aim of this thesis is to develop a tool to simplify the process of implementing a cloudburst area in different types of residential areas by estimating a manageable rain return period. The tool is meant to be used for planning by providing the user an estimated return period of which a residential area is free from flooding if implementing a nearby cloudburst area. Since the tool aims to simplify the planning process when implementing cloudburst areas, it should be easy to use. Therefore, the tool is designed to require minor input information that is available. Following this, the tool was developed to be used with the flooded volume of a 100-year rain (with a climate factor of 1.2) since this can be extracted from the structure plans.

The tool was developed by evaluating flooded volumes generated by rain from return periods in the range of 10-100 years, in different residential areas. The evaluation was conducted by establishing graphs which is a commonly used approach to describe the correlation between rain return period and other parameters (Arosio et al., 2020; Martina et al., 2020; Mediero et al., 2022).

The tool was developed by following a research design that can be seen in Figure 3.1. The research design included the selection of areas and site characteristics to investigate. The selected areas were modeled in the hydrodynamic modeling software MIKE+. First, the areas were modeled without cloudburst areas and this is defined as *the current situation*, and secondly, with cloudburst areas defined as *the future situation*. For the current situation, different rain loads from rain return periods between 10 to 100 years were modeled, while for the future situation, only the rain load from a 100-year rain was modeled. The results from the simulation of the current situation were processed and analysed separately for each selected area. Further, an analysis of the site characteristics was conducted to provide an understanding of how these affected the results. From the results of the current situation, a correlation between rain return period and runoff volume was established and this was used to develop the tool. The results from the future situation were used to analyse the utilization of the cloudburst areas and hence, to evaluate the accuracy of the tool.

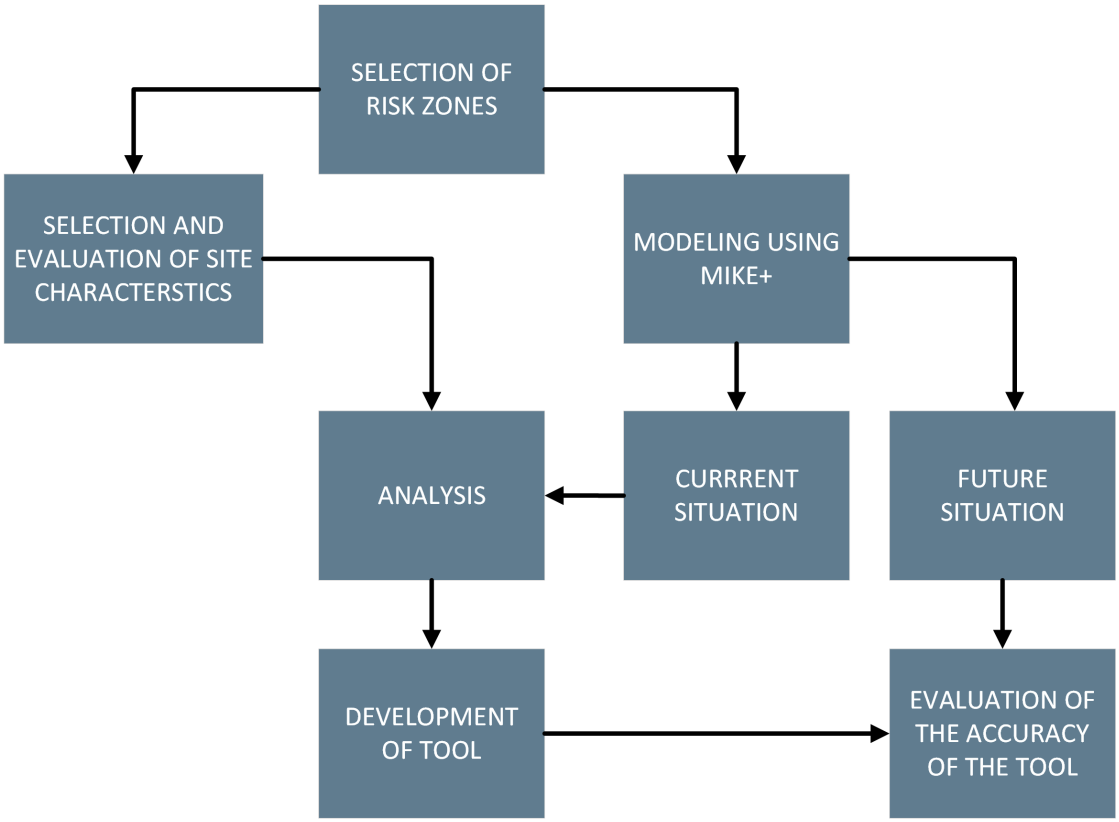

Figure 3.1: A conceptual description of the research design used in this study.

The following sections include a description of all steps conducted in this study. An overview of the structure of the methodology and the content within each section is presented in the following list:

- **Case study area**: The case study area is the City of Gothenburg and this section provides a brief description of the flood management in the city.
- **Selection of risk zones**: In Gothenburg, four residential areas (defined as *risk zones*) were selected and used for the development of the tool. This section describes the process of choosing the risk zones and requirements that were considered. Further, this section includes a presentation of the selected risk zones.
- **Selection of site characteristics**: To evaluate the similarities and dissimilarities between the results for the different risk zones, different site characteristics were analysed. In this section, the process of choosing which site characteristics to analyse is described. Further, a description of each site characteristic in each risk zone is presented coupled with observations from a study visit to all risk zones (conducted 9th of May, 2023).
- **Modeling in MIKE+**: In this study, a MIKE+ model for flood mapping of Gothenburg was provided from DHI and Kretslopp och vatten. This section provides a general description of the provided model, the selections of simulations to model, and modifications made to the model for this study. Also, a description of the uncertainties in the model.

- **Analysis**: From the modeling, results were extracted and processed to develop the tool. This section includes a description of the extracted results, the methodology for processing the results, and the steps conducted to develop the final tool.

3.3 Case study area

The City of Gothenburg serves as the case study in this thesis. Following the flood risk supplement to the comprehensive plan from 2019, the City of Gothenburg has initiated and developed several strategies to increase resilience against cloudbursts and floods. In Gothenburg, the department Kretslopp och vatten has developed 15 structure plans following the objectives defined in the comprehensive plan, see Figure 3.2 (Kretslopp och vatten, 2021c). The aim of structure plans is to clarify and support planning and to identify needed cloudburst infrastructure to minimize flood consequences (Kretslopp och vatten, 2021a). The structure plans include flood mapping due to a 100-year rain with a climate factor of 1.2 and also recommendations for different cloudburst facilities (such as cloudburst areas, paths, and steering measures).

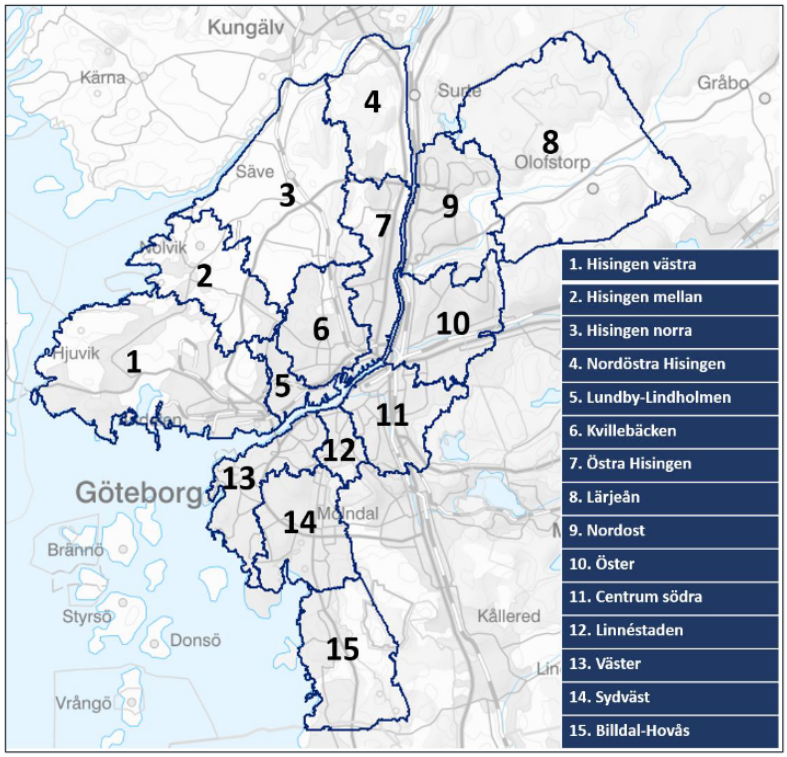

Figure 3.2: Map over Gothenburg with the 15 structure plans displayed (Kretslopp och vatten, 2021b). *(Published with approval from C. Karlsson DHI and D. Karlsson Kretslopp och vatten.)*

3.3.1 Selection of risk zones

For each structure plan, a hydrodynamic model has been established to conduct flood mapping. In this thesis, the model from structure plan West (see number 13 in Figure 3.2) was used and hence, all risk zones are residential areas located within this structure plan. This structure plan was selected based on recommendations from DHI and Kretslopp och vatten (C. Karlsson & D. Karlsson, personal communication, January 23, 2023).

Following the aim of this thesis, it was required to determine the number of risk zones to evaluate. Henrichs (2003) describes that a study should include an adequate number of perspectives, however, as few to avoid fatigue and to ensure that the process remains manageable. In this thesis, a total of four risk zones were selected based on evaluations of the structure plan West and in discussions with DHI and Kretslopp och vatten. The number of risk zones was considered suitable since it provided a diversity of types of residential areas which was required to fulfill the aim. Further, four risk zones enable an extensive comparison of the results and site characteristics of the zones. The risk zones were selected based on the following criteria:

- Different types of residential areas.
- A residential area with an adjacent recommended cloudburst area.
- The cloudburst area decreases the flood within the residential area.
- The cloudburst area is not included in a larger chain of cloudburst facilities. This means that the cloudburst area is designed to decrease the risk of flooding in the residential area without several other measures.

The selected risk zones are Furåsen, Högen, Majvallen, and Såggatan. A study visit to each risk zone was carried out on the 9th of May 2023 and images of each zone can be seen in Figures A.2, A.4, A.6, and A.8 in Appendix A. Furåsen and Högen are located outside the city center while Majvallen and Såggatan are located in the central parts of Gothenburg. In Furåsen and Högen the main building type is townhouses with gardens. Majvallen and Såggatan consist of apartment buildings and planted courtyards near or enclosed by the buildings. The apartment buildings in Majvallen have an open structure while the apartment buildings in Såggatan have an enclosed structure. In Figure 3.3, all risk zones are visualized together with the cloudburst areas recommended by Kretslopp och vatten (2021b). In the figure, additional recommendations for cloudburst facilities near the residential area are visualized as well.

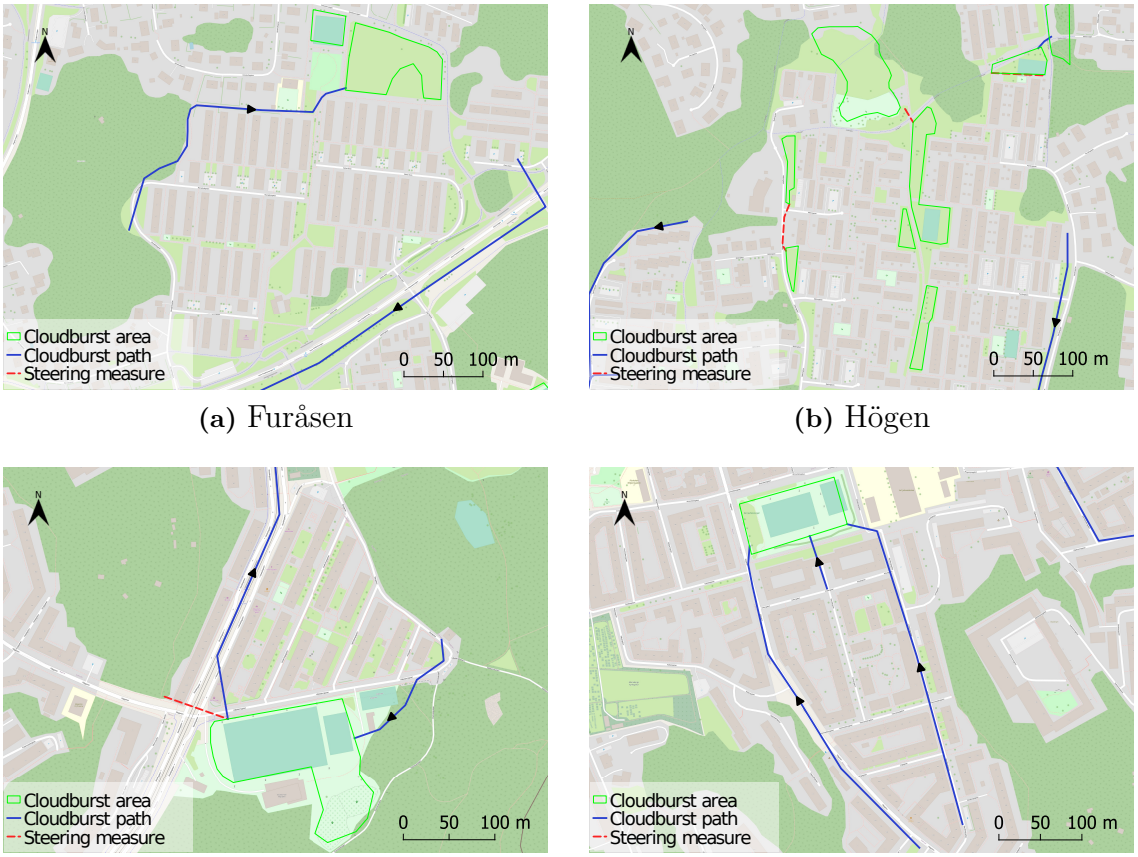

(a) Furåsen **(b)** Högen

(c) Majvallen **(d)** Såggatan

Figure 3.3: The selected risk zones with the cloudburst facilities recommended by Kretslopp och vatten (based on Kretslopp och vatten (2021b)). The legend describes the representation of cloudburst areas, paths, and steering measures.

Each risk zone has been divided into a residential area and a cloudburst area, see Figure 3.4. The residential area was determined to be all buildings close to the recommended cloudburst area where the flood decreased when implementing the cloudburst area. The decrease in flood was evaluated using the tool Vatten i Staden (2023). Further, the cloudburst areas used in this study were the ones recommended in structure plan West.

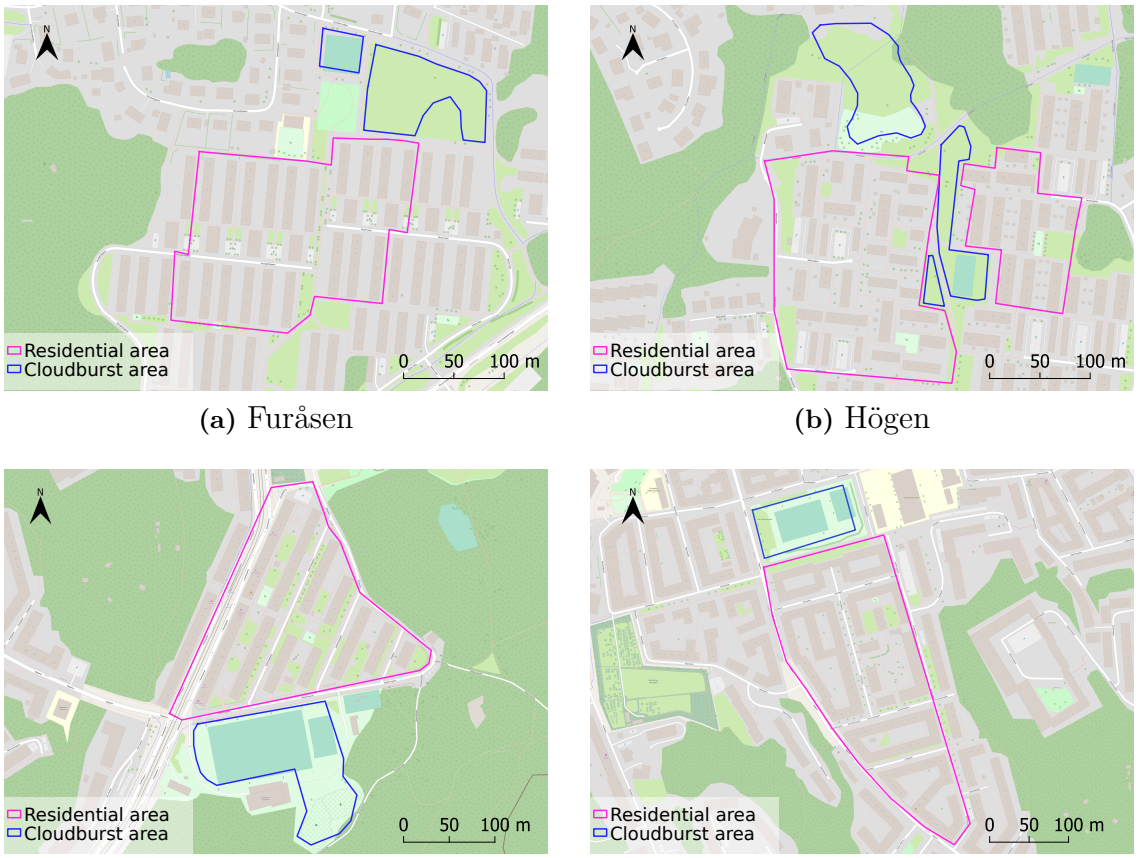

(a) Furåsen **(b)** Högen

(c) Majvallen **(d)** Såggatan

Figure 3.4: The residential (pink outlined area) and cloudburst area (blue outlined area) within each risk zone.

The size of all residential and cloudburst areas are presented in Table 3.1. The table displays similar sizes for all risk zones, however, Såggatan has the largest residential area and the smallest cloudburst area.

Table 3.1: Size of residential and cloudburst area in each risk zone.

Area	Furåsen	Högen	Majvallen	Såggatan
Residential area $[m^2]$	34924	47197	36983	50197
Cloudburst area $[m^2]$	9152	12192	14672	7264

3.3.2 Selection of site characteristics

The selection of site characteristics was determined based on the literature collected and presented in section 2.3. All characteristics that were determined to be analysed in this thesis have been identified by literature as important factors that influence urban floods. Further, these characteristics are commonly mentioned and used in flood analysis of urban areas. The selected characteristics are:

- **Topography**: Several studies state topography as one of the dominant factors influencing flooding (Huang et al., 2019; Qi et al., 2020; Walczykiewicz & Skonieczna, 2020; Zhang, 2020).
- **Infiltration**: Infiltration highly influences urban floods and is associated with the high degree of imperviousness in cities (P. Luo et al., 2022; Ren et al., 2020; Qi et al., 2020; Walczykiewicz & Skonieczna, 2020; Wang et al., 2022).
- **Sewer network**: Insufficient sewer networks increase urban floods and residential areas with combined sewer networks are more vulnerable (Evans & Orman, 2013; Jha et al., 2012; Prokić et al., 2019).

The runoff coefficient is a factor used to describe the proportion of precipitation that results in runoff (Tegelberg & Svensson, 2013). The runoff coefficient is not a site characteristic, however, a parameter used to quantify different parameters (topography, infiltration, building structure). Thus, runoff coefficients provide easily comparable results, in terms of numbers, and therefore, runoff coefficients for all risk zones were calculated.

In the following sections, the characteristics of all zones and the methodology used to calculate the runoff coefficient are described.

3.3.2.1 Topography

The elevation of the catchment areas was analysed for each risk zone. The catchment area refers to the land area from which the runoff flow towards the same direction and in this case, ends up in the risk zone. Information (e.g. area, storage capacity, land use) regarding each catchment area was gathered in Scalgo Live and a shp-file was extracted for further analyse in QGIS. The inclination of each catchment area was calculated by dividing the difference in height (m) between the highest and lowest point of each catchment area by the shortest distance (m) between the points (both measured in QGIS). Table 3.2 displays the size, depression storage capacity, and inclination for the catchment area of each risk zone. The table shows large differences between the catchment areas where Furåsen is influenced by a catchment area that is significantly larger than the other areas, however, with the smallest inclination. Further, the table shows the smallest catchment area of Såggatan. The location and topography of the catchment areas are visualized in Figures B.1 and B.2, in Appendix B.

Table 3.2: Catchment area characteristics for all risk zones.

	Furåsen	**Högen**	**Majvallen**	**Såggatan**
Area [m^2]	3590000	300000	310000	130000
Depression storage capacity [m^3]	129244	4765	783	4344
Inclination [%]	1.8	4.5	7.3	4.6

The topography within each zone was analysed using QGIS and can be seen in Figure 3.5. The common denominator for all zones is that the residential areas are

located in a depression when compared to the surroundings. The figures visualize a similar topography for Furåsen and Högen where the middle areas of each zone have the lowest elevation. In Majvallen, the residential area slopes towards the larger road on the west side, which is a low point, while Såggatan has the lowest point in the northern parts.

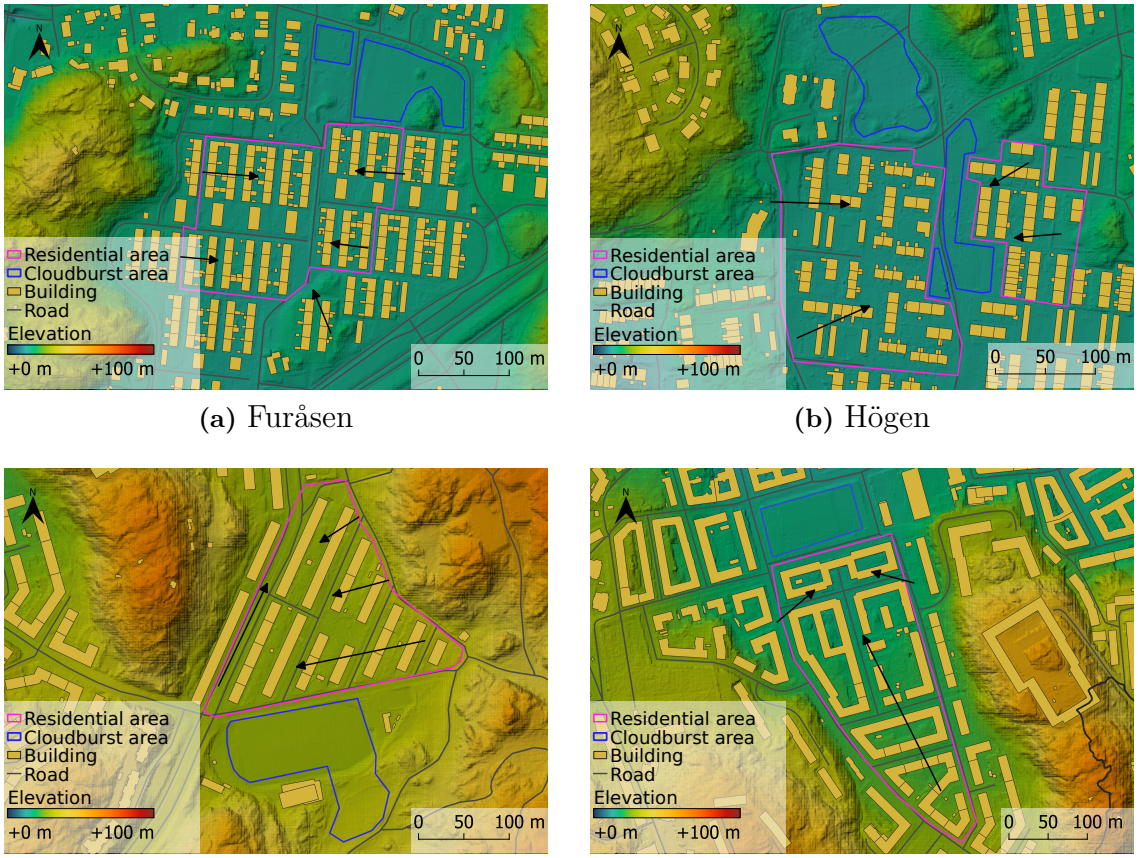

(a) Furåsen **(b)** Högen

(c) Majvallen **(d)** Såggatan

Figure 3.5: Topography for each risk zone, arrows represent water flow direction © *Lantmäteriet*. The legend describes the representation of residential areas, cloudburst areas, buildings, and roads. Also, the color legend is used to describe elevation reaching from +2 m (blue) to +100 m (red).

In Figure 3.5 it is visualized that the proposed cloudburst areas in Furåsen and Högen (today larger grass areas) are situated upstream of the residential area. The topographical characteristics imply that runoff from northern upstream areas will pass the grass areas before entering the residential areas. Both Furåsen and Högen have the lowest elevation in the middle of the residential areas, and in Högen an additional cloudburst area is located here. This implies that the runoff entering the residential area of Högen will end up in this cloudburst area if it can flow unhindered.

Majvallen is surrounded by steep areas with slopes directed against the zone in almost all directions, see Figure 3.5. In the figure, it is visualized that the proposed cloudburst area (today a soccer field) in Majvallen is located upstream of the res-

idential area. The soccer field should therefore reduce the runoff flowing from the southern areas into the residential area. However, runoff from the southeastern and eastern areas will most likely end up in the residential area. The road west of the residential area is lower elevated than the residential area and will therefore hinder runoff from entering the residential area.

The recommended cloudburst area (today a soccer field) at Såggatan is located downstream of the residential area. The topography in Figure 3.5 implies that runoff from all parts of the residential area will flow towards the soccer field. However, one building that extends over the entire area in the opposite direction from the inclination of the risk zone is visualized in Figure 3.5 and this building will hinder the runoff. The building was visited during the study visit where an opening in the middle of the apartment building was observed, hence runoff will be able to flow through the building, see Figure A.8 in Appendix A. The residential area in Såggatan is on the east side surrounded by higher elevated areas with slopes directed against the residential area. Runoff from these areas will most likely end up in the residential area since there is no upstream grass area that can reduce the runoff.

The inclination of each risk zone was calculated using the same methodology as for the catchment areas and is presented in Table 3.3.

Table 3.3: The inclination of each risk zone.

	Furåsen	**Högen**	**Majvallen**	**Såggatan**
Inclination [%]	1.0	1.4	2.8	2.6

Depressions larger than 20 m^3 within each risk zone were evaluated in Scalgo Live. The information was exported to and illustrated in QGIS and could be obtained in Figure 3.6. The figure shows that a large part of the residential areas in especially Såggatan but also Högen are depressions. For Högen, the upstream grass area is also a depression. Furåsen has depressions in some parts of the upstream grass area and in the middle of the residential area. In Majvallen the figure shows no depression in the upstream soccer field and just smaller ones in the residential area.

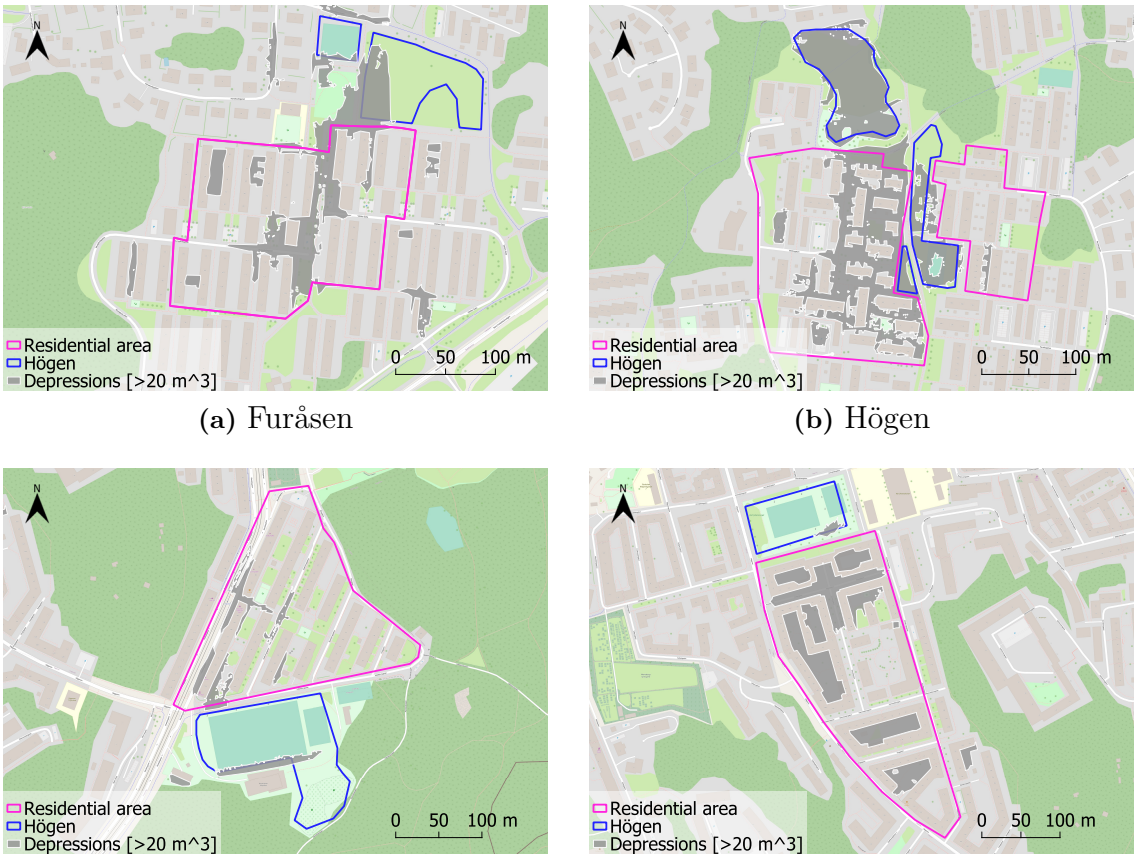

(a) Furåsen **(b)** Högen

(c) Majvallen **(d)** Såggatan

Figure 3.6: Depressions (volume $> 20\ m^3$) within each risk zone © *Lantmäteriet*. The legend describes the representation of residential areas, cloudburst areas, and depressions.

3.3.2.2 Infiltration

The land covers in the catchment areas, risk zones, and residential areas were analysed. For the catchment areas, the amount of impermeable areas were extracted from Scalgo Live. For the risk zones and residential areas, the analyses were performed by observing the infiltration parameters used in the model. For both the risk zones and residential areas, the area that was classified as impermeable in the model where divided by the total area, and by this, the percentage of impermeable land cover in each area was calculated. The percentages of impermeable land cover in the catchment areas, risk zones, and residential areas are presented in Table 3.4.

Table 3.4: Percentage of impermeable land cover in the catchment areas, risk zones, and residential areas for each risk zone.

Impermeable land cover	Furåsen	Högen	Majvallen	Såggatan
Catchment area [%]	36	37	19	50
Risk zone [%]	62	49	77	78
Residential area [%]	83	67	80	84

The results in Table 3.4 show the largest percentage of impermeable areas for Såggatan considering all areas. All zones show a similar trend where the catchment area has the lowest percentage of impermeable areas while the residential areas have the highest.

3.3.2.3 Runoff coefficient

The runoff coefficient, φ, is a factor used to quantify the proportion of precipitation that results in runoff (Tegelberg & Svensson, 2013). The coefficient depends on evaporation, infiltration, and retention and is dependent on spatial characteristics (Hayes & Young, 2005). The runoff coefficient is a unitless factor with a ratio of 0-1 where 0 implies no runoff and 1 indicates that all rain falling over the area will generate runoff (Hayes & Young, 2005). In this thesis, three runoff coefficients were calculated for both the total and catchment area of each zone. First, a coefficient for short-term precipitation (φ_{short}) was estimated by using the recommendations given in Svenskt Vatten (2016). Thereafter, runoff coefficients for 10- and 100-year rain (φ_{10y} and φ_{100y}) were calculated based on recommendations provided in Tegelberg & Svensson (2013).

Svenskt Vatten has defined standard values for the runoff coefficient for short-term rains based on land use and topography, see Table C.1 in Appendix C (Svenskt Vatten, 2016). For areas that include different land use or topography, it is possible to calculate a comprehensive runoff coefficient by dividing a large area into smaller areas. This can be done by using Equation 3.1 together with the values presented in Table C.2 in Appendix C (Svenskt Vatten, 2016).

$$\varphi = \frac{A_1\varphi_1 + A_2\varphi_2 + ... + A_i\varphi_i}{A_1 + A_2 + ... + A_i} \tag{3.1}$$

A_i: Catchment area for the limited area [ha]
φ_i: Runoff coefficient for each limited area [-]

For the calculation of φ_{short}, the residential areas and recommended cloudburst areas were analysed separately, and summarized using Equation 3.1. The residential areas within each zone were defined as either open construction (Majvallen), closed construction with vegetation (Såggatan), or townhouses (Furåsen and Högen), see Table C.1. In Table C.1, the coefficient differs depending on the steepness, and following the inclinations presented in Table 3.3 Furåsen was considered as flat, Högen as slightly steep, and Majvallen and Såggatan as steep. Further, all recommended cloudburst areas were defined as cultivated land, grass area etcetera, see Table C.2. In Såggatan, the cloudburst area consists of an artificial turf soccer plan though, however, a stormwater investigation performed by Sweco (Berntzon, 2019) defines the runoff coefficients of artificial turfs as 0.1. The runoff coefficients for the catchment areas were calculated using the areas of different land uses provided in Scalgo Live and the coefficients in Table C.2.

The φ_{10y} and φ_{100y} were estimated to enable an understanding of the increase in the generation of runoff for cloudburst events. The runoff coefficient for permeable areas increases during long and/or more intensive rains due to reduced infiltration capacity according to Svenskt Vatten (2016). To consider the reduced infiltration capacity during cloudburst events, a German methodology, included in Tegelberg & Svensson (2013), was used. The methodology includes the ratio of impermeable area (%), the gradient of the area (%), and the rain intensity (l/(s · ha)) to estimate the runoff coefficient. The graphs used for this methodology can be seen in Figure C.1 in Appendix C. The inclinations and imperviousness used as input to the graphs are presented in Tables 3.2, 3.3, and 3.4. Further, the rain intensities for both return periods were calculated by Equation 2.1 and using a duration of 30 minutes.

3.3.2.4 Sewer network

The sewer network for each zone was extracted from the model and is illustrated in Figure 3.7. The figure shows the stormwater manholes and the pipe network. All zones except Majvallen contain a separated network, displayed as a stormwater network in the figure, while Majvallen contains both combined and separated networks.

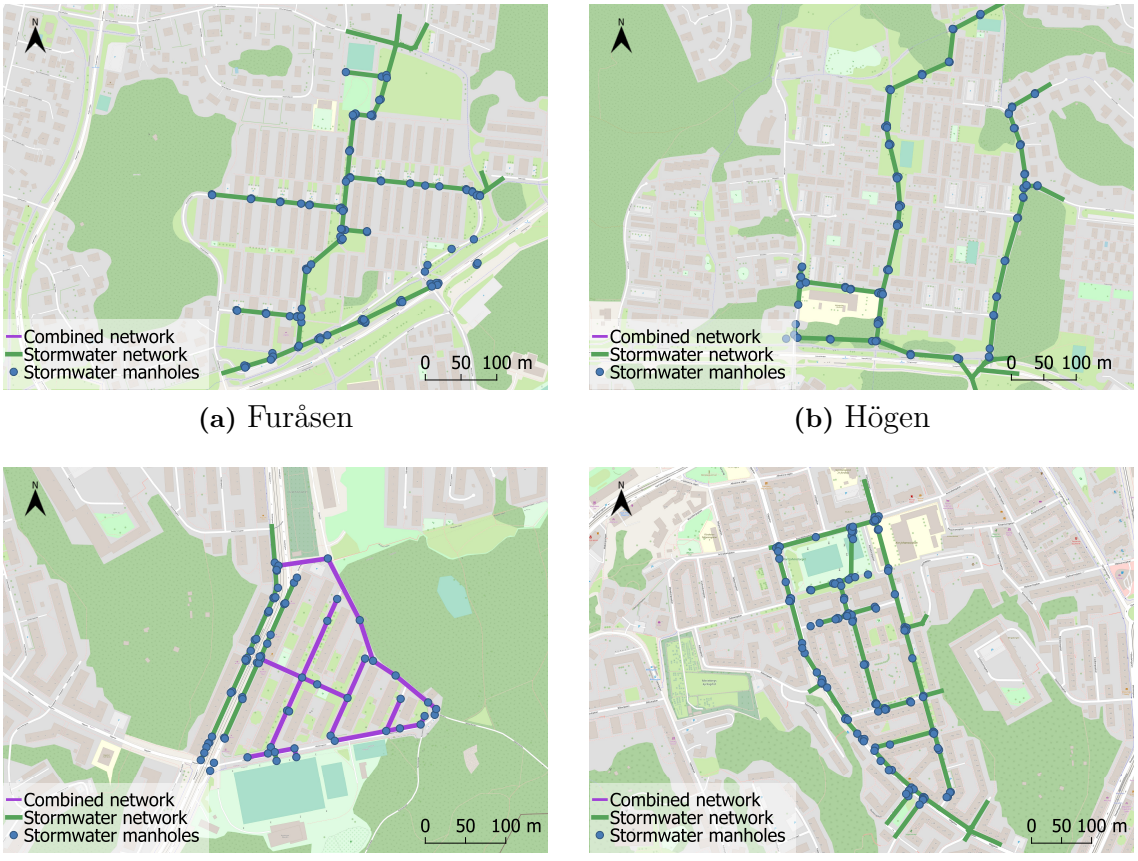

(a) Furåsen **(b)** Högen

(c) Majvallen **(d)** Såggatan

Figure 3.7: The sewer network in each risk zone. The legend describes the representation of the manholes and sewer networks based on the type of system. *(Published with approval from C. Karlsson DHI and D. Karlsson Kretslopp och vatten.)*

Figure 3.7 only includes the public network since this is the network included in the model. During the study visit to all risk zones, several additional manholes were identified for all risk zones. For instance, in the model, Högen includes just one pipe in the middle of the risk zone but in reality, several manholes were observed within the blocks of the residential area which most likely are connected to the pipe.

3.4 Modeling in MIKE+

To develop the tool, different rain events have been modeled in MIKE+. The model that was used in this study was originally developed by DHI and modified for this study. In the following sections, the original model is described followed by an explanation of the modifications for the purpose of this study.

3.4.1 Original model from DHI

The original model was built in 2020 in MIKE 21 FM, and MIKE Urban and was used to construct structure plan West (number 13 in Figure 3.2). The model was designed as a coupled 1D/2D model where the collection system was defined by a 1D network and the overland by 2D grids ($4 \cdot 4\ m^2$) (Kretslopp och vatten, 2021a). The collection system was based on the existing network, distributed by the City of Gothenburg, consisting of stormwater, wastewater, and combined sewer networks (Kretslopp och vatten, 2021a). The 2D domain (topography) was based on a topography model that was established in 2017 by height-scanning conducted by the City of Gothenburg (Kretslopp och vatten, 2021a). By using the grids in the 2D domain, hydrodynamic processes such as surface runoff, infiltration, and rain intensity were included in the model (Kretslopp och vatten, 2021a). The infiltration capacity was determined based on soil properties and land use and defined by porosity, soil thickness, initial water content, infiltration rate, and leakage rate (Kretslopp och vatten, 2021a). The porosity and soil thickness were fixed values and permitted an infiltration capacity of 120 mm excluding the initial water content. The infiltration and leakage rate were also fixed values and dependent on the soil properties. The initial water content was not fixed and depended on both soil properties and rain intensity.

To develop structure plan West, a 100-year rain with a climate factor of 1.2 was modeled. The 100-year rain was a CDS rain with a duration of six hours. The CDS rain was divided into three phases with varying rain intensities: pre-rain, peak-rain, and post-rain (Kretslopp och vatten, 2021a). The simulation was conducted in two steps:

- **Initial simulation**: In the initial simulation, the 1D network and the pre-rain were included. The simulation was made to represent the conditions in the sewer network due to the pre-rain and resulted in a hotstart file (DHI, 2023a).
- **Main simulation**: The main simulation included the coupled 1D/2D model and both the peak- and post-rain. Further, the simulation included the hotstart file created in the initial simulation and thereby, a representation of the

filling degree within the sewer network due to the pre-rain. From the main simulation, two result files were generated, one containing the maximum values, and one containing a dynamic representation of the results over the simulated time. The result files included for instance depth and flow intensity.

A conceptual model of the simulation setup with the rain phases and simulation steps is displayed in Figure 3.8.

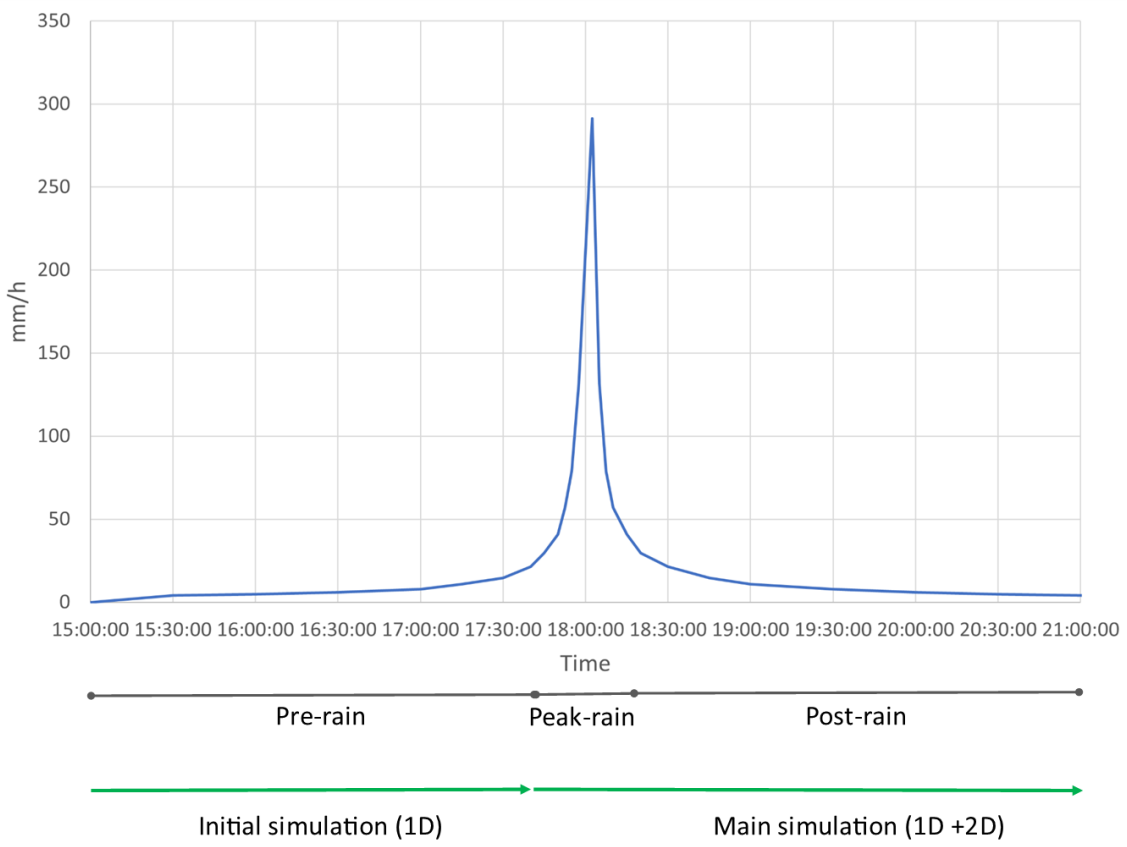

Figure 3.8: The simulation setup used in the original model with the rain intensities (mm/h) for each time step used for the simulation of the 100-year CDS rain (climate factor 1.2) (based on Kretslopp och vatten (2021c)). The figure also includes the division of the rain event and the two steps used for the simulation.

3.4.2 Simulations conducted in this thesis

The original model created by DHI was converted from MIKE21 FM and MIKE Urban to MIKE+ in this study. The MIKE+ model was a coupled 1D/2D model and included structure plan West. The following sections include descriptions of the different simulations, the modifications made to the model, and the model uncertainties.

3.4.2.1 Selection of simulations

In this study, eleven simulations were modeled. Each simulation represented a return period (T) and was simulated either with or without cloudburst areas. Ten of the simulations were used to develop the tool and did not include the cloudburst area (the current situation). The last simulation was used to analyse the improvement due to the implementation of cloudburst areas and, hence, included the recommended cloudburst areas (the future situation). An overview of the simulations is visualized in Table 3.5.

Table 3.5: The modeled simulations for each situation. All return periods (T) are simulated with $c_f = 1.2$.

Situation	**Description**	**Return period T [years]**
Current	Without cloudburst areas	10, 20, 30, 40, 50, 60, 70, 80, 90, 100
Future	With cloudburst areas	100

The interval of simulations used to develop the tool was selected based on the structure plans and guidance from DHI and Kretslopp och vatten (C. Karlsson & D. Karlsson, personal communication, February 16, 2023). A 100-year rain (climate factor 1.2) was determined to be used as the maximum return period since this is the return period evaluated in the structure plans. A 10-year rain (climate factor 1.2) was determined to be used as the minimum return period. Ten simulations within the selected interval were considered a sufficient number of simulations to evaluate the relation between flooded volume and rain return period. In addition, the number of ten simulations provided an evenly distributed range of T.

3.4.2.2 Modifications made in the original model

The same simulation setup as in the original model (initial and main simulation) was used in this study, see Figure 3.8. Modifications were made in the input data and differed between the two situations (current and future).

The modifications made in the model to simulate the current situation were related to the different return periods. For each return period, an associated rain load was used and represented by a CDS rain with a duration of six hours and a climate factor of 1.2. The rain loads were calculated based on the recommendation in *P104* provided by Svenskt Vatten (2011) and are presented in Table D.1 in Appendix D. The rain loads were used as boundary conditions and assigned in two different parts in the model setup:

- **Boundary conditions**: The rain load was inserted as a time series for the full duration.
- **2D precipitation**: The total pre-rain load was assigned to all grids to describe the water depths due to the pre-rain. The total pre-rain load for each return period is presented in Table D.2 in Appendix D.

Further, the rain loads for each return period were used to calculate the initial water content for different soil types using an Excel sheet provided by DHI. The initial water contents for different soil types were assigned as boundary conditions to each grid in the tab *2D infiltration*. The initial water contents for each of the simulations are presented in Table D.3 in Appendix D.

The simulation of the future situation only included a 100-year rain, equal to the original model, and thereby no modifications associated with the rain loads were required. However, modifications were made to the topography defined in the 2D domain. The topography was adjusted by lowering the surface of each cloudburst area within the risk zones to an infinite depth using MIKE Zero (a complementary software to MIKE+, developed by DHI). By using infinite depths, the cloudburst areas are assigned to be able to store all water that can enter the cloudburst area.

3.4.2.3 Model uncertainties

The original model was used to simulate a 100-year rain and has been calibrated in comparison to rain events of a similar magnitude (Kretslopp och vatten, 2021a). No calibration has been conducted for rain events from return periods smaller than 100 years and hence, there are uncertainties regarding the accuracy of the results when modeling these scenarios. The uncertainties are associated with infiltration capacity, sewer network capacity, and manhole placements and increase for return periods with rain loads that approach the infiltration and sewer network capacity (Kretslopp och vatten, 2021c). By that, the model uncertainties increase when the rain intensity decrease.

The model that has been used is a complex and large model, depending on a major amount of input data and settings. The model has been failing during some simulations, especially for high return periods with large rain loads. These simulations have therefore been simulated several times, without changing any settings or input data, until the whole simulation was finished. Consequently, there are uncertainties considering the model since the exact same simulation both failed and finished. Further, different simulations have been conducted on two different computers with different data performances and this is assumed to create variance within the results.

During this thesis, two limitations have been identified in the model. First, simplifications consider the representation of manholes within all risk zones. During the study visit, the locations of manholes in the model were compared to the manholes observed at the risk zones, and several manholes were identified to be excluded from the model. This affected the sewer network capacity in the model, and hence, the magnitude of floods within the residential areas. Secondly, the representation of one of the apartment buildings located in Såggatan. For this apartment building, an opening that would allow for water to flow downstream has been excluded from the model. This influenced the magnitude of floods within the residential area in Såggatan.

3.5 Analysis

Several steps of processing and analyzing were required to develop the tool from the results provided in the modeling. An overview of the structure of the analysis and the content within each section is presented in the following list:

- **Selection of results**: This section includes a description of the selection of results to use and also, the definition of flood used in this thesis.
- **Extraction of depth, $d_{\geq 0.2m,T}$ and d_T**: In this section, the methodology used to extract the depths from the simulations in MIKE+ is described.
- **Calculation of flooded volume, $V_{d\geq 0.2m,T}$ and $V_{tot,T}$**: In this study, two types of volumes were calculated. In this section, the methodology used to calculate these volumes is described.
- **Calculation of $R_{1,T}$ and $R_{2,T}$**: In this section, the variable $R_{1,T}$ and $R_{2,T}$ is described together with the methodology used to calculate these. $R_{1,T}$ was the variable used to develop the tool, and $R_{2,T}$ was the variable used for further understanding of the flooded volume.
- **Development of tool**: This section includes a description of the methodology used to develop the tool. This includes the development of one graph for each risk zone based on $R_{1,T}$, analyse of the graphs, and the development of the tool.

3.5.1 Selection of results

To be able to develop the tool, it was required to determine the definition of flood to be used. The flood definition was determined in collaboration with DHI and Kretslopp och vatten, and was influenced by the definition of flood used in the structure plans in Gothenburg (Kretslopp och vatten, 2021c, 2021b). In the structure plans, floods are divided by depth and location, and floods with depths above or equal to 0.2 m, either close to a building or on an asphalt surface, are considered unwanted (Kretslopp och vatten, 2021c). Following this, the results used to develop the tool were floods with depths above or equal to 0.2 m in the residential areas, thereby close to buildings. In this study, these floods were described by two variables: depth $d_{\geq 0.2m,T}$ and volume $V_{d\geq 0.2m,T}$. To enable an evaluation of the cloudburst areas, the total floods (i.e. with all depths) in the cloudburst areas were included in the analysis. Further, the total floods were used to evaluate the flood characteristics within each residential area. The total floods were also described by two variables: depth d_T and volume $V_{tot,T}$. Further, the maximum flow intensity $FI_{max,T}$ was included in the analysis to visualize the flow paths within each risk zone.

From the volumes, two ratios were calculated for all residential areas for all return periods T for the current situation. The ratio between $V_{d\geq 0.2m,T}$ and $V_{d\geq 0.2m,100}$ was named $R_{1,T}$ and was included in the development of the tool. The ratio between $V_{d\geq 0.2m,T}$ and $V_{tot,T}$ was named $R_{2,T}$. and was not included in the development of the tool but included in the analysis.

For this thesis, only the maximum values for floods were considered, hence the result files with maximum values from the simulations were used. Further, the volumes, depths, and flow intensities were analysed for both the current and future situations while the ratios only were calculated for the current situation. The different variables included in the analysis of the current and future situations are summarized and visualized in Table 3.6 together with a description.

Table 3.6: Description of the variables used to describe the results. All variables except $R_{1,T}$ and $R_{2,T}$ were analysed for both current and future situations. The ratios were calculated for the current situation.

Variable	Description	Unit	Area	Simulations	Collected by
$FI_{max,T}$	Flow intensity	$m^3/s/m$	R/C	R: T=10&100 C: T=10&100	Result file
$d_{\geq 0.2m,T}$	Average depth $\geq$ 0.2 m	m	R	T=10-100	Extraction
d_T	Average depth	m	R/C	R: T=10-100 C: T=100	Extraction
$V_{d\geq 0.2m,T}$	Volume with depth $\geq$ 0.2m	m^3	R	T=10-100	Calculated from $d_{\geq 0.2m,T}$
$V_{tot,T}$	Total volume	m^3	R/C	R: T=10-100 C: T=100	Calculated from d_T
$R_{1,T}$	$V_{d\geq 0.2,T}/V_{d\geq 0.2,100}$	-	R	T=10-100	Calculated from $V_{d\geq 0.2,T}$
$R_{2,T}$	$V_{d\geq 0.2,T}/V_{tot,T}$	-	R	T=10-100	Calculated from $V_{d\geq 0.2,T}$ & $V_{tot,T}$

C=Cloudburst area, R=Residential area, T=Return period [years]

3.5.2 Extraction of depth, $d_{\geq 0.2m,T}$ and d_T

The results from MIKE+ were processed using MIKE Zero. The model included the entire structure plan West, and hence, it was required to limit the results to the selected risk zones. Therefore, a selection was constructed for each residential area and each cloudburst area within the risk zones. The selections were created by importing shp-files of each area (created in QGIS) into MIKE Zero. By the development of selections, it was possible to evaluate the results within each specific area separately. The $d_{\geq 0.2m,T}$ and d_T were extracted from the result files by using these selections.

The depth ($d_{\geq 0.2m,T}$) was extracted for all residential areas in each simulation (both for the current and the future situation). In the residential area, all grids with depths $\geq$ 0.2 m were selected, and the average depth of these grids was extracted as $d_{\geq 0.2m,T}$.

The depth (d_T) was extracted for all residential areas for each simulation for the current situation and for all cloudburst areas for the 100-year rains simulations for

both current and future situations. This depth was extracted following the same methodology as for $d_{\geq 0.2m,T}$, however, the average of all depths was used.

3.5.3 Calculation of flooded volume, $V_{d\geq 0.2m,T}$ and $V_{tot,T}$

The flooded volume $V_{d\geq 0.2m,T}$ was calculated for all residential areas, for each simulation of both current and future situations. The volume was calculated by the depth ($d_{\geq 0.2m,T}$), the number of grids with depths $\geq$ 0.2 m ($n_{d\geq 0.2m,T}$), and the area of the grids (A_{grid}) that were used in the model ($4 \cdot 4\ m^2$) by using Equation 3.2.

$$V_{d\geq 0.2m,T} = d_{\geq 0.2m,T} \cdot n_{d\geq 0.2m,T} \cdot A_{grid} \tag{3.2}$$

$V_{d\geq 0.2m,T}$: Flood volume with depths $\geq$ 0.2 m for a T-year rain $[m^3]$
$d_{\geq 0.2m,T}$: Average depths $\geq$ 0.2 m for a T-year rain $[m]$
$n_{d\geq 0.2,T}$: Number of grids with depths $\geq$ 0.2 m for a T-year rain $[-]$
A_{grid}: Area of grids ($4 \cdot 4\ m^2$) $[m^2]$
T: Rain return period $[year]$

The total volume ($V_{tot,T}$) was calculated for all residential areas for each simulation for both current and future situations and for all cloudburst areas for the 100-year rain simulations for both the current situation and future situation. The total volume ($V_{tot,T}$) was calculated by the depth (d_T), the number of grids with a flood (n_T), and the area of the grids (A_{grid}) by using Equation 3.3.

$$V_{tot,T} = d_T \cdot n_T \cdot A_{grid} \tag{3.3}$$

$V_{tot,T}$: Total flood volume (all depths) for a T-year rain $[m^3]$
d_T: Average depth for a T-year rain $[m]$
n_T: Number of grids with flood for a T-year rain $[-]$
A_{grid}: Area of grids ($4 \cdot 4\ m^2$) $[m^2]$
T: Rain return period $[year]$

3.5.4 Calculation of $R_{1,T}$ and $R_{2,T}$

The ratios $R_{1,T}$, and $R_{2,T}$ were calculated for all the residential areas, for each T for the current situation. The ratio $R_{1,T}$ was calculated by $V_{d\geq 0.2m,T}$ and $V_{d\geq 0.2m,100}$, see Equation 3.4. This enabled a comparison of $V_{d\geq 0.2m,T}$ for different return periods, regardless of the size of the risk zone and the flood volume.

$$R_{1,T} = \frac{V_{d\geq 0.2m,T}}{V_{d\geq 0.2m,100}} \tag{3.4}$$

$R_{1,T}$: Ratio [-]
$V_{d\geq 0.2m,T}$: Flood volume with depths $\geq$ 0.2 m for a T-year rain $[m^3]$
$V_{d\geq 0.2m,100}$: Flood volume with depths $\geq$ 0.2 m for a 100-year rain $[m^3]$
T: Rain return period $[year]$

The ratio $R_{2,T}$ was calculated by $V_{d\geq 0.2m,T}$ and $V_{tot,T}$, see Equation 3.5.

$$R_{2,T} = \frac{V_{d\geq 0.2m,T}}{V_{tot,T}} \tag{3.5}$$

$R_{2,T}$: Ratio [-]
$V_{d\geq 0.2m,T}$: Flood volume with depths $\geq$ 0.2 m for a T-year rain $[m^3]$
$V_{tot,T}$: Total flood volume (all depths) for a T-year rain $[m^3]$
T: Rain return period $[year]$

3.5.5 Methodology to develop the tool

To develop the tool, ten $R_{1,T}$ (one for each return period) were calculated for each risk zone. These were plotted as points in a diagram. Thereafter, a trend line was created for each risk zone by interpolating the points in Excel. For the interpolation, the trend line with the highest coefficient of determination, a.k.a R^2, was selected for each risk zone separately. R^2 is defined as the measure of the variation of dependent variables (Chicco et al., 2021), and a high R^2 indicates low variation. Table 3.7 describes the function for the graphical representation used for each risk zone together with R^2.

Table 3.7: Functions for the graphical representation and corresponding R^2, for each risk zone.

Risk zone	**Function**	R^2
Furåsen	Power	0.998
Högen	Polynomial of second degree	0.999
Majvallen	Polynomial of second degree	0.998
Såggatan	Power	0.996

The four graphs were all plotted in one diagram. By using $R_{1,T}$ for developing the graphs, the graphs approached each other for higher return periods, since $R_{1,100}$ is 100% for all risk zones. Thereby, an analysis of the similarities and dissimilarities between the risk zones was conducted for lower return periods and especially focused on $R_{1,10}$. The lower ratios were compared along with an evaluation of the

site characteristics for all risk zones. Modeling uncertainties were also included in the evaluation. By this analysis, the risk zones with similar $R_{1,T}$, and site characteristics were determined to be included in the development of the tool. The tool was developed by plotting the ratios from the selected risk zones in one diagram. From the ratios, an interpolated trend line was created by a polynomial equation of the third degree since this received the highest R^2. The equation describes $R_{1,T}$ in relation to T and is the basis of the tool, see the yellow line (A) in Figure 3.9.

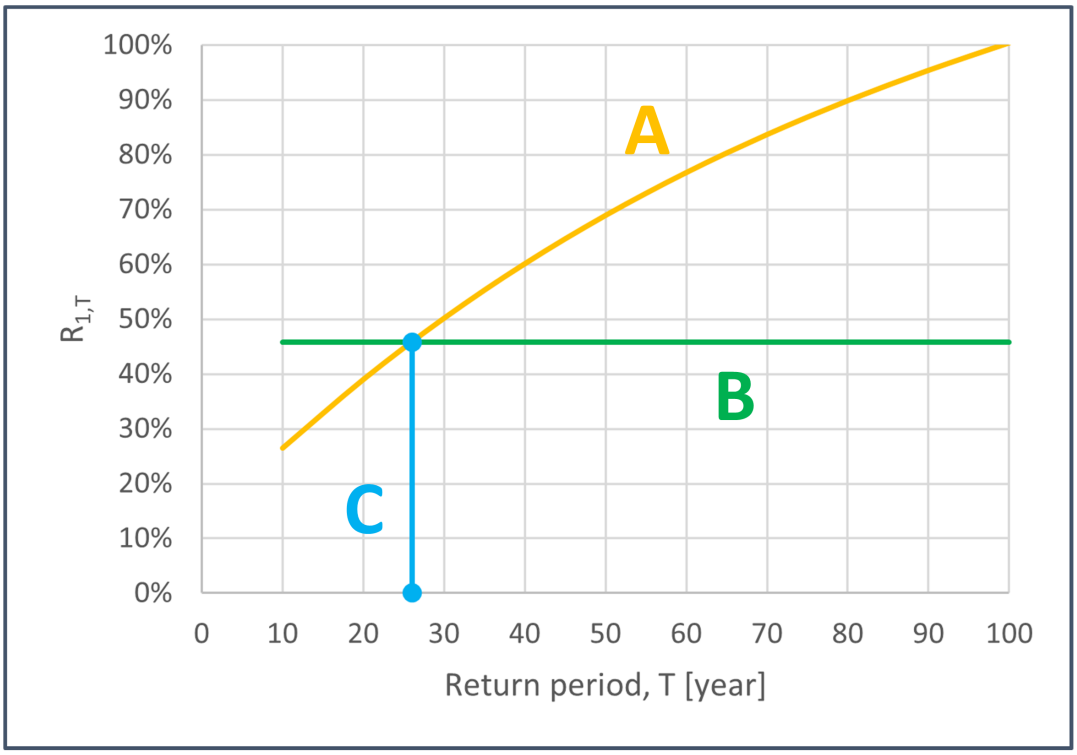

Figure 3.9: A conceptual model of the tool where (A) represents $R_{1,T}$, (B) represents $R_{available}$, and (C) provides the manageable T-year rain.

$R_{available}$ was included in the tool to describe the ratio between available volume for a cloudburst area ($V_{available}$) and $V_{d\geq 0.2m,100}$ in the residential area, see the green line (B) in Figure 3.9. In the tool, $R_{available}$ is calculated by Equation 3.6.

$$R_{available} = \frac{V_{available}}{V_{d\geq 0.2m,100}} \tag{3.6}$$

$R_{available}$: Ratio [-]
$V_{available}$: Available volume for a cloudburst area $[m^3]$
$V_{d\geq 0.2m,100}$: Flood volume with depths $\geq$ 0.2 m for a 100-year rain $[m^3]$

The tool was created in Excel and programmed to identify the intersection between lines A and B in Figure 3.9. The intersection is described by the blue line (C) which

provides the user with an estimated T-year rain. The estimated T describes the return period for which $V_{available}$ is equal to $V_{d \geq 0.2m,T}$. By that, the tool provides the T where no flood will occur in the residential area if implementing the cloudburst area and enabling all $V_{d \geq 0.2m,T}$ to reach the cloudburst area.

4

Results & Discussion

The following chapter includes results from the quantitative data collection conducted using MIKE+ and MIKE Zero. The chapter is divided into three sections, current situation, implementation of cloudburst area, and final tool. Additionally, this chapter will include a discussion of the results.

4.1 Current situation

The objective of this study is to develop a tool that describes the correlation between return period and flooding and that could be used in flood management considering the implementation of cloudburst areas in different residential areas. Based on the objective, the approach is to primarily evaluate the current situation (i.e. no cloudburst areas are implemented) as this is the situation analyzed when using the tool.

4.1.1 Runoff coefficients

The calculated runoff coefficients for short-term precipitation (φ_{short}) and 10- and 100-year rain (φ_{10y} and φ_{100y}) in each catchment area are presented in Table 4.1. The table visualizes the largest runoff coefficients for the catchment area of Såggatan considering all rain events. Further, the catchment area of Majvallen has the smallest φ_{short} and φ_{10y}, and Furåsen has the smallest φ_{100y}.

Table 4.1: Runoff coefficients for each catchment area, for short-term precipitation and cloudbursts with the intensities of 10- and 100-year rains (climate factor 1.2).

Runoff coefficient φ [-]	**Furåsen**	**Högen**	**Majvallen**	**Såggatan**
Short-term precipitation φ_{short}	0.32	0.29	0.17	0.42
10-years rain φ_{10y}	0.43	0.49	0.38	0.61
100-years rain φ_{100y}	0.68	0.78	0.73	0.85

The calculated φ_{short}, φ_{10y} and φ_{100y} in each risk zone are presented in Table 4.2. Similar to the runoff coefficients for the catchment areas, the largest coefficients are seen for Såggatan for all rain events, however equal to Majvallen for φ_{10y} and φ_{100y}.

For the φ_{100y} it could be seen that the values are equal for Furåsen and Högen as well.

Table 4.2: Runoff coefficients for each risk zone, for short-term precipitation and cloudbursts with the intensities of 10- and 100-year rains (climate factor 1.2).

Runoff coefficient φ [-]	**Furåsen**	**Högen**	**Majvallen**	**Såggatan**
Short-term precipitation φ_{short}	0.30	0.29	0.37	0.55
10-years rain φ_{10y}	0.55	0.52	0.76	0.76
100-years rain φ_{100y}	0.75	0.75	0.88	0.88

4.1.2 Maximum flow intensities, $FI_{max,T}$, current situation

The $FI_{max,10}$ and $FI_{max,100}$ within the surface runoff routes are presented in Figures 4.1, 4.2, 4.3 and 4.4. By a general evaluation of these results, it is stated that roads function as natural cloudburst paths. Majvallen distinguishes from the other zones with more extensive high $FI_{max,10}$.

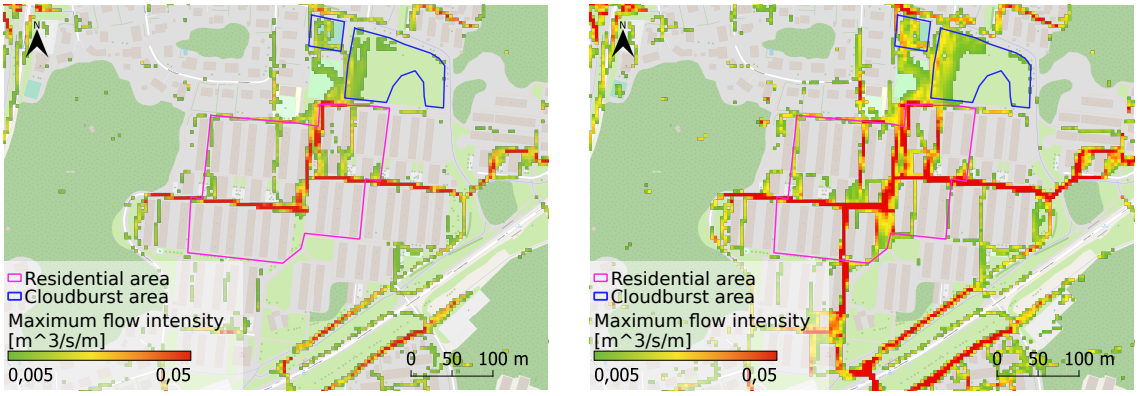

(a) $FI_{max,10}$ **(b)** $FI_{max,100}$

Figure 4.1: Maximum flow intensities during a (a) 10- and (b) 100-year rain (climate factor 1.2) in Furåsen. The legend describes the representation of residential and cloudburst areas. Also, the color scale is used to describe the flow intensities ($m^3/s/m$) from 0.005 (green) to 0.05 (red).

(a) $FI_{max,10}$ **(b)** $FI_{max,100}$

Figure 4.2: Maximum flow intensities during a (a) 10- and (b) 100-year rain (climate factor 1.2) in Högen. The legend describes the representation of residential and cloudburst areas. Also, the color scale is used to describe the flow intensities ($m^3/s/m$) from 0.005 (green) to 0.05 (red).

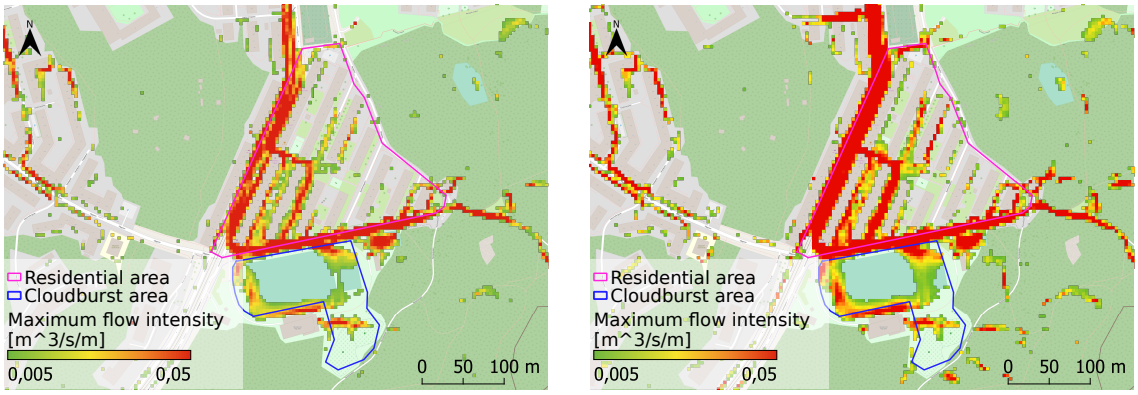

(a) $FI_{max,10}$ **(b)** $FI_{max,100}$

Figure 4.3: Maximum flow intensity during a (a) 10- and (b) 100-year rain (climate factor 1.2) in Majvallen. The legend describes the representation of residential and cloudburst areas. Also, the color scale is used to describe the flow intensities ($m^3/s/m$) from 0.005 (green) to 0.05 (red).

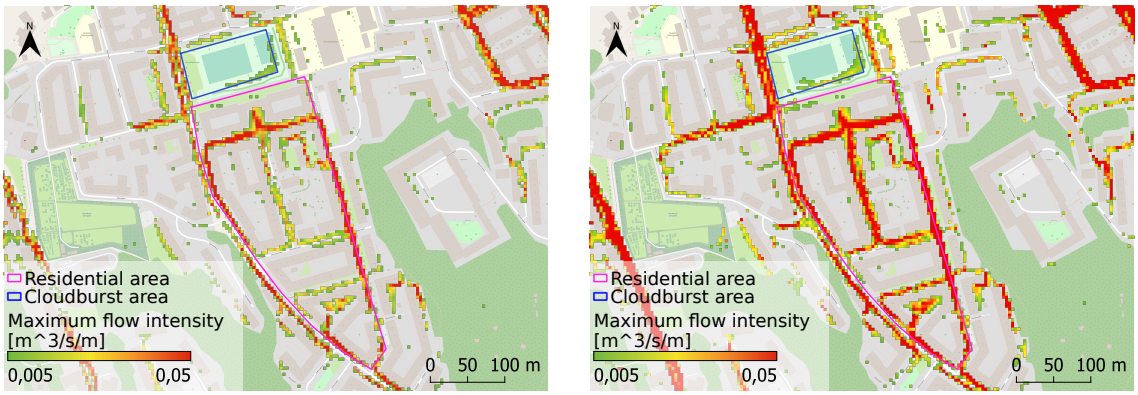

(a) $FI_{max,10}$ **(b)** $FI_{max,100}$

Figure 4.4: Maximum flow intensity during a (a) 10- and (b) 100-year rain (climate factor 1.2) in Såggatan. The legend describes the representation of residential and cloudburst areas. Also, the color scale is used to describe the flow intensities ($m^3/s/m$) from 0.005 (green) to 0.05 (red).

4.1.3 The flood in each risk zone, current situation

To enable a conceptual understanding of the flood characteristics (spread and depth) within each risk zone, the maximum flooded depths ≥ 0.2 m in the residential areas are presented in Figures 4.5, 4.6, 4.7 and 4.8. A resemblance between Furåsen, Högen, and Majvallen can be seen as the ranges of depth and spread in the zones are similar during a 100-year rain. A larger part of the upstream green areas in Furåsen and Högen are covered with water compared to Majvallen where the water is located within the residential area. At Såggatan the water accumulates in very specific locations within the residential area and no water reaches the downstream green area. The depth in Såggatan is also greater than the depth obtained for the other risk zones.

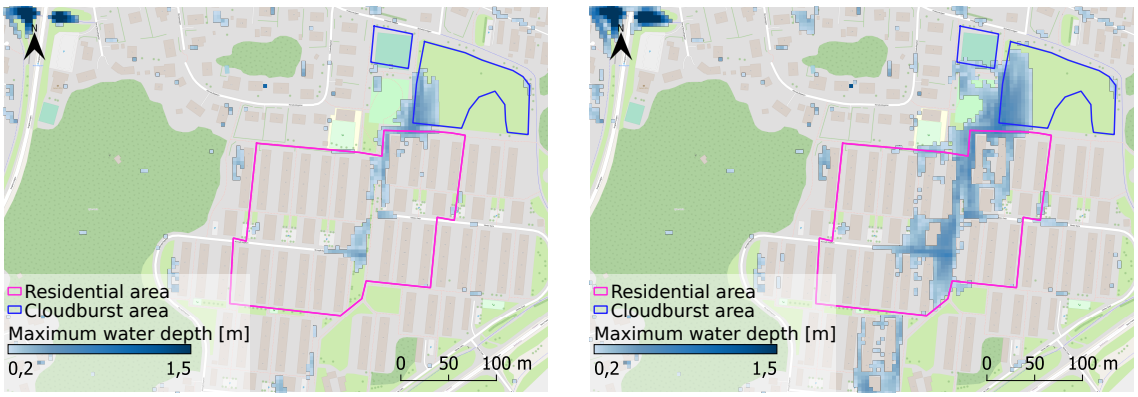

(a) T=10 years **(b)** T=100 years

Figure 4.5: Maximum flood depths ≥ 0.2 m during a (a) 10- and (b) 100-year rain (climate factor 1.2) in Furåsen. The legend describes the representation of residential and cloudburst areas. Also, the color scale is used to describe depths (m) from 0.2 (light blue) to 1.5 (dark blue).

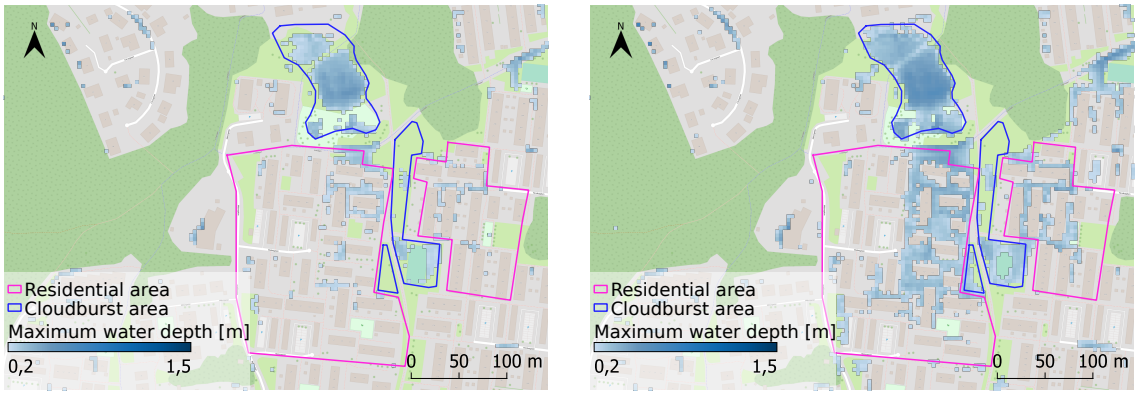

(a) T=10 years **(b)** T=100 years

Figure 4.6: Maximum flood depths $\geq$ 0.2 m during a (a) 10- and (b) 100-year rain (climate factor 1.2) in Högen. The legend describes the representation of residential and cloudburst areas. Also, the color scale is used to describe depths (m) from 0.2 (light blue) to 1.5 (dark blue).

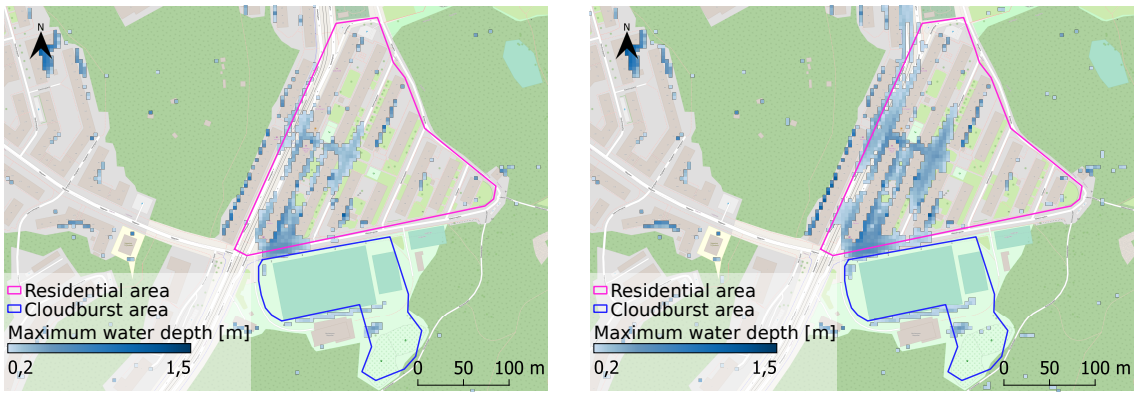

(a) T=10 years **(b)** T=100 years

Figure 4.7: Maximum flood depths $\geq$ 0.2 m during a (a) 10- and (b) 100-year rain (climate factor 1.2) in Majvallen. The legend describes the representation of residential and cloudburst areas. Also, the color scale is used to describe depths (m) from 0.2 (light blue) to 1.5 (dark blue).

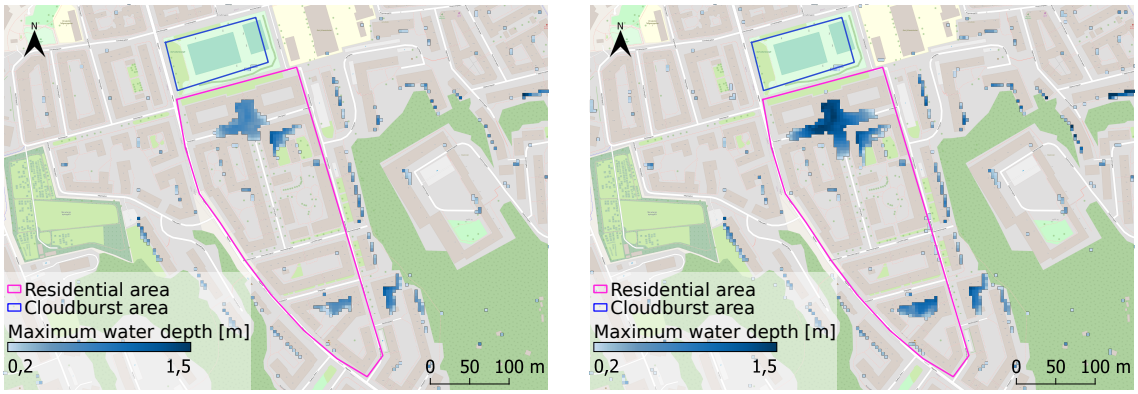

(a) T=10 years **(b)** T=100 years

Figure 4.8: Maximum flood depths $\geq$ 0.2 m during a (a) 10- and (b) 100-year rain (climate factor 1.2) in Såggatan. The legend describes the representation of residential and cloudburst areas. Also, the color scale is used to describe depths (m) from 0.2 (light blue) to 1.5 (dark blue).

4.1.4 $R_{1,T}$ for each residential area

$R_{1,T}$ is defined as the ratio between the flood volume $V_{d\geq 0.2m,T}$ for each return period (T) and $V_{d\geq 0.2m,100}$ (Equation 3.4). $V_{d\geq 0.2m,T}$ is presented in Table 4.3 for each residential area and each T.

Table 4.3: The flooded volume $V_{d\geq 0.2m,T}$ (m^3) for each risk zone and each simulated return period T (year).

	Flooded volume $V_{d\geq 0.2m}$ (m^3) for each Return period T (year)									
Risk zone	10	20	30	40	50	60	70	80	90	100
Furåsen	745	1098	1469	1636	1855	2081	2300	2464	2634	2830
Högen	860	1203	1648	1958	2243	2520	2786	2932	3102	3224
Majvallen	2002	2176	2423	2561	2724	2873	3082	3263	3442	3553
Såggatan	1844	2247	2731	2944	3210	3431	3645	3846	4076	4256

$R_{1,T}$ has been calculated for each residential area and are displayed as points in Figure 4.9. A trend line for each residential area has been established through interpolation. No general correlation between the graphs for the different residential areas can be identified since they differ considering both start value ($R_{1,10}$) and slope. However, Furåsen and Högen are approximately equivalent between $R_{1,10}$ to $R_{1,40}$ and Majvallen and Såggatan are approximately equivalent between $R_{1,40}$ and $R_{1,100}$. Further, Högen resembles Majvallen and Såggatan between $R_{1,70}$ and $R_{1,100}$.

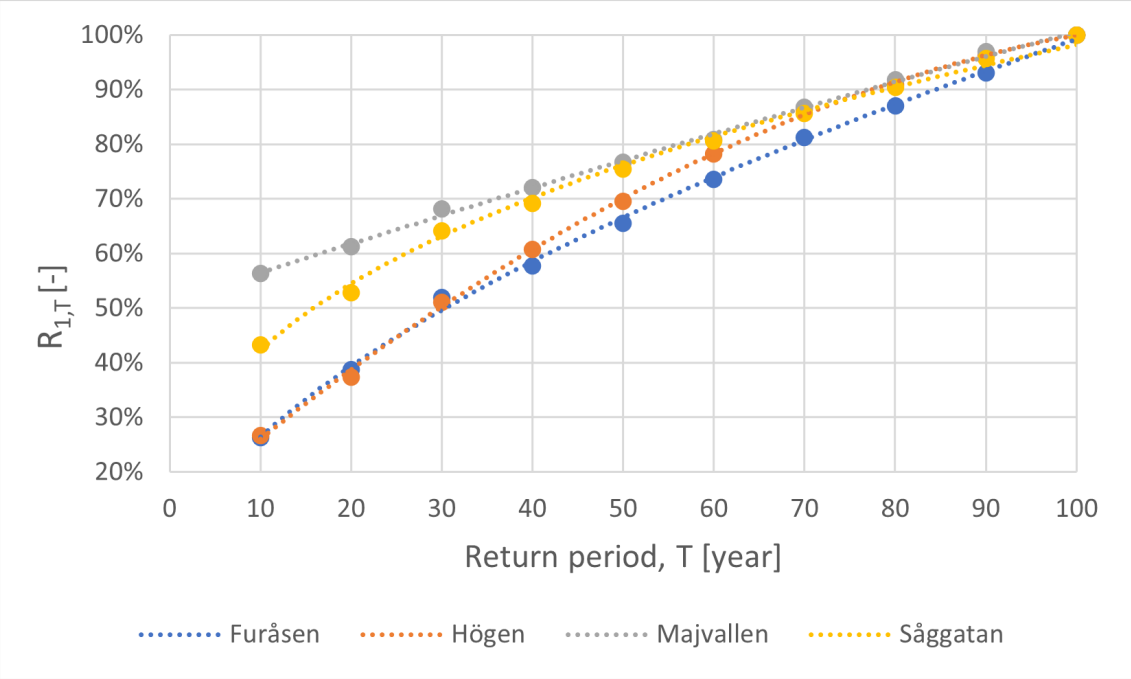

Figure 4.9: The ratio $R_{1,T}$ for each return period T and each residential area separate. Also, the interpolated trend line between the ratios of each residential area.

4.1.5 $R_{2,T}$ for each residential area

$R_{2,T}$ is defined as the ratio between the flood volumes $V_{d\geq 0.2m,T}$ and $V_{tot,T}$ for each return period (T) (Equation 3.5). $V_{tot,T}$ is visualized in Table 4.4 for each residential area and each T.

Table 4.4: The flooded volume $V_{tot,T}$ (m^3) for each risk zone and each simulated return period T (year).

	Flooded volume $V_{tot,T}$ (m^3) for each Return period T (year)									
Risk zone	10	20	30	40	50	60	70	80	90	100
Furåsen	1619	1992	2386	2573	2781	3009	3196	3362	3528	3673
Högen	2743	3037	3396	3592	3657	4017	4213	4376	4539	4670
Majvallen	3183	3344	3585	3719	3879	4013	4173	4307	4468	4575
Såggatan	2829	3198	3721	3967	4244	4490	4705	4920	5166	5351

$R_{2,T}$ has been calculated for each residential area and are presented as points in Figure 4.10. The results display similarities in slope for the graphs of Furåsen and Högen, and for Majvallen and Såggatan, respectively. The graphs for Majvallen and Såggatan display a minor increase between $R_{2,10}$ and $R_{2,100}$. This implies that a large ratio of the total floods within these residential areas has depths ≥ 0.2 m already during a 10-year rain.

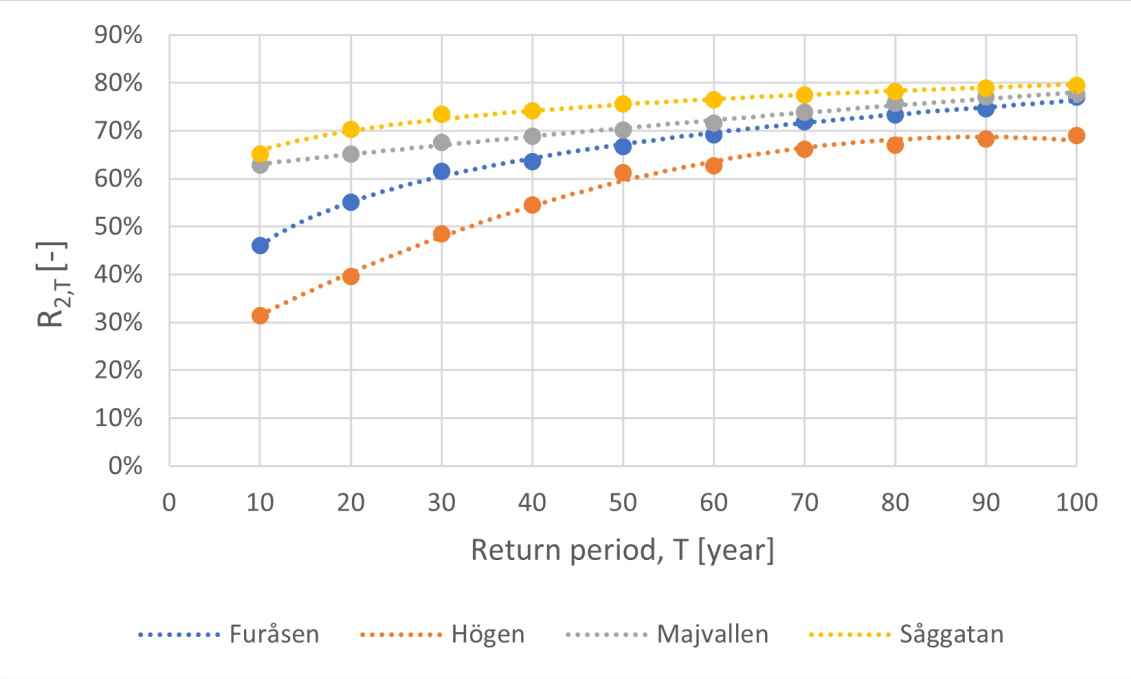

Figure 4.10: The ratio $R_{2,T}$ for each return period T and each residential area separate. Also, the interpolated trend line between the ratios of each residential area.

4.1.6 Discussion of current situation

Sections 4.1.2, 4.1.3, 4.1.4, and 4.1.5 visualized the results for the current situation, using different variables. In the following sections, these results are discussed and compared to the site characteristics described in Section 3.3.2.

4.1.6.1 Furåsen and Högen

Furåsen and Högen resemble consider most of the results for the current situation and for most of the site characteristics of the risk zones when compared to Majvallen and Såggatan. Both Furåsen and Högen have townhouses and a green area located upstream of the residential area. Additionally, both zones have a comparable topography with an inclination towards the center of the residential area. However, Furåsen and Högen differ considering the catchment areas where the catchment area for Furåsen is ten times larger than the catchment area for Högen. Additionally, the depression storage capacity in the catchment area for Furåsen is 27 times larger than in the catchment for Högen. The size of the catchment area for Furåsen implies that there will be a large amount of runoff into and within the risk zone. However, a lot of this runoff can be stored within the large depression storage and thereby, decrease the runoff entering the risk zone.

Runoff coefficients are numerical descriptions of the runoff within an area that encounters either land use and inclination (φ_{short}) or imperiousness, inclination, and rain intensities (φ_{10y} and φ_{100y}). By calculating these coefficients, it is thereby possible to compare all these site characteristics for different areas simultaneously. For the risk zones of Furåsen and Högen, which have comparable site characteristics, the

φ_{short}, φ_{10y}, and φ_{100y} are approximately equal. For the catchment areas, the φ_{short} are approximately equal despite the differences considering site characteristics. The φ_{10y} and φ_{100y} of the catchment areas are slightly higher for Högen, and this is due to the three times larger inclination for the catchment area for Högen compared to Furåsen.

The maximum flow intensities, $FI_{max,10}$ and $FI_{max,100}$ are the results with the most distinct dissimilarities between Furåsen and Högen. Both $FI_{max,10}$ and $FI_{max,100}$ are lower and more widespread within Högen compared to Furåsen. This is assumed to be influenced by the orientation of the buildings in the residential areas. In Högen, the buildings are oriented in various directions and therefore no major surface runoff routes are identified. Instead, the runoff is divided into several smaller runoff routes resulting in lower but more widespread flow intensities. In Furåsen, all buildings are placed in parallel resulting in few surface runoff routes with high flow intensities.

The maximum flood depths ≥ 0.2 m are overall similar for Furåsen and Högen and this is assumed to be due to the similar topography for the zones. For both zones, the water accumulates within depressions. Since both Furåsen and Högen have upstream grass areas that are depressions to some extent these operate as protective barriers for the residential areas. The depths for a 10-year rain are small within the residential areas for both risk zones and most water is accumulating in the upstream grass areas. The depths for a 100-year rain are more extensive and spread over the residential areas for both zones compared to the 10-year rain. There are dissimilarities observed between the risk zones for 100-year rain. In Furåsen, the flood accumulates in the center of the residential area and the western parts of the upstream grass area, and there is no major spreading in the residential area. For Högen, there is an accumulation of water in the grass area located upstream of the residential area and the flood within the residential area is widespread.

The results that are used to develop the tool are the $R_{1,T}$, i.e. the ratios between $V_{d\geq 0.2m,T}$ and $V_{d\geq 0.2m,100}$ for all return periods (T) and all residential areas. The $R_{1,T}$ are approximately equal between 10- and 40-year rains for Furåsen and Högen. Högen obtains higher $R_{1,T}$ for larger return periods ($T > 40$ year) compared to Furåsen, the differences are in the range of five percentage points. Further, the $R_{2,T}$ enables a comparison of the ratios between $V_{d\geq 0.2m,T}$ and $V_{tot,T}$ for all T, for the residential areas. Högen is the risk zone with the smallest $R_{2,T}$ for all T. Furåsen has the second smallest $R_{2,T}$ but the differences are quite large, indicating that the flood in Furåsen is deeper in comparison to Högen. The results are assumed to be reasonable due to the flood behavior previously described where Furåsen has a more concentrated flood. Consequently, a concentrated and deep flood results in larger $R_{2,T}$.

4.1.6.2 Majvallen

Majvallen has several site characteristics that are assumed to be beneficial considering resilience against urban floods. For instance, the residential area in Majvallen consists of apartment buildings that are built with open yards and that are directed along the flow direction. Thereby, no flow will be captured within the residential

area due to the building structure. Further, the catchment area of Majvallen has the lowest percentage of impermeable land cover, 19% in comparison with the other zones, 36% (Furåsen), 37% (Högen), and 50% (Såggatan), resulting in the lowest runoff coefficients for the catchment areas (φ_{short}, φ_{10y}, and φ_{100y}). Low runoff coefficients indicate a high reduction of the runoff in the catchment area and are thereby beneficial.

An aggravating site characteristic for Majvallen is the sewer network as 75% of the pipes in the residential area in Majvallen are combined. Areas with combined sewers are more vulnerable to flooding (Prokić et al., 2019) which is also obtained in the results as Majvallen has more extensive floods with large depths. A properly designed sewer network in Sweden shall be capable of handling a 10-year rain (MSB, 2013b). The 10-year rain simulated in this thesis has a climate factor of 1.2 which represents an 18-years rain without a climate factor. Consequently, it is realistic that flooding occurs during the 10-year rain scenario modeled. However, the $R_{1,10}$ for Majvallen is significantly higher than the $R_{1,10}$ for the other risk zones. Therefore, further analysis of the sewer system has been accomplished and this shows a complete use of the system's capacity even during a 10-year rain in the model. Consequently, the large flood in the results is due to limitations of the sewer network capacity in the model. During the study visit several manholes were observed that are not included in the model. Hence, it is not verified whether the lack of sewer network capacity in the model reflects the reality.

The maximum flow intensities, $FI_{max,10}$ and $FI_{max,100}$, for Majvallen are extensive and high compared to the other risk zones. The water enters from the upstream catchment area in the east corner of the residential area with a high flow intensity. Hence, the low runoff coefficients for the catchment area for Majvallen do not seem to reduce the flow intensities compared to the other zones. This is assumed to be due to the small depression storage capacity in the catchment area for Majvallen. Accordingly, the depression storage capacity seems to influence the runoff more than the site characteristics included in the runoff coefficients. For both the 10- and 100 year rains, the water follows the roads reaching from the east corner, via the west corner, to the north corner of the residential area. Hence, these roads operate as surface runoff routes with high $FI_{max,10}$ and $FI_{max,100}$ and surround the residential area. Further, high flow intensities are seen for both return periods for some of the roads within the residential area.

The residential area in Majvallen has few depressions. However, when comparing the location of the depressions and the flood depths it is seen that a majority of the floods in the residential area are located within these depressions and these floods have large depths during both the 10- and 100-year rain. Hence, despite the few depressions within the residential area these seem to highly influence the flood within Majvallen.

4.1.6.3 Såggatan

Figure 4.8 visualizes few but rather deep floods captured within the residential area of Såggatan, characteristics that distinguish it from the other risk zones. Further, a major part of the residential area in Såggatan has no flood during a 100-year rain which also differs in comparison to the other zones. The differences between Såggatan and the other zones are assumed to be highly influenced by the building structure. Såggatan consists of apartment buildings with closed yards that hinder water from passing to downstream areas. The building structure was initially assumed to capture water within all closed yards but this was not seen in the results.

Såggatan has several aggravating site characteristics. The risk zone has the highest percentages of impermeable surfaces considering both the catchment area, risk zone, and residential area. Consequently, the risk zone and the influencing catchment area have low infiltration capacities which increase the runoff, and results in the largest runoff coefficients (φ_{short}, φ_{10y}, and φ_{100y}) for both the catchment area and risk zone. Additionally, the soccer field in Såggatan is located downstream of the residential area instead of upstream as in the other zones and will therefore not reduce the runoff flowing from upstream areas.

Figure 4.8 visualizes a deep flood located in the downstream northern parts, hindered by an apartment building that functions as a barrier. This apartment building contains an opening in reality though. This opening was not included in the model and thereby, the results do not reflect reality. The opening is assumed to allow runoff to flow toward the recommended cloudburst area (today a soccer field), that is located downstream. Consequently, the excluded opening generates an overestimation of the flood in the results for Såggatan.

The maximum flow intensities, $FI_{max,10}$ and $FI_{max,100}$, for Såggatan are large for the surface runoff routes leading to the location of the previously mentioned flood. The topography shows that the risk zone has an inclination towards this location which also is a depression. Therefore, it is reasonable that there are large flow intensities directed toward this location. The catchment area for Såggatan has a large depression storage capacity which has been assumed to be beneficial to reduce the flow intensities. However, the catchment area is small and more or less only consists of the residential area though, and hence, a majority of these depressions are located within the residential area and result in floods.

Såggatan has the second highest $R_{1,T}$ for return periods up to 70 years. However, the $R_{1,10}$ are in between Majvallen and Furåsen and Högen and the ratios of Såggatan distinguish all the other zones. Further, Såggatan has the largest $R_{2,T}$ for all return periods, from 65% during a 10-year rain to 80% during a 100-year rain. This implies that a majority of the floods in Såggatan have depths ≥ 0.2 m.

4.2 Future situation

A simulation of a 100-year rain with implemented cloudburst areas has been accomplished to analyse how the cloudburst areas decrease the floods within the residential areas. In this section, results from this simulation are presented.

4.2.1 Maximum flow intensities, $FI_{max,T}$, future situation

$FI_{max,100}$ for each of the risk zones during the future situation are presented in Figure 4.11. The figure displays flow intensities within all cloudburst areas, however, the smallest is within the cloudburst area of Såggatan. Further in Såggatan, there are high flow intensities for the surface runoff routes leading to the depression that has a large flood during the current situation.

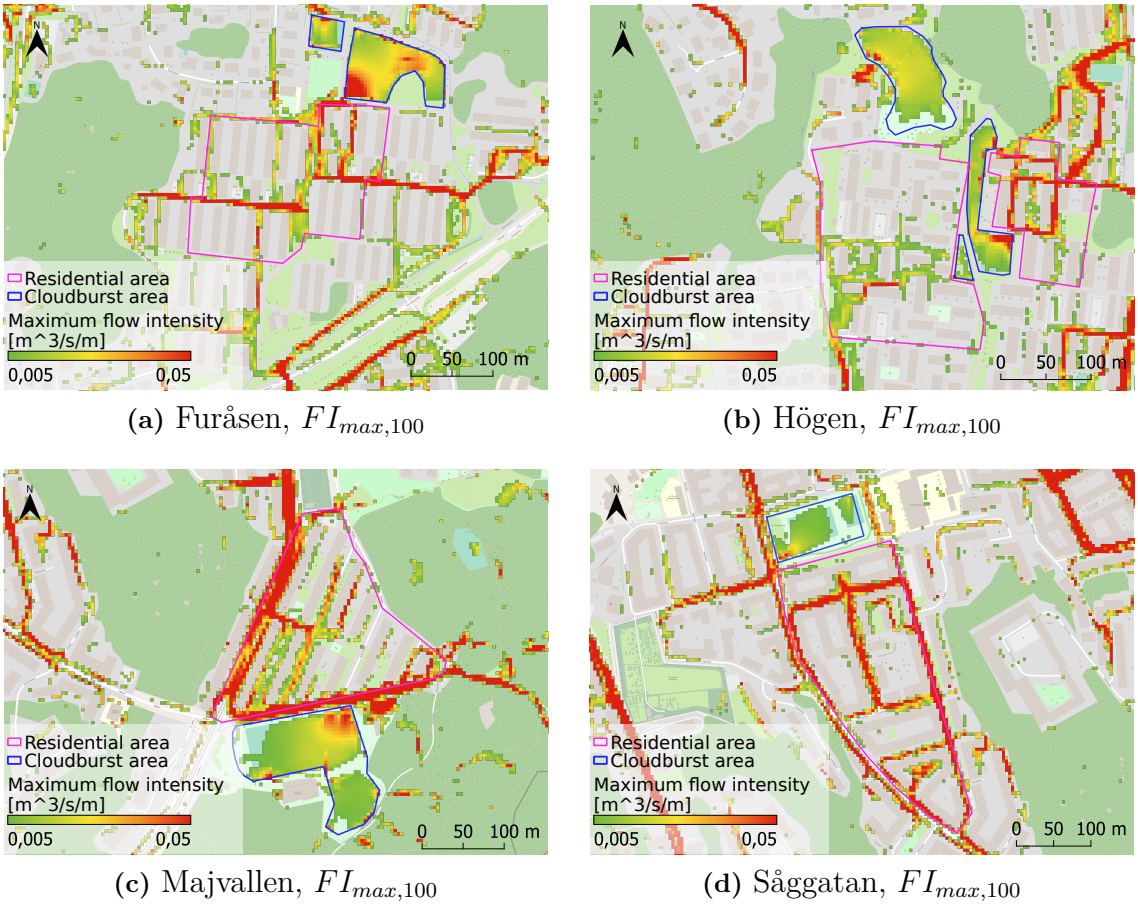

(a) Furåsen, $FI_{max,100}$

(b) Högen, $FI_{max,100}$

(c) Majvallen, $FI_{max,100}$

(d) Såggatan, $FI_{max,100}$

Figure 4.11: Maximum flow intensities during a 100-year rain (climate factor 1.2) for each risk zone. The legend describes the representation of residential and cloudburst areas. Also, the color scale is used to describe the flow intensities ($m^3/s/m$) from 0.005 (green) to 0.05 (red).

4.2.2 The flood in each risk zone, future situation

The maximum flood depths $\geq$ 0.2 m for all risk zones are visualized in Figure 4.12. The results indicate that the flood reaches the cloudburst areas in Furåsen, Högen,

and Majvallen. For Högen, there is approximately no flood within the residential area after the implementation of the cloudburst area. In contrast, Såggatan has no water (with depths $\geq$ 0.2 m) located in the cloudburst area.

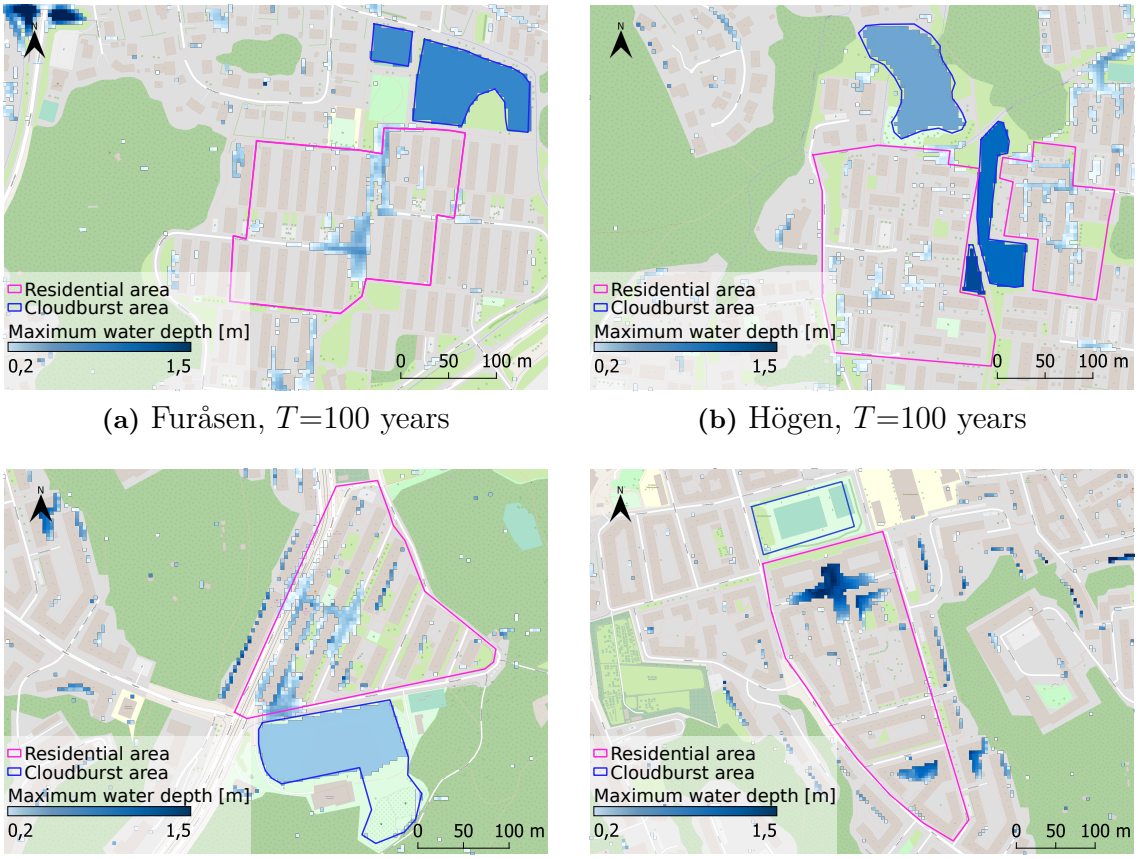

(a) Furåsen, T=100 years

(b) Högen, T=100 years

(c) Majvallen, T=100 years

(d) Såggatan, T=100 years

Figure 4.12: Maximum flood depths $\geq$ 0.2 m during a 100-year rain (climate factor 1.2) in each risk zone. The legend describes the representation of residential and cloudburst areas. Also, the color scale is used to describe depths (m) from 0.2 (light blue) to 1.5 (dark blue).

4.2.3 $V_{d\geq 0.2,100}$ and $V_{tot,100}$, current and future situations

Figure 4.13 visualizes $V_{d\geq 0.2,100}$ in the residential area and $V_{tot,100}$ in the cloudburst area, for current and future situations and for all risk zones. The results indicate that the implementation of cloudburst areas decreases $V_{d\geq 0.2,100}$ within the residential areas of Furåsen, Högen, and Majvallen. For Såggatan, there is a small increase in $V_{d\geq 0.2,100}$ for the future situation though, and this increase is assumed to be due to the variance within the results, generated from using different computers. This is one of the uncertainties with the model and is further described in Section 3.4.2.3.

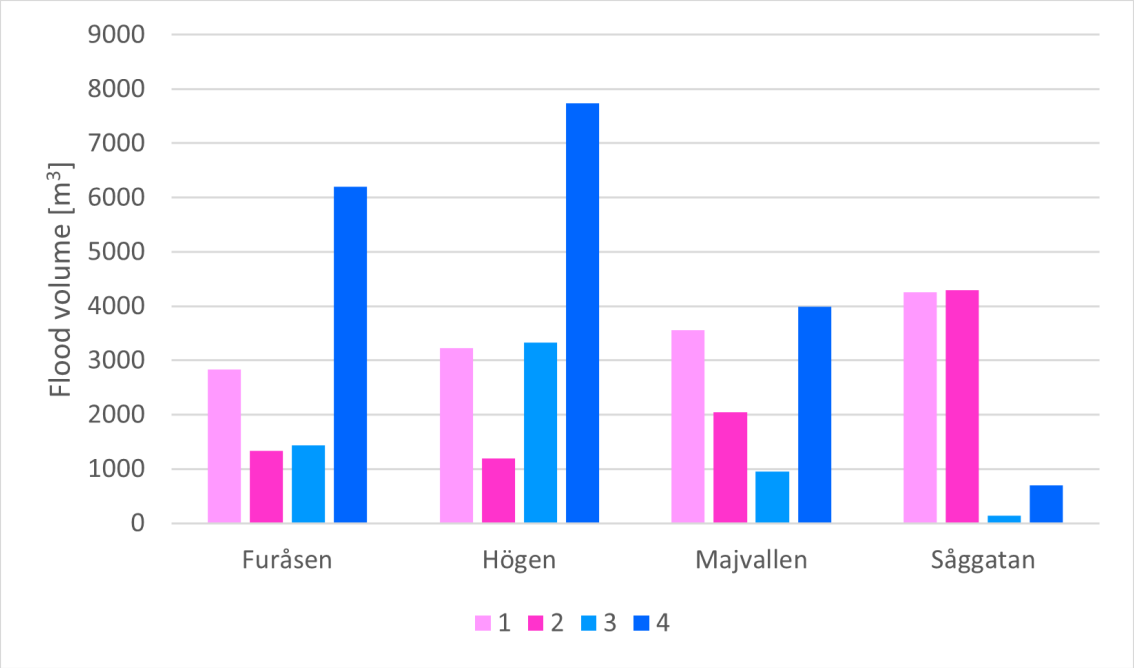

Figure 4.13: Maximum flood volume (with depths $\geq$ 0.2 m) $V_{d\geq 0.2m,100}$ in the residential area (1) *before* and (2) *after* implementation of cloudburst area, and maximum total volume $V_{tot,100}$ in the cloudburst area (3) *before* and (4) *after* implementation. All volumes are represented by a 100-year rain (climate factor 1.2).

4.2.4 Discussion of future situation

From analysing the results from the future situation it is stated that all cloudburst areas, except for the one in Såggatan, reduce the floods within the residential areas. The result for Såggatan is assumed to be an incorrect representation of reality due to the excluded opening in the apartment building. The cloudburst areas in Furåsen, Högen, and Majvallen store a larger volume of water ($V_{tot,100}$) after implementation than the flood volume ($V_{d\geq 0.2m,100}$) within the residential areas before implementation. Hence, these cloudburst areas have a larger capacity than required. However, according to the results, floods (with depths $\geq$ 0.2 m) will still occur within the residential areas of these risk zones despite the implementation of cloudburst areas.

The flow intensities $FI_{max,100}$ for the future situation changes significantly for all risk zones, except Såggatan, after the implementation of cloudburst areas. In Furåsen, Högen, and Majvallen larger flow intensities are seen for a bigger part of the cloudburst area than before. However, there are no major natural runoff routes that enable water to enter the cloudburst areas from upstream areas, and thereby, all water seems to pass via the residential areas before entering the cloudburst areas.

In the structure plans, all selected risk zones have additional cloudburst facilities that were excluded in this study, see Figure 3.3. The results previously presented indicate that these excluded cloudburst facilities are important factors that affect the consequences and severity of a cloudburst. The largest impact is seen for Såggatan where three cloudburst paths are recommended to enable the runoff within the

residential area to reach the cloudburst area. Similar observations are seen for Majvallen. In Furåsen, one path that enables water from the eastern parts to enter the cloudburst area is excluded, however, in comparison to Såggatan and Majvallen, this path is not assumed to be as vital. Högen differs from the other zones since the structure plan recommends several steering measures and smaller cloudburst areas. In Högen, a large portion of the runoff enters from the northeastern parts where a smaller cloudburst area and a steering measure are proposed to be located. Hence, these excluded facilities would reduce the flood within the residential area if implemented.

In summary, cloudburst areas are implemented to capture surface water during floods. To enable the gathering of water it is important to have an understanding of the characteristic, e.g. depressions, low points, surface runoff routes, and overall topography. To reduce the flooding within residential areas, it is necessary to ensure that the intended water (the water from the residential areas) can enter the cloudburst areas, i.e. that the cloudburst areas manage water that otherwise will cause consequences within the residential areas.

4.3 Development of tool

This study has been conducted by evaluating four different risk zones and the aim was to develop a tool that works for different residential areas. The results described in previous sections show dissimilarities between the risk zones and thereby, it was required to determine which risk zones to include in the development of the tool. This section includes a description of this selection together with an explanation of the final tool and its limitations.

4.3.1 Selection of risk zones to include in the tool

The ratio $R_{1,T}$ are the results that are the basis of the tool. The ratio $R_{1,T}$ is defined by the ratio between the flooded volume $V_{d\geq 0.2m,T}$ and $V_{d\geq 0.2m,100}$, see Equation 3.4. Consequently, these ratios highly influence the selection of risk zones to include in the tool. As described in previous sections, Majvallen has a significantly higher $R_{1,10}$ than the other zones. The $R_{1,10}$ for Majvallen implies that 56% of the $V_{d\geq 0.2m,100}$ occurs already during a 10-year rain. This $R_{1,10}$ is substantially higher than for Furåsen (26%), Högen (27%), and Såggatan (43%). When these results were analysed together with experts at DHI and Kretslopp och vatten (C. Karlsson & D. Karlsson, personal communication, April 20, 2023), the ratio was considered to be unrealistic high. Due to the large $R_{1,10}$, and since there are uncertainties regarding the accuracy of the sewer network in the model, it is assumed most accurate to exclude Majvallen when developing the tool.

The floods in Såggatan are different, in terms of spread and depth, compared to the floods in the other risk zones. The $R_{1,10}$ is also different compared to the other zones as it is lower than for Majvallen but higher than for Furåsen and Högen. Additionally, Såggatan is different than the other zones considering several site characteristics, e.g. building structure and a proposed cloudburst area located

downstream of the residential area. Due to these differences, and due to the uncertainties regarding the influence of the excluded opening in the apartment building in the model, Såggatan is excluded when developing the tool.

When comparing Furåsen and Högen, dissimilarities are found considering both site characteristics and results. However, the similarities between Furåsen and Högen are more distinct than the dissimilarities when compared to Majvallen and Såggatan. The $R_{1,T}$ for Furåsen and Högen are approximately equal for return periods $T < 40$ years. There are differences between the $R_{1,T}$ for return periods $T > 40$ years, however, the differences are in the range of five percentage points. In relation to the major differences in $R_{1,10}$ and slope for the graphs of Majvallen and Såggatan, this is considered negligible. Overall, the $R_{1,T}$ indicate a correlation between flooded volume ($V_{d\geq 0.2m,T}$) and return period for Furåsen and Högen. Following that, and since there always will be dissimilarities when comparing two independent zones, Furåsen and Högen are assumed to be adequate enough to incorporate both when developing the tool.

In summary, the tool is based on the $R_{1,T}$ for Furåsen and Högen. This implies that the tool is based on two townhouse areas, and hence, the tool is not applicable to different residential areas as it aimed to be. The aim of this thesis is to evaluate whether it is possible to develop a tool for different residential areas. Following the methodology of this thesis this is not possible.

4.3.2 Final tool

The final tool is based on the correlating $R_{1,T}$ for Furåsen and Högen. All the calculated $R_{1,T}$ for both Furåsen and Högen are plotted together in one diagram, see Figure 4.14.

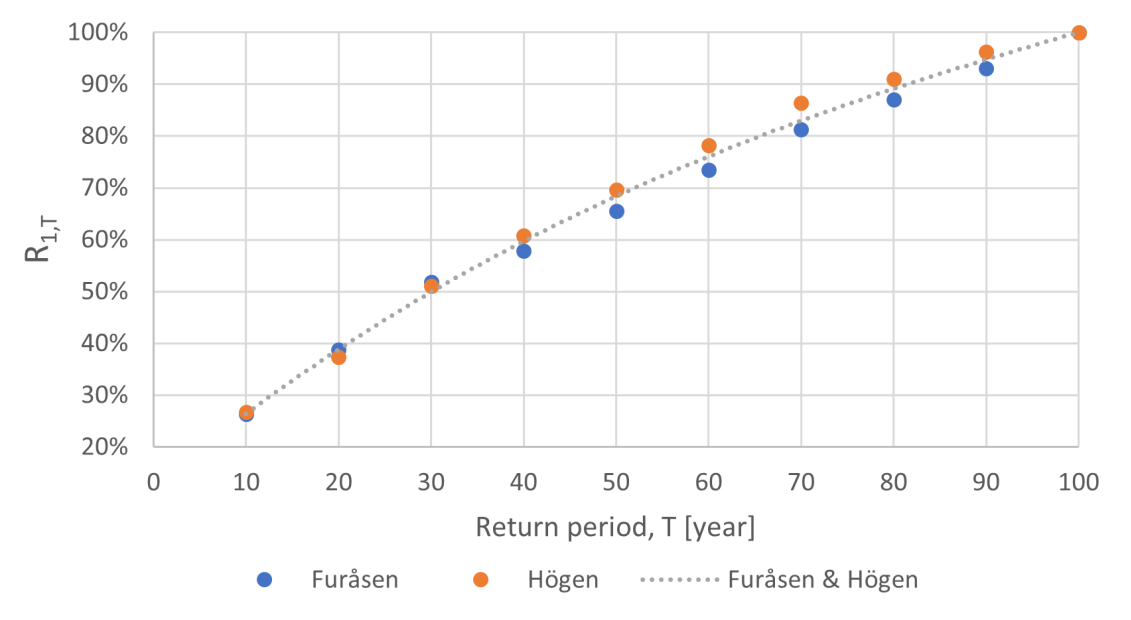

Figure 4.14: The ratio $R_{1,T}$ for each return period for the residential areas in Furåsen and Högen. Also, the interpolated trend line of these ratios.

Figure 4.14 displays the interpolated trend line which is a cubic polynomial equation, see Equation 4.1. The cubic polynomial equation was provided by Excel and selected as it receives the highest R^2 value (0.9945), following the methodology described in Section 3.5.

$$R_{1,T} = 2 \cdot 10^{-7} T^3 - 8 \cdot 10^{-5} T^2 + 0.0148T + 0.1245 \quad (4.1)$$

$R_{1,T}$: Ratio [-] (see Equation 3.4)
T: Return period [year]

Equation 4.1 is the basis of the tool and represents the $R_{1,T}$. This equation is represented by the graph (yellow line) in Figure 4.15. The tool requires two inputs:

(i) the $V_{d \geq 0.2m,100}$ (m^3) with a climate factor of 1.2
(ii) the available volume ($V_{available}$) in the planned cloudburst area (m^3)

Input *(i)* can be calculated using Equation 3.2. Input *(ii)* is determined by the user based on the evaluated site and planned volume of the implemented cloudburst area. Both inputs are used to calculate $R_{available}$ by Equation 3.6 which is represented by the horizontal line (green line) in Figure 4.15. Based on the inputs and the graph, the tool is programmed to estimate a manageable return period T which is represented by the vertical line (blue line) in Figure 4.15.

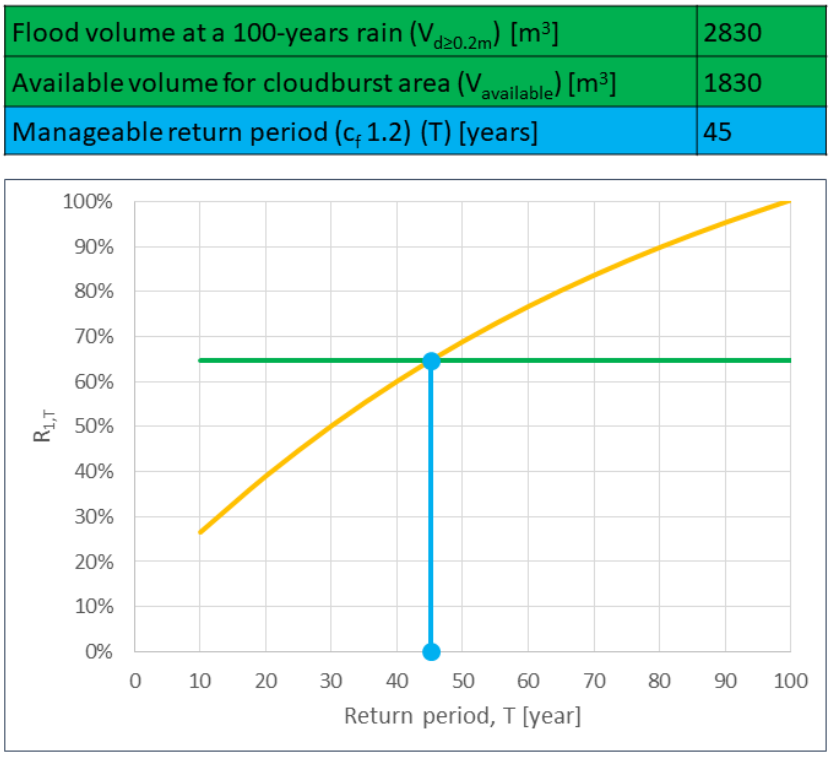

Figure 4.15: The interface of the final tool available in Excel. The green boxes represent the required input values and the blue box is the return period estimated by the tool. The yellow line represents the $R_{1,T}$ for return periods T between 10 to 100 years, the green line the $R_{available}$, and the blue line the manageable return period (T).

The tool displayed in Figure 4.15 is based on and assumed to be reliable for residential areas with townhouses. Since the tool is based on just two risk zones it is considered impossible to prove whether it is reliable or not and, to verify the tool, it would have been preferable to test it on other residential areas with townhouses. However, it is important to mention that the results for Furåsen and Högen, despite both similarities and dissimilarities considering site characteristics, indicate a correlation between the $R_{1,T}$ for the evaluated return periods T.

The example in Figure 4.15 represents Furåsen, using a depth of 0.2 m for the cloudburst area, and visualizes a manageable return period of 45 years with a climate factor of 1.2. The return period depends on whether only the floods (with depths $\geq$ 0.2 m) within the residential area are able to enter the cloudburst area or not. For instance, if the cloudburst area is occupied by runoff entering from other floods, the capacity of a 45-year rain will be an overestimation. Hence, it is important to ensure that all intended flood volumes enter the cloudburst area. The tool is developed to be used during preliminary studies and the capacity is just an estimation, however, reachable if all influencing aspects are considered during the design process.

By estimating a manageable return period, the tool has the potential to provide the user with information that can be used as arguments in the cloudburst management process. For instance, many residential areas are dense and there might be a limited available area to implement a cloudburst area. Therefore, it is impossible for some residential areas to implement enough volume of cloudburst areas to be able to manage a 100-year rain. For such residential areas, the tool can be used to provide information regarding which return period the cloudburst area can manage. This information can then be used as arguments for decision-makers when evaluating different options to increase the resilience of flooding.

4.4 Research uncertainties

The study aimed to describe different residential areas by one general correlation between flood volume and rain return period. This required several assumptions, and hence, uncertainties were generated. Uncertainties in research are unavoidable but important to address. In the following section, the uncertainties within both the methodology used and the results will be described.

The tool is based on a correlation established for just two risk zones with townhouses. The correlation for these risk zones is strong but has not been verified in other residential areas with townhouses. Thereby, there are major uncertainties regarding the accuracy of the tool. Establishing a correlation based on just two risk zones that is accurate for all other residential areas with townhouses is assumed impossible. To be able to establish a general correlation for all residential areas with townhouses following the methodology used in this study, the correlation needs to be tested in at least three additional risk zones with townhouses and verified for all these. If the correlation had been tested in three additional risk zones and verified within all these zones, the correlation would be assumed to be general for residential areas with townhouses. However, if the correlation were verified in just two or fewer, an

evaluation of affecting factors would be required. Thereafter, it would be required to determine whether it is appropriate to proceed following the division used in this study or to divide residential areas with townhouses in subgroups based on different site characteristics. Another methodology that could have been appropriate to use, would be to establish the correlation based on $R_{1,T}$ from a large number of risk zones with townhouses. If such a methodology had been used, the graph could have been established by selecting the mean value of $R_{1,T}$ for each return period T. However, such an approach would require modeling of a large number of risk zones and would therefore be a time-consuming process.

In this study, the division of residential areas was based on type (i.e. building type and structure) and the types used were townhouses, apartment buildings in open structures, and apartment buildings in enclosed structures. The tool is based on a correlation between two risk zones with similar types of residential areas, but also with similar topography, sewer network, and location of the proposed cloudburst area (upstream of the residential area). The correlation was not identified in the risk zones with other types of residential areas which also differ considering the other site characteristics. From this study, the building type and structure are assumed to highly influence the ratios $R_{1,T}$. However, it is not clear how the other site characteristics influence the ratios. For instance, in the initial part of this study, Majvallen was assumed to have similarities in comparison to Furåsen and Högen that are predominant to the dissimilarities. This assumption was due to the building structure that, despite consisting of apartment buildings, resembled with an open structure and a large fraction of green areas in the residential area. However, the $R_{1,T}$ for Majvallen were significantly higher than for Furåsen and Högen, and consequently, the site characteristics that are dissimilar were predominant. Following that, there are uncertainties considering the accuracy of the division used in this thesis. It is uncertain if it is sufficient to only divide residential areas considering building structure and type or if there are other site characteristics that are required to be included in the division. Since no other site characteristics have been considered during the development of the tool, there are uncertainties regarding the accuracy of the tool. For instance, it is uncertain if the tool is able to estimate an accurate manageable return period if it is used for a residential area with townhouses that differs in site characteristics from Furåsen and Högen (e.g. that are steep or has a combined sewer network).

The tool is based on a ratio, $R_{1,T}$, that has the flood volume for the 100-year rain $V_{d\geq 0.2m,100}$ as the denominator. Thereby, the differences in $R_{1,T}$ between the different risk zones will decrease with increasing return periods since all $R_{1,100}$=100%, i.e. all graphs will approach each other for return periods approaching 100 years. Thereby, the start value ($R_{1,10}$) is the fundamental ratio that determines the slope of the graph, and the risk zones included in the development of the tool were selected since they had similar $R_{1,10}$. However, there are uncertainties considering the accuracy of the model used in this study when simulating rain intensities that approach the infiltration and sewer network capacity. Since $R_{1,10}$ represents the lowest return period, this is the ratio with the largest uncertainties. In summary, there are uncertainties regarding the accuracy of the ratios that were most important when

selecting risk zones to include in the tool. To ensure the accuracy of these ratios, it would be appropriate to calibrate the model used in this study for the 10-year rain (with a climate factor of 1.2).

In this study, modeling is used to describe reality. Such methodology requires assumptions and hence, generates uncertainties. The incomplete representation of the sewer network affects the results by overestimating the floods. However, there are uncertainties about the magnitude in which the limited representation of the sewer network affects the results. For instance, several manholes were excluded in the representation of both Furåsen and Högen but these zones seem to be able to manage a 10-year rain quite well. In Majvallen, several manholes were excluded from the model as well, however, resulting in large floods during a 10-year rain. To determine how the limited representation of the sewer network influences the results in the different risk zones, further analysis of the sewer network would have been appropriate. Both to evaluate the sewer network capacity in the model, but also to identify the number and location of excluded manholes and connected pipes. It would also be appropriate to include both public and private sewer networks.

5

Conclusion & further research

In this chapter, the conclusions of this study and the answers to the research questions are presented. Suggestions of areas to be further researched are also described.

5.1 Conclusions

This thesis aimed to develop a tool to simplify the process of implementing a cloudburst area in different types of residential areas by estimating a manageable return period. Based on the results from this thesis, it is concluded that it is possible to develop such a tool following the proposed methodology. However, the tool has certain limitations that decrease its applicability. For instance, the tool is only developed for residential areas with townhouses and not different residential areas. Further, the tool is developed based on two similar townhouse areas and has not been verified for other residential areas with townhouses. Consequently, due to both the limitations regarding the applicability and the uncertainties regarding the accuracy it is unsure if the tool actually simplifies the process of implementing cloudburst area. Therefore, there is a need for further development and verification of the tool.

To fulfill the aim, three research questions were formulated. The first question included an evaluation of the possibility to create a tool to estimate the increase in flood resilience due to the implementation of a cloudburst area. The study reveals that with the methodology used it is possible to create such a tool. The results display that even during the implementation of cloudburst areas with an infinite volume capacity there will be floods (with depths ≥ 0.2 m) in the residential areas though, hence there is a need for additional measures to ensure that the water enters the cloudburst area. Consequently, the tool estimates a manageable return period that is accurate if all flooded volumes ($V_{d\geq 0.2m,T}$) within the residential area and, exclusively this volume, are able to enter the cloudburst area. An important conclusion from the study is thereby that to reach the maximum capacity of a cloudburst area, it is essential to evaluate whether other measures are required or not. Also, to evaluate which location is the most suitable for a cloudburst area in relation to the residential area.

The second question considered whether there is a general relationship between flooded volume and rain return period for the selected areas or not. Based on the results, no such relationship has been identified. A relation was found for two of

the areas, that both consisted of townhouses, however, was not verified in the other areas, consisting of apartment buildings. Consequently, a correlation was established but is not general for all the selected residential areas.

Following the third research question, several site characteristics were identified to influence the floods within the residential areas. The study revealed that different site characteristics affect different risk zones. The site characteristics that have been identified to influence floods in this study are:

- **Topography**: The location, size, and depth of depressions were identified as dominant characteristics to influence floods in all risk zones, which agrees with the findings in other studies. Considering floods (with depths ≥ 0.2 m), topographical characteristics that allow for water to accumulate in specific locations, and hence that generate floods with large depths, were identified as aggravating.
- **Catchment area**: The limited depression storage of the catchment area of Majvallen were identified to increase the amount of runoff ending up in the residential area. Further for Furåsen, a large depression storage capacity was identified to decrease the amount of runoff ending up in the residential area.
- **Location of larger green areas:** For Furåsen and Högen, the results show that the locations of the upstream green areas were important since these acted as barriers and hindered runoff to enter the residential areas.
- **Building structure**: The building structure in Såggatan was identified as important since it captured runoff in specific locations.
- **Sewer network capacity**: The lack of sewer network capacity in Majvallen was identified to increase the floods during low return periods.

5.2 Further research

There are several aspects that would be desirable to study further when summarizing this study. This section will provide suggestions for possible areas of future studies:

- This study identified a correlation between two areas with similar land use and building structure, that possibly could be found in other similar areas. Based on the results, a recommendation for future research is to continue evaluating similar areas to verify the correlation. If a correlation can be established the recommendation is to analyse other types of areas separately.
- The results from this study agreed with the literature study where several physical parameters were mentioned to influence flood characteristics. Future studies should investigate and compare the influence of different parameters, for instance by conducting a sensitivity analysis.
- This study was conducted on request from Kretslopp och vatten and DHI where their vision was to develop a tool for simplification of cloudburst management in the City of Gothenburg. Their vision has been interpreted and

further developed by the research group. To increase the usability of the tool it would be desirable to conduct an interview study or survey to gather information from potential users regarding their needs. For instance, to create an understanding of which information that is easily accessible to be used as input data and/or to determine whether a tool that gives an acceptable estimation for similar areas or a perfect estimation for a few areas is more usable.

References

Alshammari, E., Rahman, A. A., Rainis, R., Seri, N. A., & Fuzi, N. F. A. (2023). The Impacts of Land Use Changes in Urban Hydrology, Runoff and Flooding: A Review. *Current Urban Studies*, *11*(01), 120–141. doi: 10.4236/cus.2023.111007

Arosio, M., Martina, M. L., & Figueiredo, R. (2020). The whole is greater than the sum of its parts: A holistic graph-based assessment approach for natural hazard risk of complex systems. *Natural Hazards and Earth System Sciences*, *20*(2), 521–547. doi: 10.5194/nhess-20-521-2020

Ata, R., Goeury, C., & Hervouet, J. M. (2014). *TELEMAC-2D Software.* Ontario: Canadian Hydraulics Centre. Retrieved from `http://www.opentelemac.org/downloads/MANUALS/TELEMAC-2D/telemac-2d_user_manual_en_v7p0.pdf`

Bell, E., Bryman, A., & Harley, B. (2019). *Business research methods* (5th ed.). Oxford: Oxford University Press.

Berntzon, L. (2019). *Dagvattenutredning för Tjurbergsparken.* Stockholm. Retrieved from `https://edokmeetings.stockholm.se/welcome-sv/namnder-styrelser/radet-till-skydd-for-stockholms-skonhet/mote-2020-10-05/agenda/dagvattenutredningpdf?downloadMode=download`

Boverket. (2010). *Mangfunktionella ytor: Klimatanpassning av befintlig bebyggd miljo i stader och tatorter genom gronstruktur.* Boverket. Retrieved from `https://www.boverket.se/globalassets/publikationer/dokument/2010/mangfunktionella_ytor.pdf`

Brunner, G. W. (2023). *HEC-RAS River Analysis System HEC-RAS 2D User's Manual.* Retrieved from `https://www.hec.usace.army.mil/confluence/rasdocs/r2dum/latest`

Bruwier, M., Maravat, C., Mustafa, A., Teller, J., Pirotton, M., Erpicum, S., ... Dewals, B. (2020). Influence of urban forms on surface flow in urban pluvial flooding. *Journal of Hydrology*, *582*. doi: 10.1016/j.jhydrol.2019.124493

Chen, J., Hill, A. A., & Urbano, L. D. (2009). A GIS-based model for urban flood inundation. *Journal of Hydrology*, *373*(1-2), 184–192. doi: 10.1016/j.jhydrol.2009.04.021

Chicco, D., Warrens, M. J., & Jurman, G. (2021). The coefficient of determination R-squared is more informative than SMAPE, MAE, MAPE, MSE and RMSE in regression analysis evaluation. *PeerJ Computer Science*, *7*, 1–24. doi: 10.7717/PEERJ-CS.623

CRED. (n.d.-a). *Frequently asked questions.* Retrieved from `https://www.emdat`

.be/frequently-asked-questions

CRED. (n.d.-b). *The International Disaster Database.* Retrieved from https://www.emdat.be

DHI. (2023a). *MIKE+ Collection System User Guide.* Retrieved from https://manuals.mikepoweredbydhi.help/latest/Cities/MIKE_Plus_Collection_System.pdf

DHI. (2023b). *MIKE+ Release Notes.* Retrieved from https://manuals.mikepoweredbydhi.help/2023/Release_Notes/MIKEPlus%20Release%20Notes.pdf

Di Salvo, C., Pennica, F., Ciotoli, G., & Cavinato, G. P. (2018). A GIS-based procedure for preliminary mapping of pluvial flood risk at metropolitan scale. *Environmental Modelling and Software*, *107*, 64–84. doi: 10.1016/j.envsoft.2018.05.020

Douglas, I., Garvin, S., Lawson, N., Richards, J., Tippett, J., & White, I. (2010). Urban pluvial flooding: A qualitative case study of cause, effect and nonstructural mitigation. *Journal of Flood Risk Management*, *3*(2), 112–125. doi: 10.1111/j.1753-318X.2010.01061.x

Eklund, A., Mårtensson, J. A., Bergström, S., Björck, E., Dahné, J., Lindström, L., ... Sjökvist, E. (2015). *Sveriges framtida klimat* (Vol. 14). Retrieved from https://www.smhi.se/polopoly_fs/1.165049!/Klimatologi_15%20Klimatscenarier%20f%C3%B6r%20Sverige%20-%20Bearbetning%20av%20RCP-scenarier%20f%C3%B6r%20meteorologiska%20och%20hydrologiska%20effektstudier.pdf

Eldho, T. I., Zope, P. E., & Kulkarni, A. T. (2018). Urban Flood Management in Coastal Regions Using Numerical Simulation and Geographic Information System. In *Integrating disaster science and management: Global case studies in mitigation and recovery.* Elsevier. doi: 10.1016/B978-0-12-812056-9.00012-9

European Commission. (2023, 2). *Floods.* Retrieved from https://environment.ec.europa.eu/topics/water/floods_en

Evans, T., & Orman, N. (2013). *Water Environment: a Sustainable Future?* (Second ed.). Foundation for Water Research. Retrieved from http://www.fwr.org/urbndnge.pdf

Försvarsdepartementet. (2009, 10). *Förordning (2009:956) om översvämningsrisker.* Retrieved from https://www.riksdagen.se/sv/dokument-lagar/dokument/svensk-forfattningssamling/forordning-2009956-om-oversvamningsrisker_sfs-2009-956

Göteborgs Stad. (2021). *Göteborgs Stads anvisning om hantering av skyfall.* Gothenburg. Retrieved from https://www.vattenigoteborg.se/Information/DownloadDocument?file=1.%20Styrande%20dokument/G%C3%B6teborgs%20Stads%20anvisning%20om%20hantering%20av%20skyfall.pdf&folder=downpourReports

Göteborgs Stad. (2023). *Vatten i staden.* Retrieved from https://www.vattenigoteborg.se/Downpour/ScenarioResult

Gustafsson, L.-G., & Mårtensson, E. (2017). *Vägledning för skyfallskartering.* Retrieved from https://rib.msb.se/filer/pdf/28389.pdf

Hayes, D. C., & Young, R. L. (2005). *Comparison of Peak Discharge and Runoff Characteristic Estimates from the Rational Method to Field Observations for Small Basins in Central Virginia.* Virginia: Virginia Department of Transportation. Retrieved from https://pubs.er.usgs.gov/publication/sir20055254

Henrichs, T. (2003). *Scenario Workshop Environmental Scenario Analysis.* European Environment Agency. Retrieved from http://www.gecafs.org/gecafs_meetings/2003_08_18/

Houston, D., Werritty, A., Bassett, D., Geddes, A., Hoolachan, A., & Mcmillan, M. (2011). *Pluvial (rain-related) flooding in urban areas: the invisible hazard.* Retrieved from www.jrf.org.uk

Huang, H., Chen, X., Wang, X., Wang, X., & Liu, L. (2019). A depression-based index to represent topographic control in urban pluvial flooding. *Water*, *11*(10). doi: 10.3390/w11102115

IPCC. (2021). *Climate change 2021.* Cambridge: Cambridge University Press. Retrieved from https://report.ipcc.ch/ar6/wg1/IPCC_AR6_WGI_FullReport.pdf doi: 10.1017/9781009157896

Jha, A. K., Bloch, R., & Lamond, J. (2012). *Cities and Flooding: A Guide to Integrated Urban Flood Risk Management for the 21st Century.* Washington: The World Bank. Retrieved from https://openknowledge.worldbank.org/handle/10986/2241

Justitiedepartementet. (1970). *Jordabalk (1970:994).* Retrieved from https://www.riksdagen.se/sv/dokument-lagar/dokument/svensk-forfattningssamling/jordabalk-1970994_sfs-1970-994

Kanu, C. L., Okechukwu Agu, & Egwuonwu, U. I. (2020). Management and Use of Grey Literature in Special Libraries. *International Journal of Research in Library Science*, *6*(2), 48. doi: 10.26761/ijrls.6.2.2020.1326

Keifer, C. J., & Chu, H. H. (1957). Synthetic Storm Pattern for Drainage Design. *Journal of the Hydraulics Division*, *83*(4). doi: 10.1061/JYCEAJ.0000104

Koutsoyiannis, D., & Papalexiou, S. M. (2017). Extreme Rainfall: Global Perspective. In *Handbook of applied hydrology* (Second Edition ed.). McGraw-Hill. Retrieved from https://www.itia.ntua.gr/el/getfile/1595/1/documents/Chapter74PP.pdf

Kretslopp och vatten. (2021a). *Modelldokumentation av Strukturplansmodeller.* Gothenburg. Retrieved from https://www.vattenigoteborg.se/Information/DownloadDocument?file=2.%20Kartering%20nul%C3%A4ge%20och%20strukturplaner/Modelldokumentation%20av%20Strukturplanmodeller.pdf&folder=downpourReports

Kretslopp och vatten. (2021b). *Strukturplan för hantering av översvämningsrisker: Avrinningsområde Väster.* Gothenburg. Retrieved from https://www.vattenigoteborg.se/Information/DownloadDocument?file=3.%20Strukturplansomr%C3%A5den/Strukturplan%20V%C3%A4ster.pdf&folder=downpourReports

Kretslopp och vatten. (2021c). *Strukturplan för hantering av översvämningsrisker: Metodbeskrivning.* Gothenburg. Retrieved from https://www.vattenigoteborg.se/Information/DownloadDocument

?file=2.%20Kartering%20nul%C3%A4ge%20och%20strukturplaner/Strukturplan%20Metodutveckling.pdf&folder=downpourReports

Landsbygds- och infrastrukturdepartementet. (2010). *Plan- & bygglag (2010:900).* Retrieved from https://www.riksdagen.se/sv/dokument-lagar/dokument/svensk-forfattningssamling/plan--och-bygglag-2010900_sfs-2010-900

Li, G., Liu, J., & Shao, W. (2022). Flood Risk Assessment Using TELEMAC-2D Models Integrated with Multi-Index Analysis in Shenzhen River Basin, China. *Water*, *14*(16). doi: 10.3390/w14162513

Li, X., Erpicum, S., Mignot, E., Archambeau, P., Pirotton, M., & Dewals, B. (2021). Influence of urban forms on long-duration urban flooding: Laboratory experiments and computational analysis. *Journal of Hydrology*, *603*. doi: 10.1016/j.jhydrol.2021.127034

Luo, K., & Zhang, X. (2022). Increasing urban flood risk in China over recent 40 years induced by LUCC. *Landscape and Urban Planning*, *219*(5), 1–8. doi: 10.1016/j.landurbplan.2021.104317

Luo, P., Luo, M., Li, F., Qi, X., Huo, A., Wang, Z., ... Wang, Y. (2022). Urban flood numerical simulation: Research, methods and future perspectives. *Environmental Modelling and Software*, *156*(7), 1–14. doi: 10.1016/j.envsoft.2022.105478

Marsalek, J., & Watt, W. E. (1984). Design storms for urban drainage design. *Canadian Journal of Civil Engineering*, *11*(3), 574–584. doi: 10.1139/l84-075

Martina, M. L., Arosio, M., Creaco, E., & Figueiredo, R. (2020). Indirect impact assessment of pluvial flooding in urban areas using a graph-based approach: The Mexico city case study. *Water (Switzerland)*, *12*(6), 1–18. doi: 10.3390/w12061753

Mediero, L., Soriano, E., Oria, P., Bagli, S., Castellarin, A., Garrote, L., ... Schröter, K. (2022). Pluvial flooding: High-resolution stochastic hazard mapping in urban areas by using fast-processing DEM-based algorithms. *Journal of Hydrology*, *608*(1-2), 1–21. doi: 10.1016/j.jhydrol.2022.127649

MSB. (2013a). *MSBFS 2013-1 föreskrifter om översvämningsrisker.* Myndigheten för Samh. Retrieved from https://www.msb.se/siteassets/dokument/regler/rs/c47e6d96-e159-436c-8320-8c53aa9e5694.pdf

MSB. (2013b). *Pluviala översvämningar: konsekvenser vid skyfall över tätorter, en kunskapsöversikt.* Gothenburg and Lund: Myndigheten för Samhällsskydd och Beredskap. Retrieved from https://rib.msb.se/filer/pdf/26609.pdf

Palla, A., Colli, M., Candela, A., Aronica, G. T., & Lanza, L. G. (2018). Pluvial flooding in urban areas: the role of surface drainage efficiency. *Journal of Flood Risk Management*, *11*, 663–676. doi: 10.1111/jfr3.12246

Prokić, M., Savić, S., & Pavić, D. (2019). Pluvial flooding in Urban Areas Across the European Continent. *Geographica Pannonica*, *23*(4), 216–232. doi: 10.5937/gp23-23508

Qi, M., Huang, H., Liu, L., & Chen, X. (2020). Spatial heterogeneity of controlling factors' impact on urban pluvial flooding in Cincinnati, US. *Applied Geography*, *125*, 1–10. doi: 10.1016/j.apgeog.2020.102362

Räddningsverket. (1997). *Spill- och dagvatten-ledningssystem: funktion vid oly-*

ckor. Karlstad: Räddningsverket. Retrieved from https://rib.msb.se/Filer/pdf/7471.pdf

Randa, O., Tom, Krhoda, O., George, Atela, O., Joanes, & Akala, H. (2022). Review of flood modelling and models in developing cities and informal settlements: A case of Nairobi city. *Journal of Hydrology: Regional Studies*, *43*, 1–13. doi: 10.1016/j.ejrh.2022.101188

Rangari, V. A., Umamahesh, N. V., & Bhatt, C. M. (2019). Assessment of inundation risk in urban floods using HEC RAS 2D. *Modeling Earth Systems and Environment*, *5*(4), 1839–1851. doi: 10.1007/s40808-019-00641-8

Ren, X., Hong, N., Li, L., Kang, J., & Li, J. (2020). Effect of infiltration rate changes in urban soils on stormwater runoff process. *Geoderma*, *363*(1), 1–11. doi: 10.1016/j.geoderma.2019.114158

Rosén, L., & Nimmermark, J. (2018). *FloodMan - Sustainable Flood Management Assessment Tool: Ett verktyg för samhällsekonomisk analys och hållbarhetsanalys av översvämningsskydd.* Gothenburg: Kretslopp och vatten. Retrieved from https://www.vattenigoteborg.se/Information/DownloadDocument?file=7.%20Kostnads-nyttoanalys/FloodMan%20rapport.pdf&folder=downpourReports

Samela, C., Persiano, S., Bagli, S., Luzzi, V., Mazzoli, P., Humer, G., ... Castellarin, A. (2020). Safer_RAIN: A DEM-based hierarchical filling-&-spilling algorithm for pluvial flood hazard assessment and mapping across large urban areas. *Water (Switzerland)*, *12*(6), 1–19. doi: 10.3390/W12061514

SCALGO ApS. (2023, 3). *SCALGO Live Documentation.* Retrieved from https://scalgo.com/en-US/scalgo-live-documentation/about/getting-started-1-1

Seenath, A., Wilson, M., & Miller, K. (2016). Hydrodynamic versus GIS modelling for coastal flood vulnerability assessment: Which is better for guiding coastal management? *Ocean and Coastal Management*, *120*, 99–109. doi: 10.1016/j.ocecoaman.2015.11.019

Seneviratne, S. I., Easterling, D., Rusticucci, M., Semenov, V., Alexander, L. V., Allen, S., ... Midgley, P. (2012). 3 - Changes in Climate Extremes and their Impacts on the Natural Physical Environment. In *Managing the risks of extreme events and disasters to advance climate change adaptation* (pp. 109–230). Cambridge and New York: Cambridge University Press. Retrieved from https://www.ipcc.ch/site/assets/uploads/2018/03/SREX-Chap3_FINAL-1.pdf

SMHI. (2021). *Återkomsttider.* Retrieved from https://www.smhi.se/kunskapsbanken/klimat/extremer/aterkomsttider-1.89085

SMHI. (2023). *Olika typer av översvämningar.* Retrieved from https://www.smhi.se/kunskapsbanken/hydrologi/oversvamningar/olika-typer-av-oversvamningar-1.176299

Stadsbyggnadskontoret. (2019). *Översiktsplan för Göteborg: Tematiskt tillägg för översvämningsrisker.* Gothenburg: Göteborgs Stad. Retrieved from https://www.vattenigoteborg.se/Information/DownloadDocument?file=1.%20Styrande%20dokument/Tematisk%20till%C3%A4gg%20%C3%96P%20%C3%B6versv%C3%A4mningsrisk-Bilaga.pdf&folder=downpourReports

Sun, Y., Wendi, D., Kim, D. E., & Liong, S. Y. (2019). Deriving intensity–duration–frequency (IDF) curves using downscaled in situ rainfall assimilated with remote sensing data. *Geoscience Letters*, *6*(1), 1–12. doi: 10.1186/s40562-019-0147-x

Svenskt Vatten. (2011). *P104 - Nederbördsdata vid dimensionering och analys av avloppsvatten* (First ed.). Stockholm: Svenskt Vatten AB.

Svenskt Vatten. (2016). *P110 - Avledning av dag-, drän- och spillvatten* (First ed.). Stockholm: Svenskt Vatten AB.

Svensson, G., Berg, R. P., Dahlström, B., Hernebring, C., & Olsson, J. (2020). *Nederbördsstatistik för dimensionering av dagvattensystem -State of the art.* Motala: Svenskt Vatten. Retrieved from https://vattenbokhandeln.svensktvatten.se/wp-content/uploads/2020/05/Svenskt_Vatten_M148.pdf

Tegelberg, L., & Svensson, G. (2013). *Utvärdering av Svenskt Vattens rekommenderade sammanvägda avrinningskoefficienter.* Stockholm: Svenskt Vatten Utveckling. Retrieved from http://vav.griffel.net/filer/svu-rapport_2013-05.pdf

Teng, J., Jakeman, A. J., Vaze, J., Croke, B. F., Dutta, D., & Kim, S. (2017). Flood inundation modelling: A review of methods, recent advances and uncertainty analysis. *Environmental Modelling and Software*, *90*, 201–216. doi: 10.1016/j.envsoft.2017.01.006

The European Parliament and the Council. (2007). *Directive 2007/60/EC of the European Parliament and of the Council of 23 October 2007 on the assessment and management of flood risks.* Official Journal of the European Union. Retrieved from https://eur-lex.europa.eu/LexUriServ/LexUriServ.do?uri=OJ:L:2007:288:0027:0034:en:PDF

Theland, J. (2019). *Skyfallskartering Ängelholms kommun.* Ängelholm: Sweco. Retrieved from https://www.engelholm.se/download/18.5eeea55516989c581e8357/1553154484051/2019.Sweco_Skyfallskartering%20ÃDngelholm.pdf

Tuyls, D. M., Thorndahl, S., & Rasmussen, M. R. (2018). Return period assessment of urban pluvial floods through modelling of rainfall–flood response. *Journal of Hydroinformatics*, *20*(4), 829–845. doi: 10.2166/hydro.2018.133

UN. (2023, 2). *Flood.* Retrieved from https://www.un-spider.org/flood

UNISDR. (2002). *Guidelines for Reducing Flood Losses.* United Nations Office for Disaster Risk Reduction. Retrieved from www.un.org/esa/sustdevwww.unisdr.org

UNISDR. (2015). *Sendai Framework for Disaster Risk Reduction: 2015-2030.* Sendai: United Nations Office for Disaster Risk Reduction. Retrieved from https://www.un.org/esa/sustdev/publications/flood_guidelines.pdf

Unwin, D. J. (1996). GIS, spatial analysis and spatial statistics. *Progress in Human Geography*, *20*(4), 540–551. doi: 10.1177/030913259602000408

Vogel, R. M., & Castellarin, A. (2016). Risk, Reliability, and Return Periods and Hydrologic Design. In *Chow´s handbook of applied hydrology* (Second ed., chap. 78). McGraw-Hill Education.

Retrieved from https://sites.tufts.edu/richardvogel/files/2019/04/2017_riskReliabilityReturnPeriods.pdf

Walczykiewicz, T., & Skonieczna, M. (2020). Rainfall flooding in urban areas in the context of geomorphological aspects. *Geosciences (Switzerland)*, *10*(11), 457. doi: 10.3390/geosciences10110457

Wang, Y., Li, C., Liu, M., Cui, Q., Wang, H., LV, J., ... Hu, Y. (2022). Spatial characteristics and driving factors of urban flooding in Chinese megacities. *Journal of Hydrology*, *613*(Part B), 1–12. doi: 10.1016/j.jhydrol.2022.128464

WHO. (2013). *Floods in the WHO European Region: health effects and their prevention.* Copenhagen: World Health Organization. Regional Office for Europe. Retrieved from https://apps.who.int/iris/bitstream/handle/10665/108625/9789289000116-eng.pdf?sequence=1&isAllowed=y

Xing, Y., Chen, H., Liang, Q., & Ma, X. (2022). Improving the performance of city-scale hydrodynamic flood modelling through a GIS-based DEM correction method. *Natural Hazards*, *112*(3), 2313–2335. doi: 10.1007/s11069-022-05267-1

Zhang, D. (2020). *Coefficients of Determination for Generalized Linear Mixed Models* (Doctoral dissertation, Purdue University). Retrieved from https://www.stat.purdue.edu/research/technical-reports/docs/tr20-01.pdf

Zhou, Q., Leng, G., Su, J., & Ren, Y. (2019). Comparison of urbanization and climate change impacts on urban flood volumes: Importance of urban planning and drainage adaptation. *Science of the Total Environment*, *658*, 24–33. doi: 10.1016/j.scitotenv.2018.12.184

A

Appendix: Study visit

The locations and directions of the images captured during the study visit are presented in Figure A.1 FigureA.3, Figure A.5, and Figure A.7. The pictures from the study visit are presented in Figure A.2, A.4, A.6, A.8.

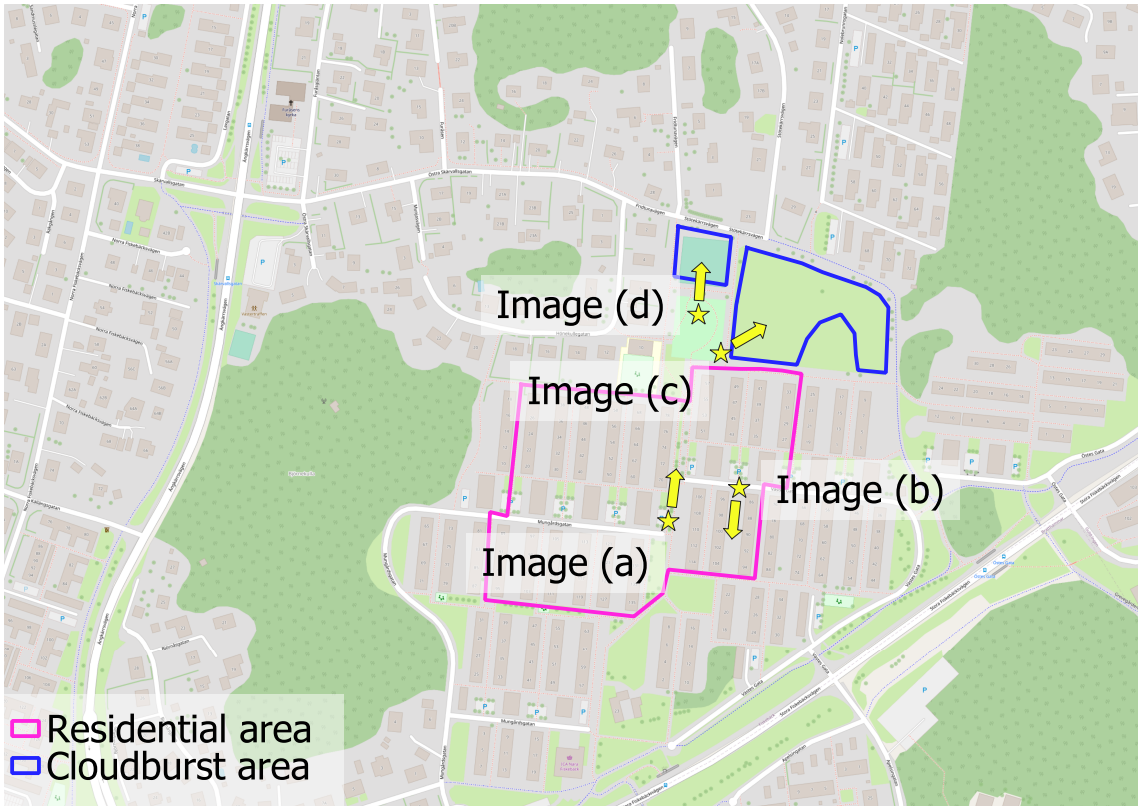

Figure A.1: The legend describes the representation of residential and cloudburst area. The stars represent the location of where the images where captured, and the arrows represent the direction of the images from the study visit to Furåsen.

(a) **(b)**

(c) **(d)**

Figure A.2: Images from the study visit to Furåsen. (a) The depression located within the central parts of the residential area. (b) The building structure in Furåsen, with one manhole that was not included in the model. (c) and (d) The recommended cloudburst areas located north of the residential area.

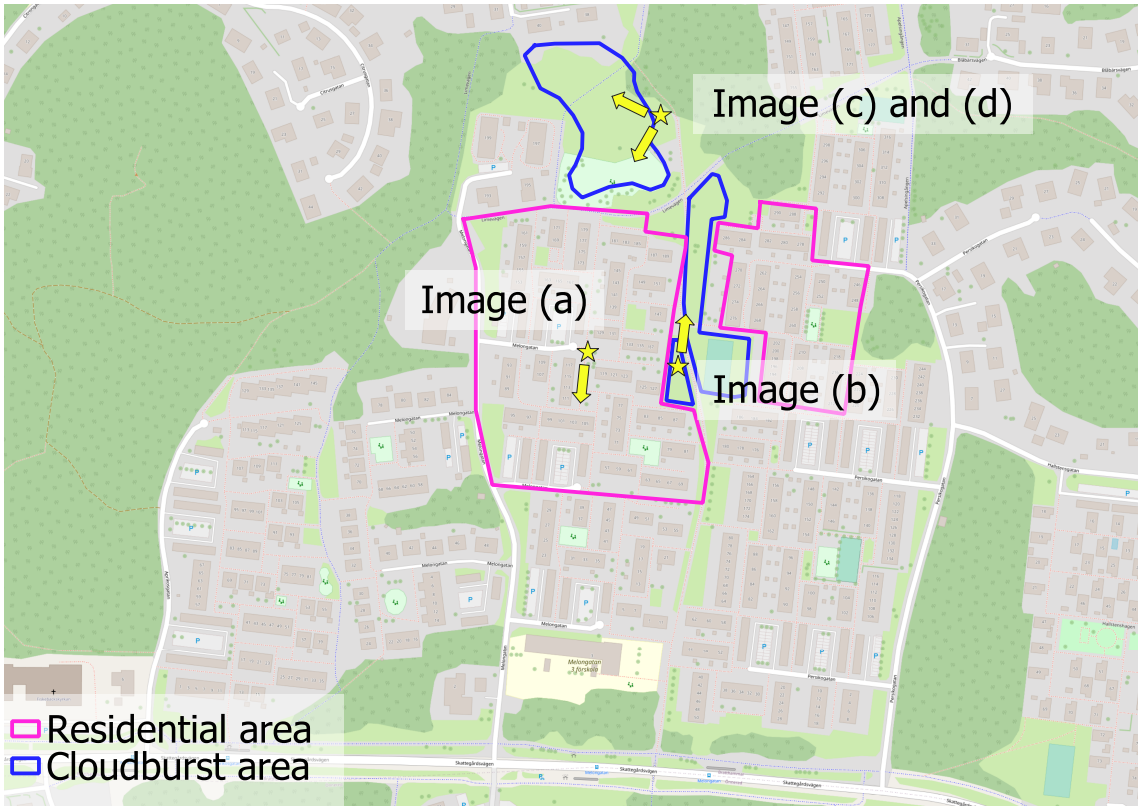

Figure A.3: The legend describes the representation of residential and cloudburst area. The stars represent the location of where the images where captured, and the arrows represent the direction of the images from the study visit to Högen.

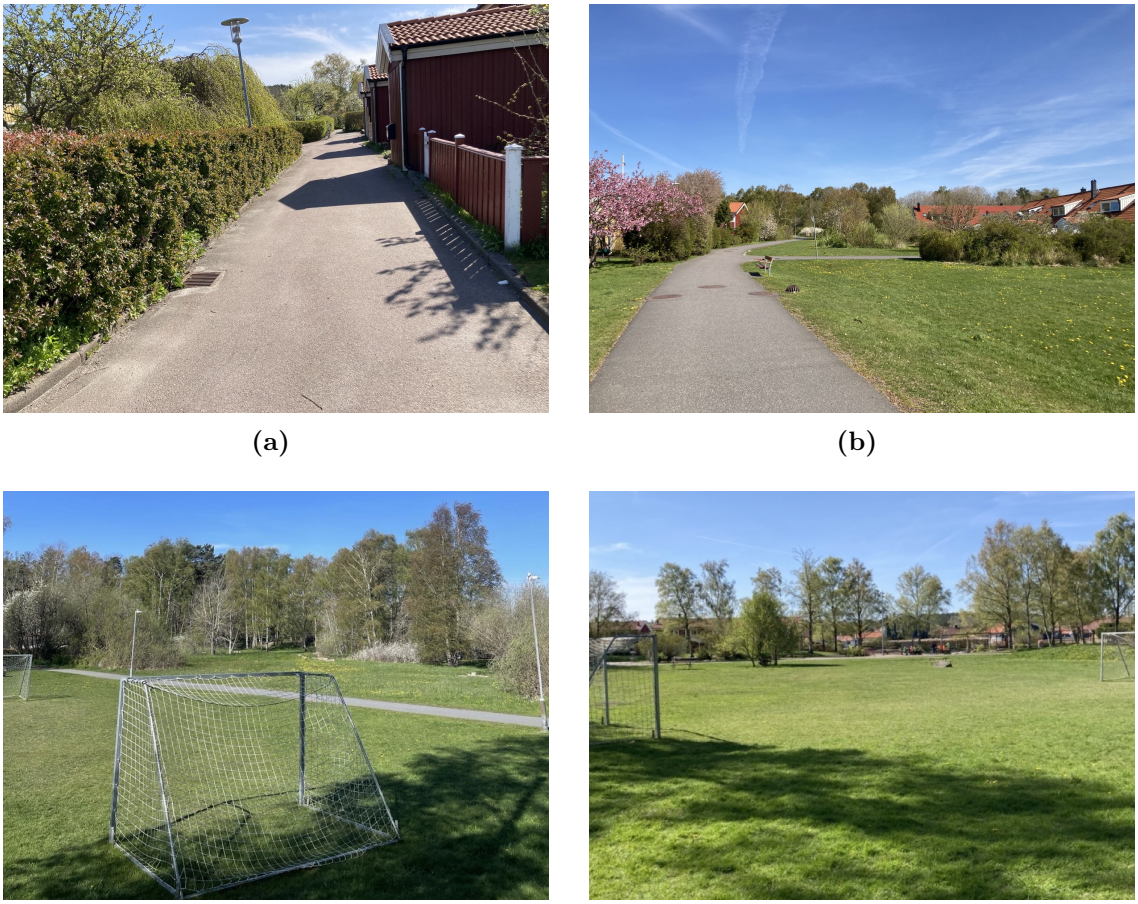

(a) **(b)**

(c) **(d)**

Figure A.4: Images from the study visit to Högen. (a) The building structure in Högen with one manhole that was not included in the model. (b) The central cloudburst area. (c) and (d) The recommended cloudburst area located north of the residential area.

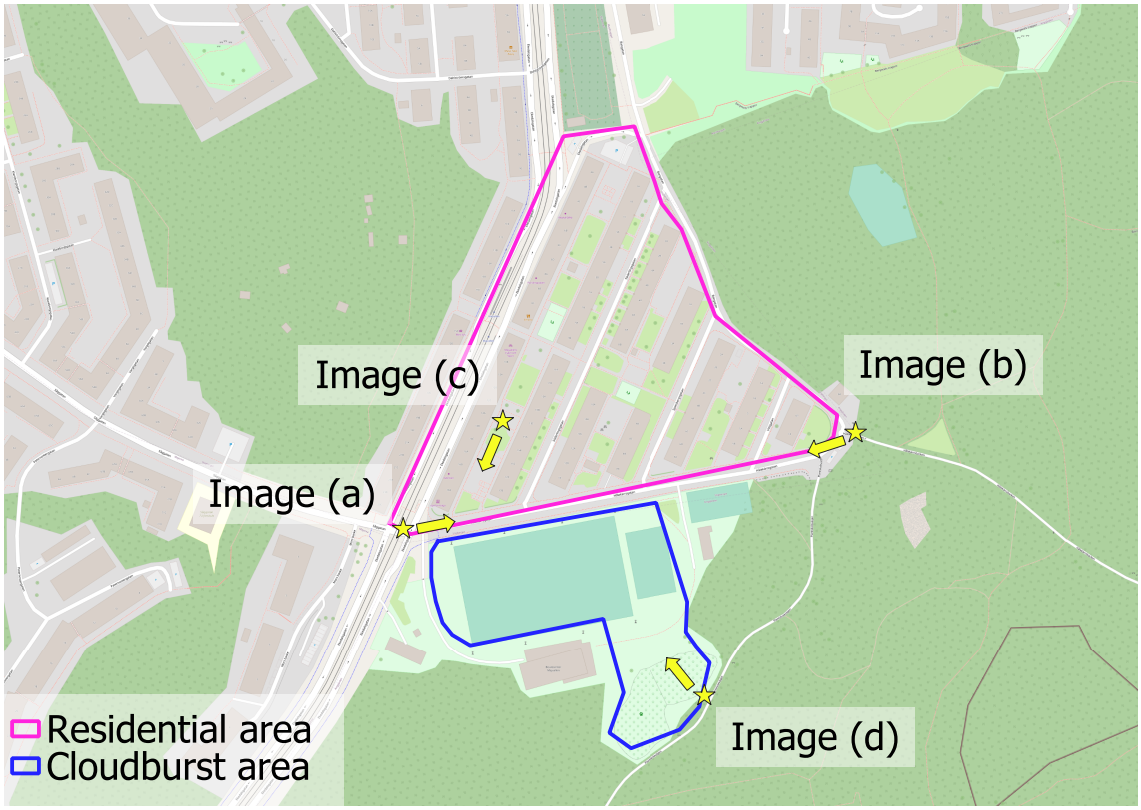

Figure A.5: The legend describes the representation of residential and cloudburst area. The stars represent the location of where the images where captured, and the arrows represent the direction of the images from the study visit to Majvallen.

(a)

(b)

(c)

(d)

Figure A.6: Images from the study visit to Majvallen. (a) and (b) The topography of the residential area. (c) The low-point in the residential area, with one manhole that was not included in the model. (d) The recommended cloudburst area.

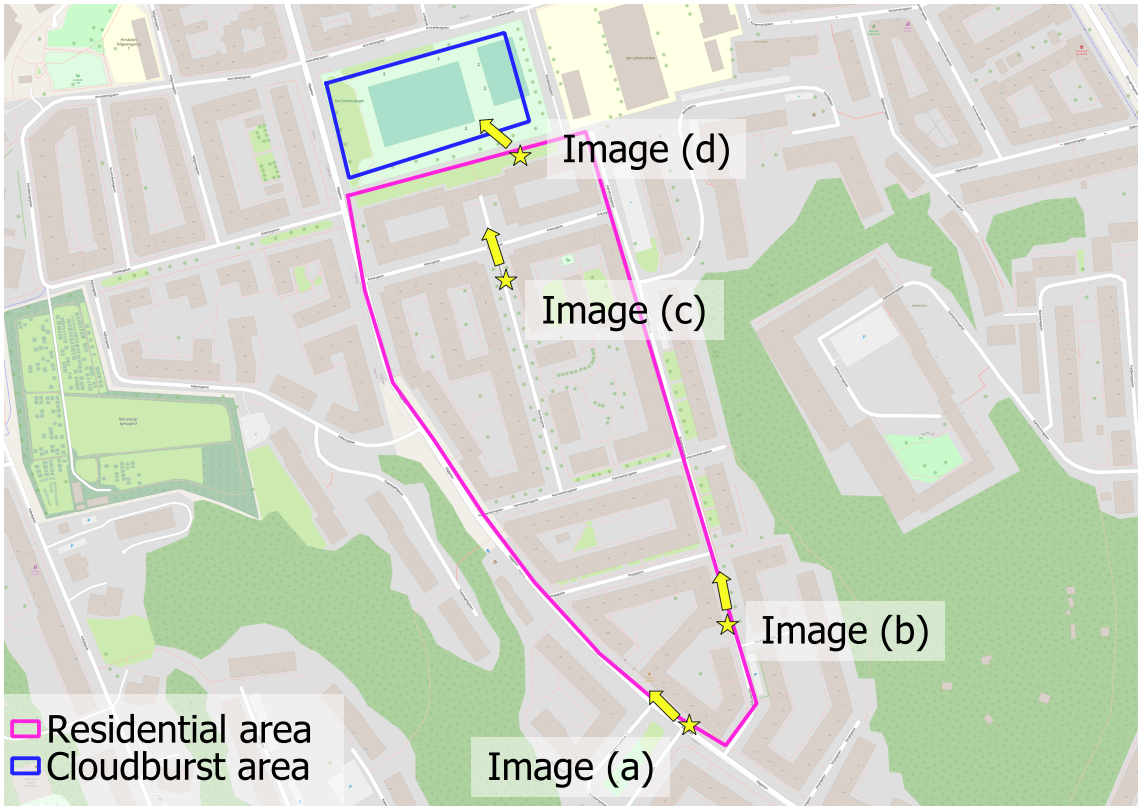

Figure A.7: The legend describes the representation of residential and cloudburst area. The stars represent the location of where the images where captured, and the arrows represent the direction of the images from the study visit to Såggatan.

(a)

(b)

(c)

(d)

Figure A.8: Images from the study visit to Såggatan. (a) and (b) The topography of the residential area. (c) The apartment building located downstream. (d) The recommended cloudburst area.

B

Appendix: Catchment areas

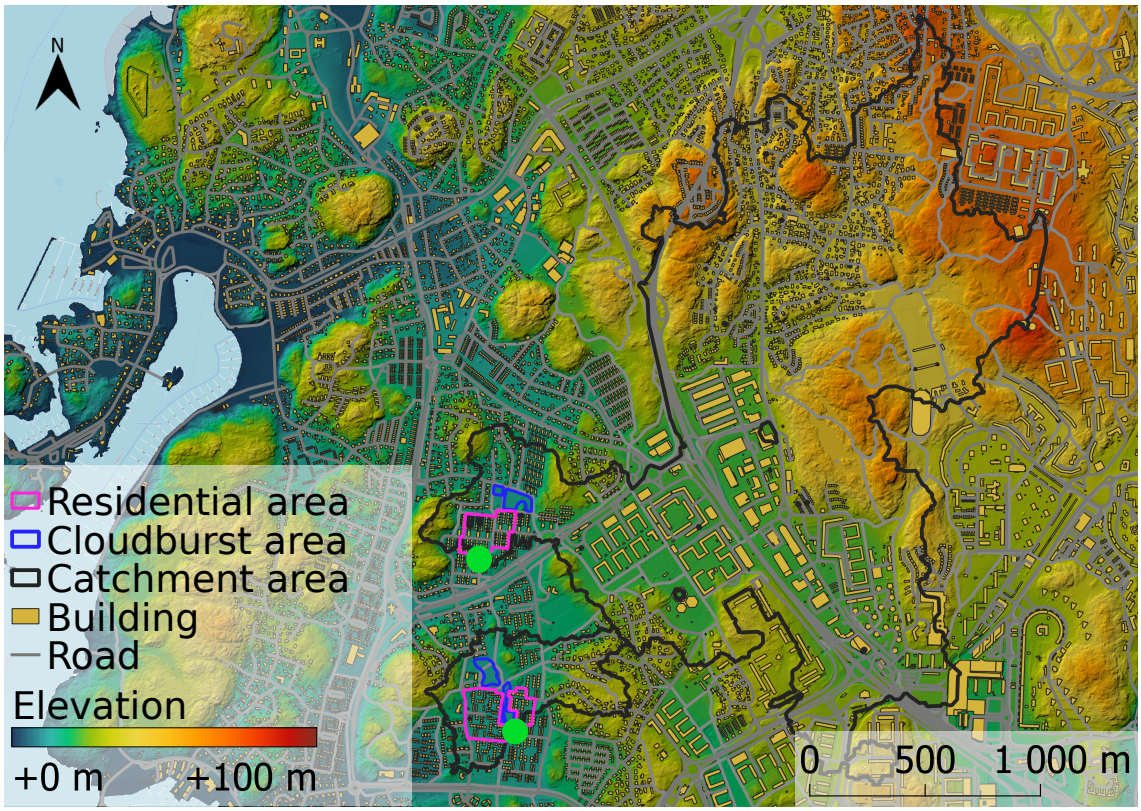

Figure B.1: The catchment area influencing Furåsen and Högen, green circles represent the outlet point © *Lantmäteriet*. The legend describes the representation of residential areas, cloudburst areas, catchment areas, buildings, and roads. Also, the color legend is used to describe elevation reaching from +2 m (blue) to +100 m (red).

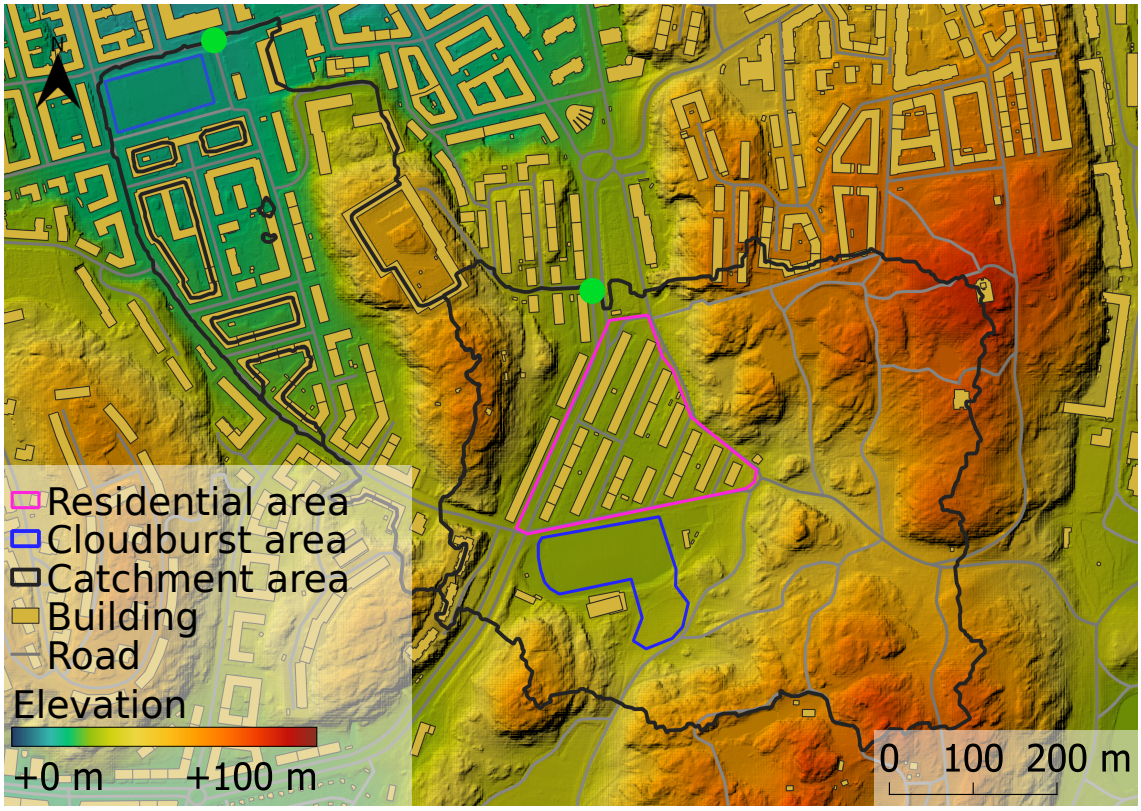

Figure B.2: The catchment area influencing Majvallen and Såggatan, green circles represent the outlet point © *Lantmäteriet*. The legend describes the representation of residential areas, cloudburst areas, catchment areas, buildings, and roads. Also, the color legend is used to describe elevation reaching from +2 m (blue) to +100 m (red).

C

Appendix: Runoff coefficient

Table C.1: Runoff coefficients for different land use, short-term precipitation (from Svenskt Vatten (2016)). *(Approved by Svenskt Vatten.)*

Land use	**Runoff coefficient** φ Limited gradient	Steep area
Closed construction method, no vegetation	0.7	0.9
Closed building style with planted yards, industrial- and school areas	0.5	0.7
Open construction method (apartment buildings)	0.4	0.6
Townhouse, chainhouse	0.4	0.6
Villas, sites (minimum construction) < 1000 m^2	0.35	0.45
Villas, sites (minimum construction) > 1000 m^2	0.2	0.3

Table C.2: Runoff coefficients for the calculation of a comprehensive runoff coefficient for an area, short-term precipitation (from Svenskt Vatten (2016)) *(Approved by Svenskt Vatten.)*.

Land use	**Runoff coefficient** φ
Roof	0.9
Concrete and asphalt surface, visible rock in steep slope	0.8
Stone-set surface with gravel joints	0.7
Road, steeply sloping mountainous park area without considerable vegetation	0.4
Visable bedrock in moderate gradient	0,3
Gravel floor and gravel path, undeveloped block of land	0.2
Park with rich vegetation and hilly mountainous woodland	0.1
Cultivated land, grass area, meadow land, etc.	0.0-0.1
Flat dense forest land	0.0-0.1

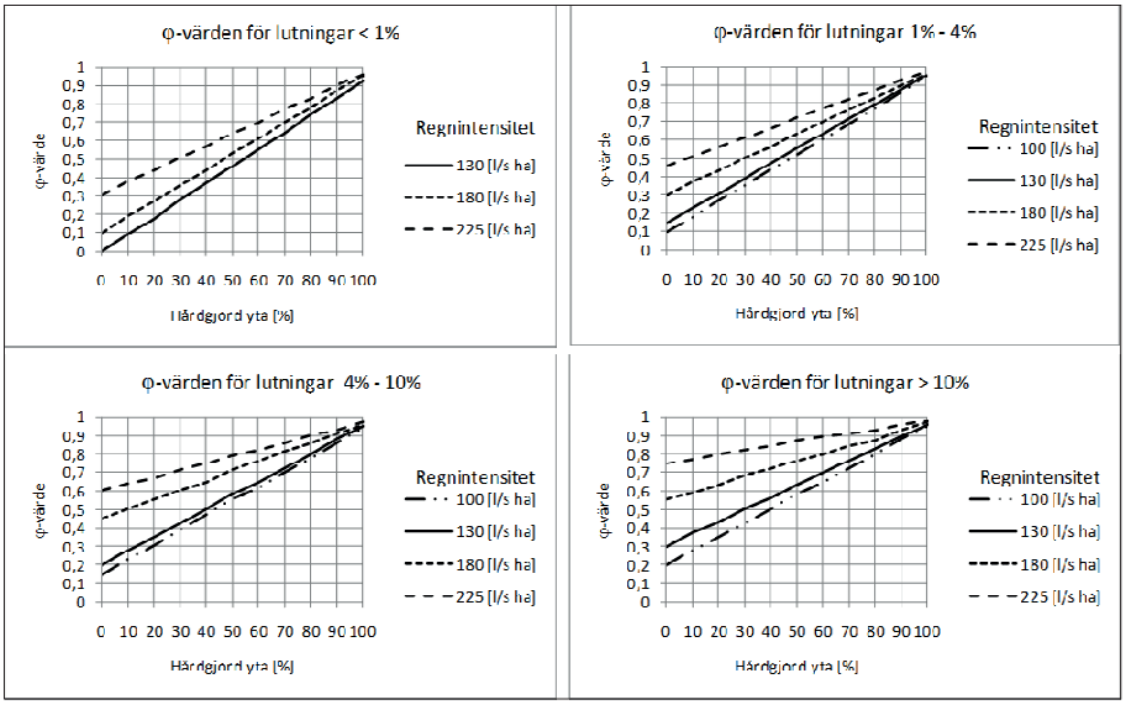

Figure C.1: Estimation of runoff coefficient according to AVT-A118 (Tegelberg & Svensson, 2013). *(Approved by Svenskt Vatten.)*

D

Appendix: Simulation details

Table D.1: The rain loads included in the model, presented as a time series for each return period. The rains are CDS rains with a climate factor of 1.2.

	Volume for each return period [mm]									
Time series	**10**	**20**	**30**	40	50	60	70	80	90	100
15:00:00	0.000	0.000	0.000	0.000	0.000	0.000	0.000	0.000	0.000	0.000
15:30:00	1.141	1.335	1.480	1.589	1.681	1.766	1.839	1.904	1.968	2.024
16:00:00	1.309	1.544	1.720	1.852	1.964	2.068	2.156	2.236	2.313	2.381
16:30:00	1.572	1.872	2.096	2.265	2.408	2.541	2.653	2.755	2.854	2.941
17:00:00	2.045	2.463	2.775	3.010	3.209	3.393	3.549	3.691	3.829	3.950
17:15:00	1.360	1.653	1.871	2.035	2.175	2.304	2.413	2.512	2.609	2.693
17:30:00	1.821	2.228	2.532	2.761	2.955	3.134	3.286	3.424	3.558	3.676
17:40:00	1.736	2.136	2.436	2.661	2.852	3.028	3.177	3.313	3.446	3.562
17:45:00	1.191	1.472	1.681	1.839	1.972	2.096	2.200	2.296	2.388	2.469
17:50:00	1.633	2.023	2.314	2.533	2.719	2.891	3.037	3.169	3.298	3.410
17:52:30	1.131	1.404	1.608	1.761	1.892	2.012	2.114	2.206	2.296	2.375
17:55:00	1.561	1.941	2.224	2.438	2.619	2.786	2.927	3.056	3.181	3.291
17:57:30	2.592	3.227	3.701	4.058	4.361	4.641	4.878	5.093	5.303	5.487
18:02:30	11.428	14.249	16.354	17.938	19.281	20.525	21.574	22.531	23.461	24.277
18:05:00	2.592	3.227	3.701	4.058	4.361	4.641	4.878	5.093	5.303	5.487
18:07:30	1.561	1.941	2.224	2.438	2.619	2.786	2.927	3.056	3.181	3.291
18:10:00	1.131	1.404	1.608	1.761	1.892	2.012	2.114	2.206	2.296	2.375
18:15:00	1.633	2.023	2.314	2.533	2.719	2.891	3.037	3.169	3.298	3.410
18:20:00	1.191	1.472	1.681	1.839	1.972	2.096	2.200	2.296	2.388	2.469
18:30:00	1.736	2.136	2.436	2.661	2.852	3.028	3.177	3.313	3.446	3.562
18:45:00	1.821	2.228	2.532	2.761	2.955	3.134	3.286	3.424	3.558	3.676
19:00:00	1.360	1.653	1.871	2.035	2.175	2.304	2.413	2.512	2.609	2.693
19:30:00	2.045	2.463	2.775	3.010	3.209	3.393	3.549	3.691	3.829	3.950
20:00:00	1.572	1.872	2.096	2.265	2.408	2.541	2.653	2.755	2.854	2.941
20:30:00	1.309	1.544	1.720	1.852	1.964	2.068	2.156	2.236	2.313	2.381
21:00:00	1.141	1.335	1.480	1.589	1.681	1.766	1.839	1.904	1.968	2.024

Table D.2: The simulated rain volumes, both total, and divided based on the type of rain. The volumes are based on the rain loads presented in Table D.1

	Volume [mm]			
Return period [year]	Total volume	Pre-rain	Peak-rain	Post-rain
10	49.610	10.983	31.200	7.427
20	60.848	13.232	38.748	8.868
30	69.234	14.910	44.381	9.943
40	75.541	16.173	48.617	10.751
50	80.894	17.244	52.213	11.438
60	85.848	18.235	55.540	12.073
70	90.029	19.072	58.349	12.609
80	93.839	19.834	60.907	13.097
90	97.547	20.576	63.398	13.573
100	100.797	21.227	65.581	13.990

Table D.3: The initial water content used in MIKE+, for each return period.

	Initial water content [%]					
Return period [year]	Hard surfaced areas	Thin layer on rock	Sand/gravel	Moraine	Elements of silt/clay, peat	Silt/clay
10	0.00	50.00	30.00	40.00	50.00	55.00
20	0.00	57.50	32.50	42.50	52.50	57.50
30	0.00	62.50	34.17	44.17	54.17	59.17
40	0.00	65.00	35.00	45.00	55.00	60.00
50	0.00	67.50	35.83	45.83	55.83	60.83
60	0.00	70.00	36.67	46.67	56.67	61.67
70	0.00	72.50	37.50	47.50	57.50	62.50
80	0.00	75.00	38.33	48.33	58.33	63.33
90	0.00	77.50	39.17	49.17	59.17	64.17
100	0.00	80.00	40.00	50.00	60.00	65.00

DEPARTMENT OF ARCHITECTURE AND CIVIL ENGINEERING
CHALMERS UNIVERSITY OF TECHNOLOGY
Gothenburg, Sweden
www.chalmers.se

CHALMERS
UNIVERSITY OF TECHNOLOGY